

Acoustofluidics 2013

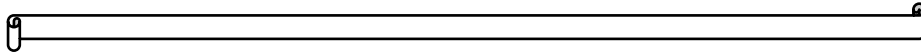
UNIVERSITY OF
Southampton

Conference Program

Lectures are held in the *Nuffield Lecture Theatre A (06/1077)*, Highfield Campus, University of Southampton.

Time	DAY 1: Thursday September 12th
10:00 onwards	Registration in the Hartley Suite (<i>Staff club, Bldg. 38</i>) and mounting posters.
10:00	USWnet Management meeting (also open to interested, non-board members) <i>Held in the Hartley Suite.</i>
13.00	Conference opening (Nuffield Lecture Theatre, Lecture Theatre A)
13.15-13.55	Keynote lecture – Tony Jun Huang "Acoustic Tweezers: Manipulating Bio-particles and Fluids Using Acoustic Waves" Department of Engineering Science and Mechanics, The Pennsylvania State University, USA
Session I – Particle Separations	
14.00-14.20	"Acoustic properties of liquids impact the separation efficiency" Per Augustsson ¹ , Sameer Deshmukh ^{1,2} , Thomas Laurell ¹ 1) Lund University, Sweden 2) Warsaw University of Technology, Poland.
14.20-14.40	"Macro-scale acoustophoresis with applications in oil water emulsion splitting" Bart Lipkens ^{1,2} , Ben Ross-Johnsrud ^{1,2} , Brian McCarthy ^{1,2} , Louis Masi ² , and Jason Dionne ^{1,2} 1) Western New England University, USA 2) FloDesign Sonics Inc., USA
14.40-15.00	"Continuous-flow ultrasonic concentration of bacteria for water quality analysis" Dario Carugo, Dyan N Ankrett, Walid Messaoudi, Nick R Harris, Martyn Hill and Peter Glynn-Jones University of Southampton
15.00-15.45	Coffee & posters in the Hartley Suite
15.45-16.10	Invited lecture – Bruce Drinkwater "Multi-element arrays for dextrous acoustic manipulation" University of Bristol, UK
Session II – Modelling 1	
16.10-16.30	"Full numerical simulation of the acoustic radiation force" Mads J. Herring Jensen ¹ and Henrik Bruus ² 1) COMSOL, Denmark; 2) Technical University of Denmark
16.30-16.50	"Theoretical And Experimental Evaluation Of The Time-Averaged Viscous Torque For The Rotation Of Micro Particles" Andreas Lamprecht, Thomas Schwarz, Jingtao Wang, Jurg Dual ETH, Zurich
16.50-17.10	"Interaction force between rigid spheres in a micro channel" Shahrokh Sepehrirahnama ¹ , Kian-Meng Lim ^{1,2} and Fook Siong Chau ¹

Time	DAY 1: Thursday September 12th
	1) National University of Singapore 2) NUS (Suzhou) Research Institute, Jiangsu.
17.10-17.20	Break
17.20-17.45	Invited lecture - Thomas Franke University of Augsburg, Germany.
17.45-18.05	"Surface Acoustic Waves for On-Demand Single Picoliter Droplet Production" Adrian Neild, David J. Collins, Kristian Helmersen, and Alan Tuncay Monash University, Australia
19:00-23:00	Conference Banquet in Hartley Suite (Staff Club, Bldg. 38 – enter by steps at far end)

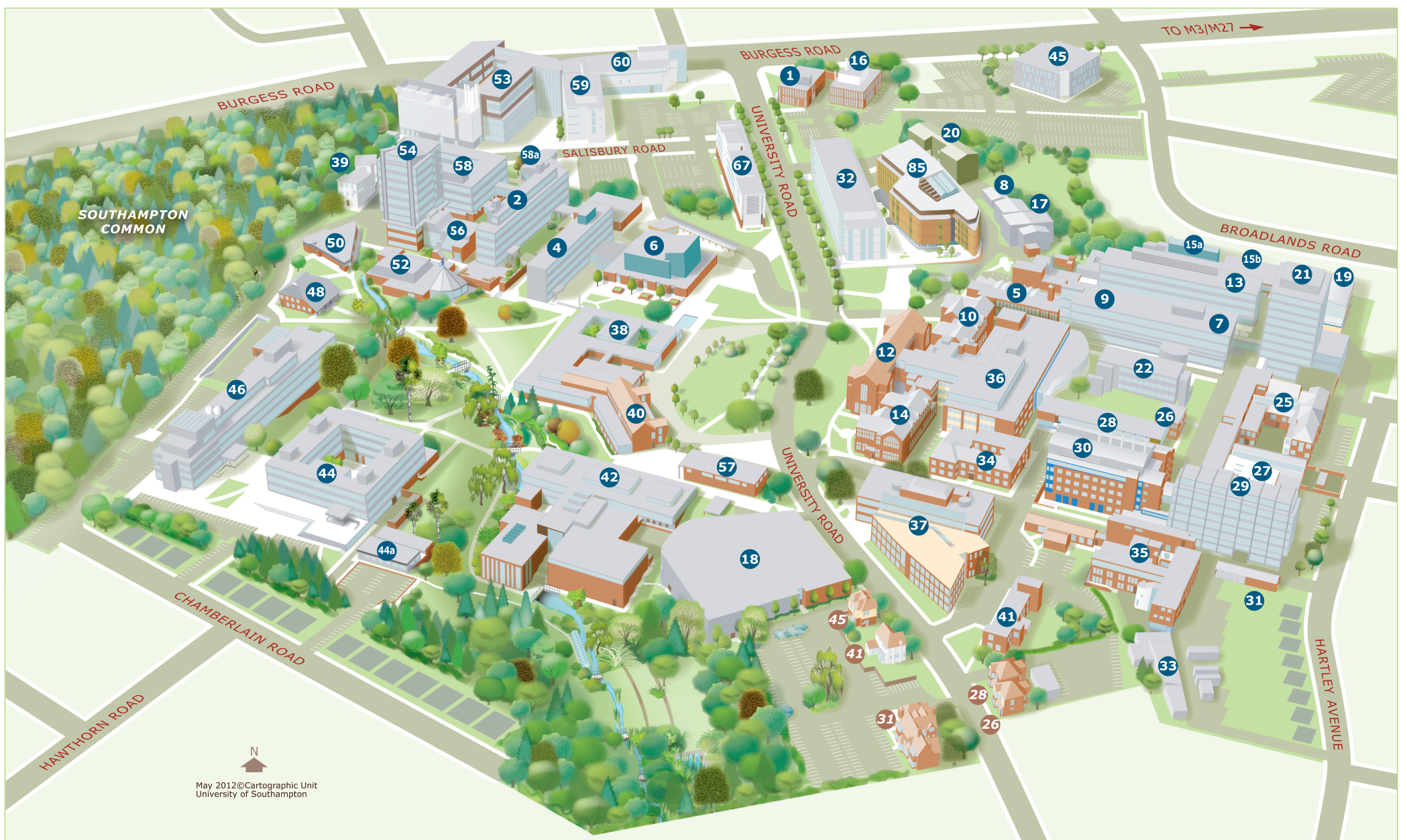


Time	DAY 2: Friday September 13th
Session IV – Modelling 2	
09.05-09.25	"Multipole expansion method for calculation of acoustic radiation force on non-spherical objects" Kian-Meng Lim ^{1,2} and Shahrokh Sepehrirahnama ¹ 1) National University of Singapore 2) NUS (Suzhou) Research Institute, Jiangsu.
09.25-09.45	"Numerical simulation of acoustophoresis for particles of arbitrary shape, size and structure" Philipp Hahn, Thierry Baasch, Jurg Dual ETH Zürich.
09.45 -10.05	"Underlying physics of the emergence of negative radiation forces on spheres illuminated by zero-order Bessel beams" Mahdi Azarpeyvand, University of Cambridge.
10.05-10.30	Coffee break and posters
Session V – Mixed ultrasound topics	
10.30-11.10	Keynote 2 – Tim Leighton "Cold water cleaning using acoustofluidics" University of Southampton
11.10-11.30	"Impedance matched channel walls in acoustofluidic systems" Ivo Leibacher, Sebastian Schatzer, Jürg Dual ETH, Zurich.
11.30-11.50	"Acoustic trapping used for bead incubation in a Luminex-based multiplex biomarker assay" Maria Tenje ¹ , Hongyan Xia ^{2,3} , Mikael Evander ¹ , Björn Hammarström ¹ , Axel Tojo ¹ , Sándor Belák ^{2,3,4} , Thomas Laurell ^{1,5} and Neil LeBlanc ^{3,4} 1) Lund University, Sweden 2) Swedish University of Agricultural Sciences, Uppsala 3) The World Organization for Animal Health (OIE) Collaborating Centre for the Biotechnology-based Diagnosis of Infectious Diseases in Veterinary Medicine Uppsala, Sweden 4) The National Veterinary Institute (SVA), Uppsala 5) Dongguk University, Korea
11.50-12.10	"Particle attraction to membranes with evanescent standing waves " Jeremy J. Hawkes, University of Manchester
12.10-12.30	"High-speed camera observation of droplet atomization and coagulation in an ultrasonic standing wave field"

Time	DAY 2: Friday September 13th
	Marina Reißweber, Felix Brand, Gerhard Lindner Coburg University of Applied Sciences and Arts
12.20-13.20	Lunch
Session VI – Biological applications	
13.20-13.45	"Live Cell Imaging in a Micro-Array of Acoustic Traps Facilitate Quantification of Natural Killer Cell Heterogeneity" A.E. Christakou ¹ , M. Ohlin ¹ , B. Vanherberghen ¹ , M.A.Khorshidi ¹ , N. Kadri ² , T. Frisk ¹ , M. Wiklund ¹ and B. Önfelt ^{1,2} 1) KTH - Royal Institute of Technology, Sweden 2) Karolinska Institute, Stockholm, Sweden
13.45-14.05	"Application of a novel perfusion bioreactor with integrated ultrasound standing wave trap for augmentation of cartilage tissue engineering" Siwei Li, Peter Glynne-Jones, Martyn Hill, Richard O C Oreffo, and Rahul S Tare University of Southampton.
14.05-14.25	"Sonoporation in the absence of contrast agent: a 'gentle' way to deliver therapeutic agents" Dyan Ankrett, Dario Carugo, Peter Glynne-Jones and Martyn Hill Univeristy of Southampton.
14.25-14.45	Coffee break
Session VII – Devices and Integration	
14.45-15.05	"Integrated acoustic micro particle manipulation and imaging system" A.L. Bernassau, M. Al-Rawhani and D.R.S. Cumming University of Glasgow
15.05-15.25	"Online Frequency Tracking in Acoustic Trapping" Björn Hammarstöm, Mikael Evander, JacobWalström, Thomas Laurell, Johan Nilsson Lund University, Sweden.
15.25-15.45	"Electronic Controlled Piezoelectric Array for Ultrasonic Particle Manipulation in an Acoustic Resonator" Han Wang ¹ , Yongqiang Qiu ¹ , Christine Demore ¹ , Sandy Cochran ¹ , Peter Glynne-Jones ² , Martyn Hill ² 1) University of Dundee, UK; 2) University of Southampton
15.45-15.55	Announcing "Acoustofluidics 2014" and closing remarks
16.00	End

Posters:

<p>"Multi-frequency characterisation of a chip for microbubble trapping" Chris Fury^{1,2}, Pierre N. G�lat^{1,2}, Philip H. Jones², Gianluca Memoli¹ 1) National Physical Laboratory, UK 2) University College of London, UK.</p>
<p>"Numerical simulation of 3D acoustophoretic motion of microparticles in an acoustofluidic device" Junjun Lei, Peter Glynne-Jones and Martyn Hill University of Southampton</p>
<p>"Acoustic trapping of Rayleigh-size particles using complex Gaussian-shape beams" Mahdi Azarpeyvand University of Cambridge</p>
<p>"Temperature dependence of acoustic streaming inside droplets induced by Lamb waves" Wei Liang, Gerhard Lindne Coburg University of Applied Sciences and Arts, Germany.</p>
<p>"Temperature Controlled Multi-Well Chip Device Using a PID Regulated Liquid Heat Exchanger" Mathias Ohlin, Martin Wiklund KTH - Royal Institute of Technology, Sweden</p>
<p>"Deformation and vibration of confined liquid droplets on a aluminium substrate excited by piezoelectric transducers" Matthias Streller, Gerhard Lindner Coburg University of Applied Sciences and Arts, Germany.</p>
<p>"Creating sheets of bronchial epithelial cells within Sonotweezers" Angela Tait, Peter Glynne-Jones, Dyan Ankrett, Martyn Hill , Donna Davies University of Southampton</p>
<p>"Acoustic streaming: a general analytical solution" Jonas T. Karlsen, Mikkel W.H. Ley, Peter B. Muller, Henrik Bruus Technical University of Denmark</p>
<p>"Ultrasonic Needle Device for Cell Membrane Disruption and Local Mixing in a Microfluidic Chip" Ida Iranmanesh, Harisha Ramachandraiah, Mathias Ohlin, Aman Russom, Martin Wiklund KTH - Royal Institute of Technology, Sweden</p>
<p>"Accelerated Cell Sorting Using In_line Sample Pre-Enrichment" Brian Warner¹, Liping Yu¹, Joe Trotter¹, Maria C. Jaimes¹, Marko Blom², Wilfred Buesink², Andreas Lenshof³, Thomas Laurell³ 1) BD Biosciences, USA; 2) Micronit Microfluidics, The Netherlands; 3) Lund University, Sweden</p>
<p>"Orientation of Erythrocytes for Flow Cytometry" Ola Jakobsson, Carl Grenvall, Thomas Laurell Lund University, Sweden</p>
<p>"Finite element modelling of cell deformation by acoustic radiation forces" Puja Mishra, Peter Glynne-Jones and Martyn Hill University of Southampton</p>
<p>"Ultrasonic Large-Scale Separation – Review and Application in Milk Fat Skimming" Linda Johansson^{1,2}, Thomas Leong^{1,2}, Pablo Juliano², Raymond Mawson², Sally McArthur¹, Richard Manasseh¹ 1) Swinburne University of Technology, Australia 2) CSIRO Animal, Food and Health Sciences, Australia</p>
<p>"Elastomeric Negative Acoustic Contrast Microparticles for Flow Cytometry Assays " Kevin W. Cushing^{1,3}, Menake E. Piyasena¹ Nick J. Carroll¹ Gian C. Maestas¹ Beth Ann Lopez¹ Bruce S. Edwards¹ Thomas Laurell³ Steven W. Graves¹ and Gabriel P. Lopez^{1,2} 1) The University of New Mexico, United States 2) Duke University, United States 3) Lund University, Sweden</p>
<p>"Modeling of the formation of bands on a multiband resonator –Comparison of two approaches: diffusion equation and two phase model" Francisco Javier Trujillo, University of New South Wales</p>



Accommodation Office	37	Maritime Engineering	28
Aeronautics, Astronautics and Computational Engineering	13 25	Mathematics	54
Biomedical Engineering	7	Mechanical Engineering	7
Boldrewood Campus (under redevelopment) (Boldrewood)		Medical Education	85
Bookshop	60	Medicine	85 96H
Career Destinations	37	Mountbatten Building	53
Cartographic Unit	44	Murray Building	58
Centre for Biological Sciences	85	Music	2
Centre for Innovation and Leadership in Health Sciences	45 67	nCATS	7
Centre for Learning & Teaching	2	Nightingale Building	67
Chemistry	27 29 30	Nuffield Theatre	6
Civil, Maritime and Environmental Engineering and Science	7 21 22 28	Ocean and Earth Science, National Oceanography Centre Southampton (Waterfront Campus)	68
Cochlear Implant Centre	19	Optoelectronics Research Centre (ORC)	46 53
Communications and Marketing	37	Physics and Astronomy	46
Early Years Centre	41	Politics	58
Economics	58	Post / Parcel Store	35
EEE Building	32	Print Centre	36
Electronics & Computer Science	1 16 20 32 46 53 59	Professional Development Unit (PDU)	27
Engineering and the Environment Student Support	22	Professional Practice in Health Sciences	45 67
Engineering Sciences	7	Professional Services	37
Engineering Materials	5	Psychology	44
Engineering Workshops	9	Rayleigh Building	15b
Environmental Sciences	7 21 22	Researcher Development and Graduate Centre (RDGC)	27
e-Science Centre	25	Research and Innovation Services (RIS)	37
Estates & Facilities	35	Research Institute for Industry	27
Eustice Building	5	R. J. Mitchell Wind Tunnel (Engineering Sciences)	17
Faraday Building	21	School of Management Executive Education	58a
Fees Office	37	Security	32
Geodata Institute	44a	Shackleton Building	44
Geography and Environment	44	Social Sciences	58
George Thomas Building	37	Social Statistics	58
Gower Building	60	Social Work Studies	58
Graduation Office	37	Sociology & Social Policy	58
Humanities - James Parkes Building (Avenue Campus)	65 65a 65b	Southampton Education School	32 34 56
Archaeology	65a	Southampton Statistical Sciences Research Institute	39
Centre for Language Study	65	Sports Hall, Fitness Centre & Swimming Pool	18
English	65	Staff Social Centre & John Arlott Room	38
Film Studies	65	Student Funds Office	37
History	65	Student Services Centre	37
Marine Archaeology	65b	Students' Union	40 42 57
Modern Languages	65	Temp Bank	4
Philosophy	65	Tizard Building	13
Human Performance Laboratory	56	Tony Davies High Voltage Laboratory	20
Human Resources	37	Turner Sims	52
Institute for Life Sciences	85	Underwater Tank	8
Institute of Sound and Vibration Research	13 19	University Health Service	48
iSolutions	2 35 54	Uni-link	57
John Hansard Gallery	50	University Post Office	60
Jubilee Sports Centre	18	Wessex Needs Assessment Centre	37
Lanchester Building	7	West Building & Old Refectory	40
Law School	4	Wolfson Building	15a
Library	10 12 14 36	Wolfson Unit for Marine Technology and Industrial Aerodynamics (WUMTIA)	15a
Main Entrance	12	Year in Industry	16
Goods Entrance, Gurney Dixon Building	10 36	Zepler Building	59
Management School	2		

University Road Houses

Chaplaincy	41 University Road
Counselling Service	28 University Road
Dental Access Centre	31 University Road

Dyslexia Services (LDC)	45 University Road
Highfield Health	31 University Road
Safety Office	26 University Road

These are University Road Houses and are not part of the main Campus Building numbering system shown above.



Acoustic Tweezers: Manipulating Bio-particles and Fluids Using Acoustic Waves

Tony Jun Huang

Department of Engineering Science and Mechanics
The Pennsylvania State University
N-330 Millennium Science Complex
University Park, PA 16802, USA
Email: junhuang@psu.edu
URL: <http://www.esm.psu.edu/huang/>

Introduction

The past few years have witnessed rapid growth in the field of acoustofluidics, *i.e.*, the fusion of acoustics and microfluidics. Acoustofluidics offers many advantages such as high biocompatibility, fast fluid actuation, contact-free particle manipulation, versatility, low cost, and compatibility with other microfluidic components. In this talk, I will first present a series of acoustic-based fluid manipulation functions, such as fast mixing, tunable and pulsatile gradient, and chemical waveform, achieved by acoustically induced bubble oscillation. Then I will summarize our recent progress on an “acoustic tweezers” technique that utilizes standing surface acoustic wave (SSAW) to manipulate particles, cells, and organisms. This technique is capable of manipulating cells and microparticles regardless of shape, size, charge or polarity. Its power intensity, approximately 10^7 times lower than that of optical tweezers, compares favorably with those of other active patterning methods. Cell viability, proliferation, and apoptosis studies have revealed it to be non-invasive. The aforementioned advantages, along with this technique’s simple design and ability to be miniaturized, render the “acoustic tweezers” technique a promising tool for various applications in biology, chemistry, engineering, and materials science.

Tunable and pulsatile chemical gradient generation

Here we demonstrate that multiple bubbles that are arranged in a ladder-like formation and oscillating in an acoustic field provide a novel and versatile method to generate tunable, pulsatile chemical gradients in microdevices. The bubbles were trapped and supported in the polydimethylsiloxane (PDMS) microfluidic channel using horseshoe structures. Each oscillating bubble, when activated, mixes the stimulus and buffer solutions locally, effectively diluting the stimulant concentration. Subsequent transport of this mixed stimulant to the next bubble in the ladder results in further dilution of the stimulant, thereby generating a spatial gradient of the stimulant across the microchannel.

Particle patterning

The acoustic tweezers device consists of a PDMS microfluidic channel and a pair of IDTs deposited on a piezoelectric substrate in a parallel (Fig. 1a) or orthogonal (Fig. 1b) arrangement. After applying a RF signal to both IDTs to generate a SSAW field, particles/cells were patterned in parallel lines or arrays. Figs. 1c and 1d show the distribution of microbeads before and after the 1D and 2D patterning processes [1]. In order to enable dynamic SSAW-based particle patterning, slanted-finger interdigital transducers (SFITs) are used instead of regular IDTs. By tuning the input signal frequency, both the frequency and originating location of the main SAW beam can be tuned, permitting dynamic control of the particle patterning. We demonstrate SSAW-based tunable patterning of HL-60 leukemia cells; the period of the two cell lines was tuned to 60 μm , 78 μm , and 150 μm .

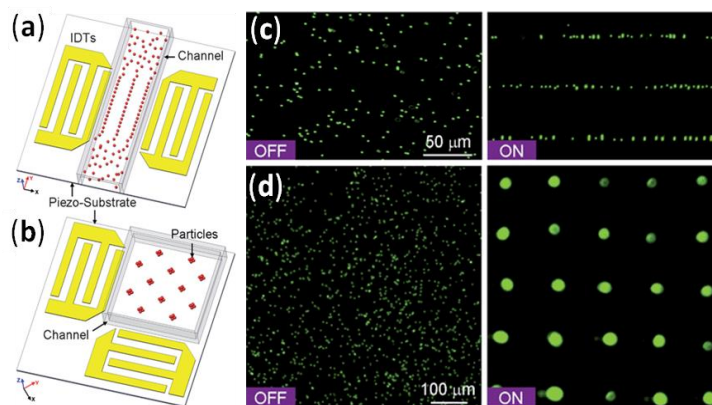


Fig. 1. SSAW-based patterning of a group of particles in stagnant fluid. Schematic of (a) 1D patterning using two parallel IDTs, (b) 2D patterning using two orthogonal IDTs (the angle between the IDTs can be changed to achieve different patterns). (c) Distribution of fluorescent microbeads before and after the 1D (SAW wavelength was 100 μm) patterning process, (d) and the 2D patterning process (SAW wavelength was 200 μm).

Single cell manipulation

When a single particle contained in stagnant fluid is exposed to a SSAW field, it will be trapped in either a pressure node or antinode (depending on the particle's properties), and it can be moved by changing the frequencies of the constituent SAWs [2]. The two pairs of chirped IDTs allow the device to move the objects trapped in the pressure nodes in x and y directions independently. Fig. 2b and 2c displays the effectiveness of this technique, manipulating a single bovine red blood cell and an entire organism *C. elegans* worm through a pre-programmed pattern. We find that a 10 μm polystyrene bead is accelerated to a velocity as high as 1.6 mm/s, and that HeLa cells exhibited no significant physiological change after being exposed to high power acoustic fields for 10 min. Such concept of tunable SSAW has also been used to achieve multichannel cell sorting [3].

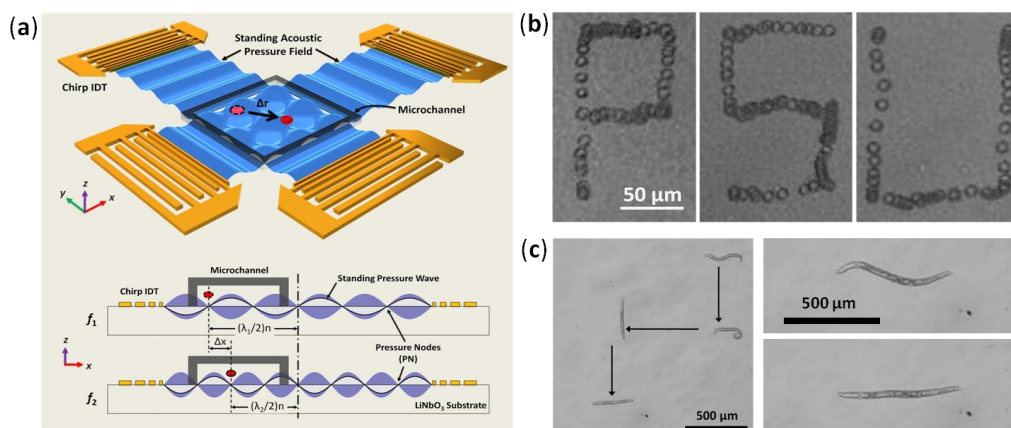


Fig. 2 (a) Device schematic and working mechanism of SSAW-based manipulation of a single particle contained in stagnant fluid (*i.e.*, acoustic tweezers). (b) Composed image of a single bovine red blood cell translated in two dimensions by changing the frequencies of the constituent SAWs. (c) Optical images showing the manipulation and stretching of a whole *C. elegans* worm.

Conclusion

Acoustic tweezers have demonstrated tremendous capability in microfluidic applications, from fluid control to particle manipulation. SSAWs have successfully been used to achieve functions of particle focusing, separation, dynamic patterning, sorting, and dexterous manipulation. Our acoustic tweezers are able to handle particles with diameters ranging from nanometer to millimeter scale. We believe that these unique advantages and functions position the acoustic tweezers to be a key enabler in many applications in biology, chemistry, medicine, and physics.

References

- [1] Jinjie Shi, Daniel Ahmed, Xiaole Mao, Sz-Chin Steven Lin, and Tony Jun Huang, Acoustic Tweezers: Patterning Cells and Microparticles Using Standing Surface Acoustic Waves (SSAW), *Lab on a Chip*, Vol. 9, pp. 2890-2895, 2009.
- [2] Xiaoyun Ding, Sz-Chin Steven Lin, Brian Kiraly, Hongjun Yue, Sixing Li, Jinjie Shi, Stephen J. Benkovic, and Tony Jun Huang, On-Chip Manipulation of Single Microparticles, Cells, and Organisms Using Surface Acoustic Waves, *Proceedings of the National Academy of Sciences of the United States of America (PNAS)*, Vol. 109, pp. 11105-11109, 2012.
- [3] Xiaoyun Ding, Sz-Chin Steven Lin, Michael Ian Lapsley, Sixing Li, Xiang Guo, Chung Yu Keith Chan, I-Kao Chiang, J. Philip McCoy, and Tony Jun Huang, Standing Surface Acoustic Wave (SSAW) Based Multichannel Cell Sorting, *Lab on a Chip*, Vol.12, pp. 4228-4231, 2012.

Acoustic properties of liquids impact the separation efficiency in acoustophoretic washing

Per Augustsson¹, Sameer Deshmukh^{1,2}, Thomas Laurell¹

¹Division of Nanobiotechnology
Department of Electrical Measurements
Lund University
S-221 00 Lund, Sweden
Email: Per.Augustsson@emat.lth.se

¹Department of Microbioanalytics
Warsaw University of Technology,
Warsaw, Poland
Email: sdeshmukh@ch.pw.edu.pl

Key findings

We have developed a method to increase the washing efficiency for particle rich suspensions in acoustophoretic carrier liquid exchange systems. A 0.73% reduction in acoustic impedance of the input suspending liquid relative to that of the re-suspension liquid led to a reduction in molecular contamination by 90% in the washed samples. Acoustic radiation pressure on the liquid interface between the liquids is speculated to prevent the suspending liquid from being dragged along with the particles into the zone of the re-suspension liquid.

Introduction

Microchannel acoustophoresis have grown profoundly and have found its utility in niche as well as mainstream applications for precise handling and manipulation of microparticles. Previous work by Hawkes et al. [1], Petersson et al. [2] and Augustsson et al. [3] have demonstrated that particles and cells can be re-suspended in new carrier liquid in continuous flow acoustophoresis devices, **Fig. 1**. The efficiency of these devices, as evaluated by comparing the amount of recovered particles to the transfer of a molecular contaminant, has been shown to be strongly affected by the concentration of particles in the processed samples hitherto limiting the technique to particle concentrations below ~1% volume.

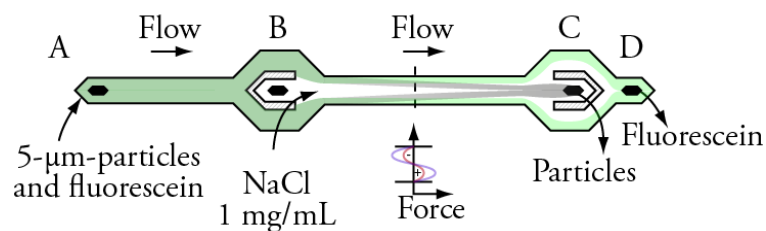


Fig. 1. Acoustophoretic re-suspension of particles in continuous flow. The 2 MHz ultrasound actuation results in a pressure node along the channel center. Particles are drawn toward this node and will, for a sufficiently high pressure amplitude, exit through the central outlet (C) while minute objects such as fluorescein molecules will remain in their flow laminated path and exit through the side's outlet (D).

Experiment

The experiments were performed on a previously described chip for particle washing and particle sorting [4], **Fig. 1**. Sample containing 5-µm-beads and fluorescein enter through inlet A and is flow laminated on both sides of a re-suspension liquid entering through the central inlet B. A NaCl concentration of 1 mg/mL was maintained in the central stream in all experiments. The acoustic properties of the sample liquid was altered relative to that of the central liquid by addition of either 5 mg/ml or 10 mg/mL NaCl. We studied the trifurcation outlet region of the chip for different particle concentrations and for different acoustic energies, optically and by collecting samples that were analysed regarding particle- and fluorescent concentration, respectively.

Results and discussion

Fig. 2 (a-c) shows the trifurcation outlet region of the chip for 0, 6 and 9 V actuation and a NaCl-concentration of the suspending liquid of 5 mg/mL whereas the central re-suspension liquid is of NaCl concentration 10 mg/mL. The sample has thus lower acoustic impedance ($Z = \rho c$) than the central stream. Fig. 2 (d-f) shows the corresponding images for a sample NaCl concentration of 10 mg/mL. When comparing Fig. 2 (b) and 2 (e) it is evident that the lower salt concentration leads to a more pronounced clearance of fluorescein in the region close to the focused beads. This is further supported by the measured fluorescence intensities in samples collected from the central outlet, Fig. 2 (j and k). This indicates that washing efficiency can be improved by lowering the acoustic impedance of the suspending liquid.

The broadening of the fluorescein band is likely to be caused by hydrodynamic drag from the particles as they move towards the central node. We speculate that the lower acoustic impedance of the suspending liquid leads to a force on the liquid interface between sample and re-suspension liquid that counteract the disturbance caused by the drag.

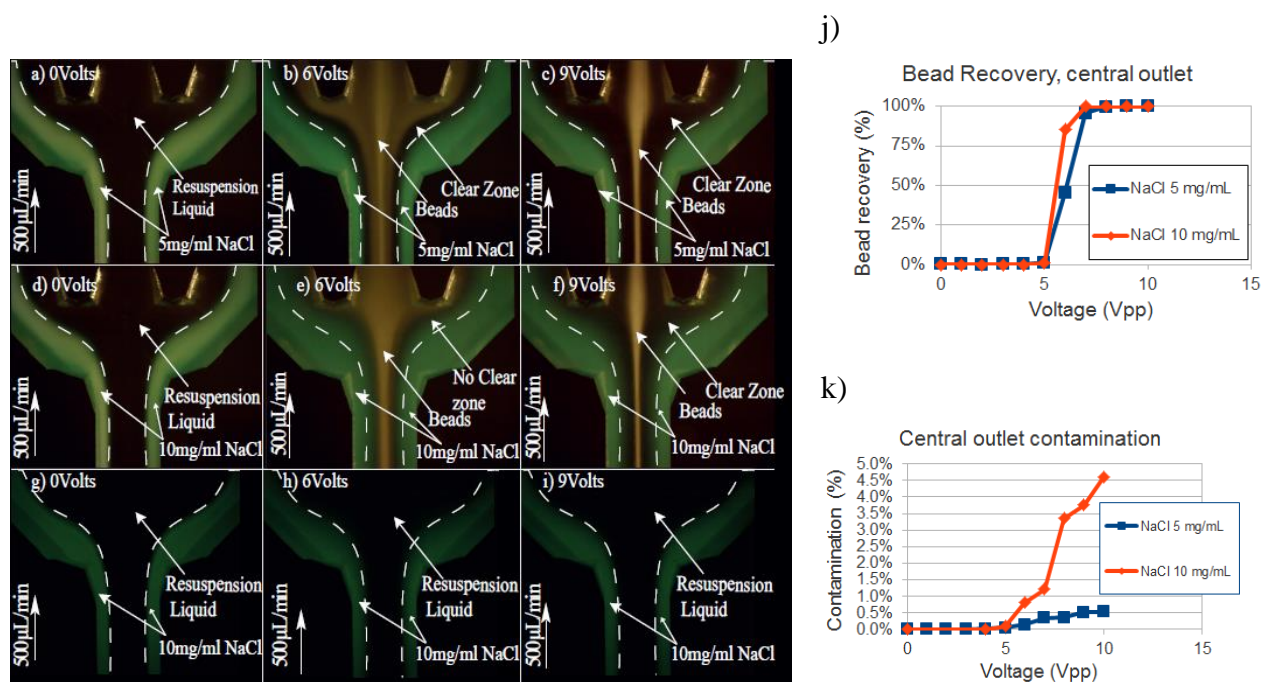


Fig. 2. (a-f) Fluorescence images of the outlet region of the channel for increasing actuator voltage and for suspensions of different NaCl-concentrations. (g-i) Control experiment with no beads in the side streams. (j and k) Plot of bead recovery and fluorescein contamination, respectively, in the central outlet.

Conclusion

Acoustic properties can be tailored to stabilize liquid interfaces in microchannel acoustophoresis so as to improve the separation of particles from minute objects.

References

- [1] Hawkes, J. J. et al., Continuous cell washing and mixing driven by an ultrasound standing wave within a microfluidic channel. *Lab on a chip*, 4(5), 446–52 (2004).
- [2] Petersson, F. et al., Carrier medium exchange through ultrasonic particle switching in microfluidic channels. *Analytical chemistry*, 77(5), 1216–21 (2005).
- [3] Augustsson, P. et al., Decomplexing biofluids using microchip based acoustophoresis. *Lab on a chip*, 9(6), 810–8 (2009).
- [4] Augustsson, P. et al., Microfluidic, Label-Free Enrichment of Prostate Cancer Cells in Blood Based on Acoustophoresis. *Analytical chemistry* (2012).



Macro-scale acoustophoresis with applications in oil water emulsion splitting

Bart Lipkens^{1,2}, Ben Ross-Johnsrud^{1,2},
Brian McCarthy^{1,2}, Louis Masi², and Jason Dionne^{1,2}

¹Department of Mechanical Engineering
Western New England University
1215 Wilbraham Road, Box S-5024
Springfield, Massachusetts, 01119, USA
Email: blipkens@wne.edu

²FloDesign Sonics Inc.
380 Main Street
Wilbraham, Massachusetts, 01095, USA
Email: b.lipkens@fdsonics.com

[Preference is for oral presentation at the conference]

Introduction

The last decades have seen a significant amount of development of microfluidic devices that employ acoustofluidics for the separation and manipulation of particles and cells. The recent tutorial papers in acoustofluidics [1] are testament to these efforts. Most of the efforts take place at the micro-scale and lead to the development of MEMS (Microelectromechanical Systems) devices. There is however a second focus on systems that employ ultrasonic standing waves that span many wavelengths [2]. Our technology fits in the latter category. The technology is that of a large scale acoustophoretic separation platform that employs three-dimensional standing waves and operates at large volumetric flow rates. Ultrasonic standing waves are used to trap, i.e., hold stationary, the secondary phase particles in a fluid stream. This is achieved when the acoustic radiation force exerted on the particles is stronger than the combined effect of fluid drag and buoyancy force. The action of the acoustic forces on the trapped particles results in concentration, agglomeration and/or coalescence of particles and droplets. Heavier than water particles are separated through enhanced gravitational settling, and lighter particles through enhanced buoyancy. The technology has the potential to be economic, efficient, sustainable, environmentally benign, and suitable for use in the oil separation of produced water. Produced water is water that is generated when oil and gas are extracted from the ground. Produced water contains emulsified oil with a majority of droplet sizes in the range of 3-8 micron.

Experiment

Previously [3] we reported on the design of a 1" by 2" acoustophoretic flow separator powered by a PZT-8 2 MHz transducer for the separation of oil from oil water emulsions. A schematic of the system is shown in Fig. 1. The emulsions were created by mechanically shearing the oil in a centrifugal pump until a stable emulsion is obtained. Particle size measurements of the emulsion indicated that the majority of the oil droplets have diameters in the range of three to five micron. Separation experiments were performed for a SAE 30 non-detergent motor oil in water emulsion at a concentration of 1000 ppm and flow rates of 500 ml/min. The transducer was driven at acoustic resonance frequencies. The transducer was operated at power levels of 20 W. Excellent separation efficiencies were obtained, i.e., better than 90% oil separation efficiency for a single pass by a single transducer setup.

Here we report on the application of the acoustophoretic separator for the oil separation of real emulsion streams such as produced water. Two different samples of actual produced water from an oil well in Texas were obtained. The first stream is produced water recovered directly from the well head. This sample has the highest amount of free organic compounds. The second stream is from the Salt Water Disposal (SWD) stream that is typically re-injected back into the ground after initial processing. This processed stream still contains significant amounts of residual oil.

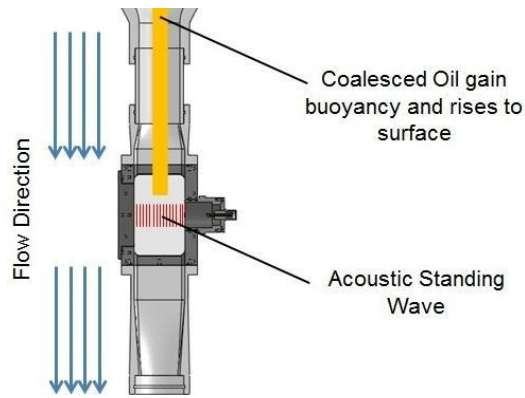


Fig. 1. Schematic of the acoustic phase separation system.

A feasibility study was performed on these two stream samples. Fig. 2 (a) shows a photo of trapped oil droplets in the acoustic standing wave and agglomerated droplets rising out of suspension. Fig. 2(b) shows a sample of the processed SWD stream pre-treatment (left) and post-treatment (right). Hydrocarbons are clearly present in the SWD stream, seen in the bottle on the left side of the photograph, but have mostly been filtered out of the stream by the acoustic separation technology, as seen in the bottle on the right side. A similar successful test was performed on the sample harvested from the well head.

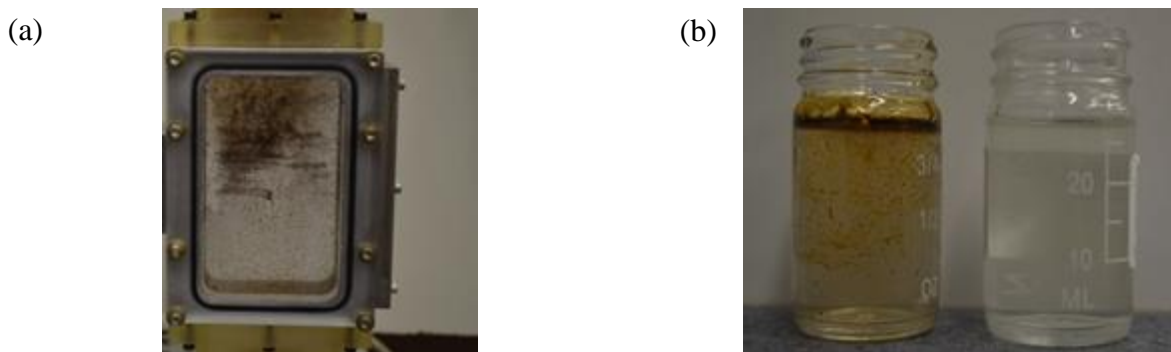


Fig. 2. (a) Photo of acoustophoretic system with hydrocarbon droplets, some trapped in the acoustic standing wave and others rising out of suspension after agglomeration in the standing waves, and (b) Photo of original (pre-treatment) produced water from the Salt Water Disposal Stream (Left) and post-treatment stream after processing with FD Sonics' acoustic separation technology (Right).

Conclusion

We have measured the acoustophoretic separation of emulsified hydrocarbons from actual produced water samples. One sample was directly harvested from the well head of a Texas oil well. The second sample was obtained after initial processing of the produced water, but still contained significant amounts of emulsified oil. Results show that the large volume flow rate acoustophoretic separator is successful in concentrating, agglomerating and coalescing the oil droplets, subsequently followed by actual separation of the oil out of suspension.

References

- [1] H. Bruus, J. Dual, J. Hawkes, M. Hill, T. Laurell, J. Nilsson, S. Radel, S. Sadhalg, and M. Wiklund, *Forthcoming Lab on a Chip tutorial series on acoustofluidics: Acoustofluidics—exploiting ultrasonic standing wave forces and acoustic streaming in microfluidic systems for cell and particle manipulation*, Lab Chip, 2011, 11, 3579-3580.
- [2] J. Hawkes and S. Radel, *Acoustofluidics 22: Multi-wavelength resonators, applications and considerations*, Lab Chip, 2013, 13, 610 - 627.
- [3] J. Dionne, B. McCarthy, B. Ross-Johnsrud, L. Masi, and B. Lipkens, *Large volume flow rate acoustophoretic phase separator for oil water emulsion splitting*, Proceedings of Meetings on Acoustics, Vol. 19, 045003 (2013) and J. Acoust. Soc. Am. Vol. 133, No. 5, May 2013, pp. 3237, 165th Meeting Acoustical Society of America and 21st International Congress on Acoustics.

Continuous-flow ultrasonic concentration of bacteria for water quality analysis

Dario Carugo¹, Dyan N Ankrett¹, Walid Messaoudi¹, Nick R Harris², Martyn Hill¹ and Peter Glynne-Jones¹

¹*Electro-Mechanical Engineering, Faculty of Engineering and the Environment, University of Southampton, Southampton, UK*

²*Department of Electronics and Computer Science, University of Southampton, Southampton, UK*

Introduction

Degradation of water quality can impact on both population health and at an industrial level. The detection of pathogens in water is carried out *via* laborious off-line analyses, making it difficult to promptly identify the source of contamination. The main obstacle in the implementation of rapid detection methods is represented by the low concentration of microorganisms in water. Manipulation of microscale bodies by acoustophoresis has been recently exploited for concentration of suspended biological cells and particles. However, acoustic manipulation of microorganisms $\sim 1\mu\text{m}$ in size represents a considerable challenge and only few studies have demonstrated concentration of particles $< 2\mu\text{m}$ in diameter [1, 2]. Here we report the development of an ultrasonic device for high-throughput concentration of bacteria in a continuous-flow format. The device is based on a thin-reflector (TR) arrangement [3] and its performance is compared with half-wave (HW) resonators.

Experimental

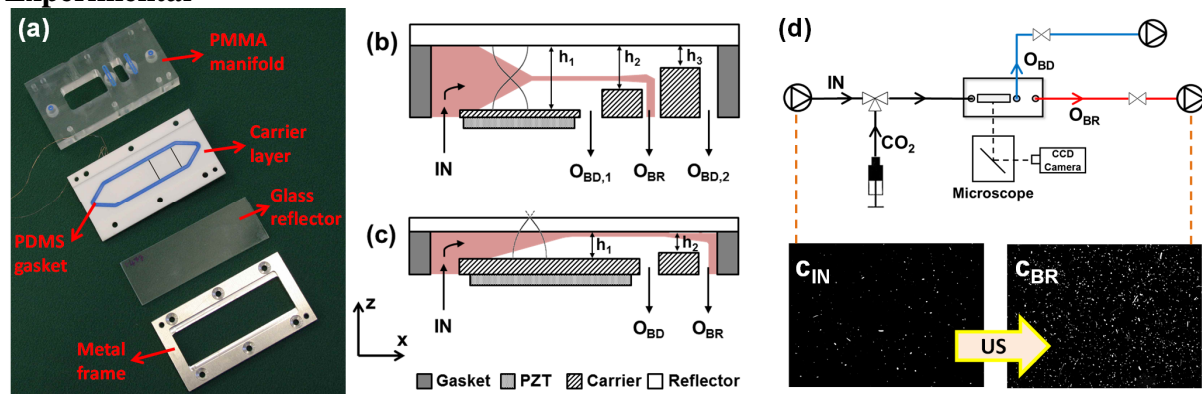


Fig. 1. (a) Photograph of multi-layered resonators' components. (b) Schematic of HW resonator. An USW was generated; bacteria were focused in a small volume centred on approximately the channel centreline and collected through the bacteria-rich outlet (O_{BR}). Bacteria-depleted fluid was withdrawn from $O_{BD,1}$ and $O_{BD,2}$. $h_1=380\mu\text{m}$ (active region), $h_2=250\mu\text{m}$ and $h_3=80\mu\text{m}$. (c) Schematic of TR resonator. An USW was generated; bacteria were moved towards the reflector surface and confined in a thin volume of fluid. Bacteria-depleted fluid was withdrawn from O_{BD} , and bacteria-rich fluid from O_{BR} . $h_1=128\mu\text{m}$ (active region), and $h_2=80\mu\text{m}$. (d) Schematic of the experimental set-up for the operation of TR resonator. 100% CO_2 was injected within the device to prevent bubbles formation. Shut-off valves were installed to selectively control liquid/gas distribution.

Devices comprised of a multi-layered structure (Figure 1a-c). A PZT transducer was employed to generate the acoustic wave and was coupled with a ceramic matching layer. The

walls of the fluidic chamber were formed by a moulded PDMS gasket and the reflector layer by a glass sheet (thickness: 1mm in HW, 170 μm in TR). A 1-D transfer impedance model was employed to predict the position of the pressure nodes and define the thickness of each layer. Iterative optimization of the acoustic operating conditions was performed by two means, (i) qualitative microscope observation of bacteria flow behaviour and (ii) quantitative z -scan analysis to determine the spatial distribution of bacteria in the fluid layer. In TR resonator, the reflector surface was coated with trichloro(1H,1H,2H,2H-perfluorooctyl)silane in order to minimise bacterial attachment. The reflector layer was stabilised by means of transversal metal bars in order to prevent glass bending. Device performance was assessed using *Escherichia coli* K12 as a model microorganism. Bacteria were fluorescently stained and suspended in PBS at a concentration of $\sim 10^4$ bacteria/ml. ImageJ *Particle Analyzer* was employed for bacteria counting and the determination of concentration increase, $\theta = c_{BR}/c_{IN}$.

Results

Both TR and HW devices were capable of effectively manipulating bacteria, as revealed from microscope observations and z -scan analyses (Figure 2a-b). Notably, in TR resonators the large majority of bacteria were moved to the reflector surface under US exposure. TR was capable of achieving significantly higher increase in bacteria concentration compared to HW (Figure 2c). This is likely due to: (i) the acoustic response in TR is less sensitive to variations in the reflector and fluid layer thickness compared to HW [3]; (ii) there are positive forces directed towards the reflector surface from every location within the fluid layer [3]; and (iii) the interface area between bacteria-rich and bacteria-depleted layers is reduced.

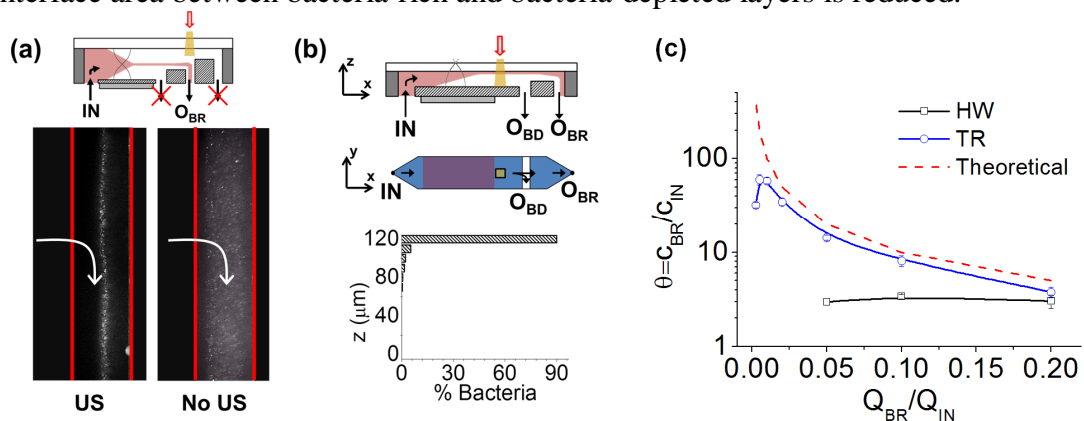


Fig. 2. (a) Fluorescent microscope images of *E. coli* flowing into O_{BR} in the presence (left) and in the absence (right) of ultrasound (HW resonator; $f=1.46\text{MHz}$, $2.5V_{pp}$, $Q_{IN}=20\text{ml/h}$). (b) z -scan analysis of the fluid layer in a TR resonator ($f=823\text{-}828\text{kHz}$ sweep, $20V_{pp}$, $Q_{IN}=20\text{ml/h}$). (c) Bacteria concentration increase (θ) achieved with TR and HW devices, compared with the theoretical trend. ($Q_{IN}=20\text{ml/h}$, $N = 3$). Y-axis is in Log scale.

Conclusion

We demonstrated the use of US to concentrate flowing suspensions of *E. coli*. The TR was capable of achieving significantly higher concentration increments (up to ~ 60 -fold increase, under high-throughput conditions). Although there is still a large margin for performance improvement - as manifested by the comparison with theoretical values - these devices could find potential application in on-line water quality analysis systems.

Acknowledgements

This work was supported by the EU-funded AQUALITY project (FP7-SME-2011-286601).

References

- [1] R. Townsend, M. Hill, N. Harris and M. McDonnell, *Ultrasonics*, 2008, **48**, 515-520.
- [2] N. Harris, M. Hill, R. Townsend, N. White and S. Beeby, *Sensors and Actuators B: Chemical*, 2005, **111**, 481-486.
- [3] P. Glynne-Jones, R. J. Boltryk, M. Hill, N. R. Harris and P. Baclet, *JASA*, 2009, **126**, EL75-EL79.

Dexterous acoustic tweezers using multi-element arrays

Bruce Drinkwater¹, Charles Courtney¹, Alon Grinenko¹, Marc Scholz¹, Phillip Bassindale¹, Paul D. Wilcox¹, Martyn Hill², David Cumming³ and Sandy Cochran⁴

¹Department of Mechanical Engineering,
University of Bristol,
Bristol, BS8 1TR,
United Kingdom.
Email: b.drinkwater@bristol.ac.uk

²Faculty of Engineering and the Environment,
University of Southampton,
Southampton, SO17 1BJ,
United Kingdom

³School of Engineering,
University of Glasgow,
Glasgow, G12 8QQ,
United Kingdom.

⁴Institute for Medical Science and Technology,
University of Dundee,
Dundee, DD2 1FD,
United Kingdom.

Introduction

Acoustic tweezers have attracted significant recent research activity leading to capabilities that rival more established manipulation technologies such as optical tweezers. In parallel, applications of acoustic tweezer technology are growing rapidly [1,2]. These developments are set against a background of a significant body of work on the acoustic radiation forces on particles and the use of devices based on simple one-dimensional standing waves to perform operations such as particle filtering and sorting [3]. For an acoustic tweezer to be dexterous it must be able to not only to trap particles, but to manipulate them flexibly, for example by moving different particles or groups of particles independently and producing a variety of different particle distributions. This paper aims to describe and discuss the recent emergence of these dexterous particle manipulation devices.

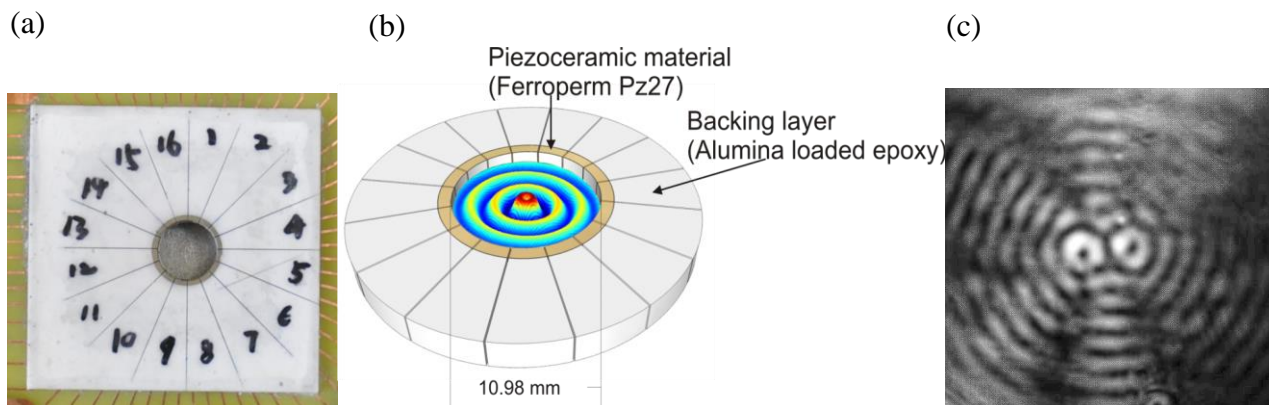


Fig. 1. (a) Photograph of a 16-element array fabricated from an annular ring of piezoceramic material. (b) schematic representation of the array device showing the key components and the acoustic pressure field generated. Note the pressure minima in the centre of the field which can be used to trap and move particles. This is formed from a vortex field and the pressure distribution is shaped like a first order Bessel function. (c) shows a Schlieren image of two traps which can also be formed and independently manipulated in the same device.

Achieving dexterity of manipulation with array-based devices

Figure 1 shows an example array-based device [4]. The use of arrays of active elements enables a wide variety of acoustic pressure fields to be generated as seen in Fig 1(c). In this way a given device can be reconfigured to generate multiple and moveable field patterns and it is this that leads to dexterous manipulation. The requirement for reconfigurability necessitates the design devices that are non-resonant in at least one dimension: in this way the acoustic fields are not dependent solely on device geometry. One attractive approach to generating a wide range of desired acoustic

fields within a device is to solve the inverse problem [5]: how to best excite the sources to achieve the desired field?

Results

Here we use the array-based devices described above to produce a wide variety of acoustic pressure fields. Critically, arrays enable reconfigurability so that a given device can generate multiple and moveable field patterns leading to the completion of complex assembly tasks as shown below in Fig. 2. Importantly, the design of these devices requires them to be non-resonant in at least one dimension as shown in Fig 1, so that the fields are not dependent solely on device geometry. Ideas from optical tweezers such as vortex fields are also shown to be applicable to acoustic devices as they enable trapping, translation and rotation.

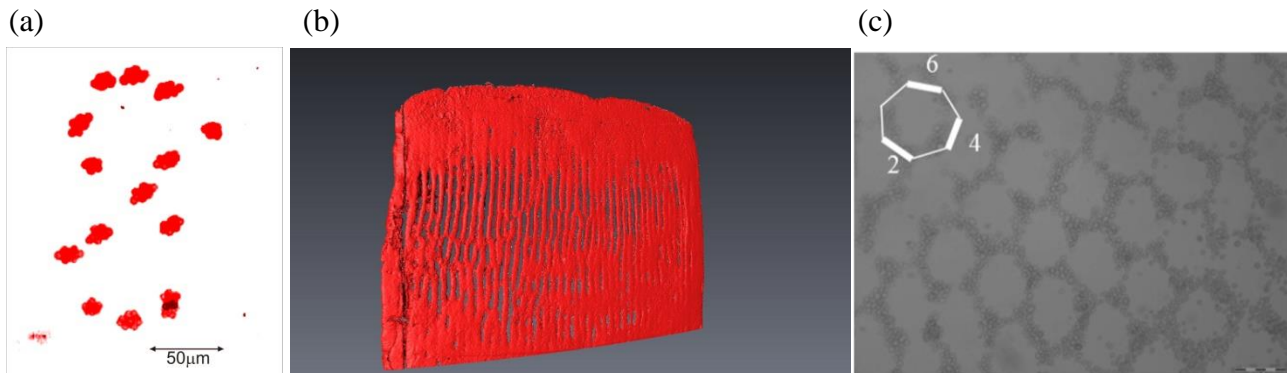


Fig. 2. (a) Manipulation of an agglomerate of 10 1µm polystyrene microspheres in a figure of eight. 14 separate photographs were summed to create this composite view. The contrast was adjusted and a false red colour added to aid viewing. (b) an X-ray CT image of a composite material assembled using ultrasonic manipulation. This structure was composed of 15µm diameter fibre each around 50 microns in length. (c) MDCK cells patterned using a heptagonal manipulation device [6].

Conclusion

The possible application areas for dexterous acoustic tweezers are vast and many avenues are yet to be explored. Recent progress has shown exciting possibilities in applications, such as tissue engineering and the assembly of composite materials. In both these cases the requirement is to carefully construct complex assemblies with microscale precision. It is also interesting to consider the complimentary developments of optical tweezers, and how together these devices might find even more widespread application.

References

- [1] Lee, J., Lee, C., Kim, H. H., Jakob, A., Lemor, R., Teh, S.-Y., ... Shung, K. K. (2011). Targeted cell immobilization by ultrasound microbeam. *Biotechnology and bioengineering*, 108(7), 1643–50.
- [2] Ding, X., Lin, S.-C. S., Kiraly, B., Yue, H., Li, S., Chiang, I.-K., ... Huang, T. J. (2012). On-chip manipulation of single microparticles, cells, and organisms using surface acoustic waves. *Proceedings of the National Academy of Sciences of the United States of America*, 109(28), 11105–9.
- [3] Glynn-Jones, P., Boltryk, R. J., & Hill, M. (2012). Acoustofluidics 9: Modelling and applications of planar resonant devices for acoustic particle manipulation. *Lab on a chip*, 12(8), 1417–26.
- [4] Grinenko, A., Wilcox, P. D., Courtney, C. R. P., & Drinkwater, B. W. (2012). Proof of principle study of ultrasonic particle manipulation by a circular array device. *Proceedings of the Royal Society A: Mathematical, Physical and Engineering Sciences*, 468(July), 3571–3586.
- [5] Courtney, C. R. P., Drinkwater, B. W., Demore, C. E. M., Cochran, S., Grinenko, A., & Wilcox, P. D. (2013). Dexterous manipulation of microparticles using Bessel-function acoustic pressure fields. *Applied Physics Letters*, 102(12), 123508.
- [6] Bernassau, A. L., Gesellchen, F., MacPherson, P. G. A., Riehle, M., & Cumming, D. R. S. (2012). Direct patterning of mammalian cells in an ultrasonic heptagon stencil. *Biomedical microdevices*, 14(3), 559–64.

Full numerical simulation of the acoustic radiation force on suspended microparticles including thermoviscosity

Mads J. Herring Jensen⁽¹⁾ and Henrik Bruus⁽²⁾

⁽¹⁾COMSOL A/S
DK-2800 Kongens Lyngby, Denmark

⁽²⁾Department of Physics
Technical University of Denmark
DTU Physics, building 309
DK-2800 Kongens Lyngby, Denmark

URL: www.staff.dtu.dk/bruus/researchgroup

Introduction

The acoustic radiation force is used for particle and cell handling in acoustofluidic systems. Theoretical studies of this force have developed by taking increasingly more complex physical aspects into account: From incompressible particles in ideal fluids (King, 1934), via compressible particles in ideal fluids (Yosioka and Kawasima, 1955) and general treatment for small particles in ideal fluids (Gorkov, 1962), to general theoretical schemes for the radiation force in viscous fluids by Doinikov [1] and by Danilov and Mironov [2] as well as specific treatment of microparticle acoustophoresis in viscous fluids by Settnes and Bruus [3]. In this work we extend this development to a numerical simulation including more completely the effect of thermoviscosity on the radiation force.

Theory

The governing perturbation equations for the thermoacoustic fields are standard textbook material [4, 5, 6]. The first-order equations expressed in terms of T_1 , p_1 , and \mathbf{v}_1 are,

$$\begin{aligned} -i\omega T_1 &= D_{\text{th}} \nabla^2 T_1 - i\omega \frac{\alpha T_0}{\rho_0 c_p} p_1, & -i\omega \rho_0 \mathbf{v}_1 &= -\nabla p_1 + \eta_0 \nabla^2 \mathbf{v}_1 + \beta \eta_0 \nabla (\nabla \cdot \mathbf{v}_1) \\ & & -i\omega p_1 &= \frac{\rho_0 c_0^2}{\gamma} \left[-i\omega \alpha T_1 - \nabla \cdot \mathbf{v}_1 \right], \end{aligned} \quad (1)$$

where D_{th} is the thermal diffusivity, c_p the isobaric specific heat capacity, α the coefficient of isothermal expansion, c_0 the speed of sound, and $\beta \approx 1/3$ the ratio of bulk to shear viscosity. The thermal and viscous penetration depth $\delta_{\text{th}} = \sqrt{2D_{\text{th}}/\omega} \approx 0.15 \mu\text{m}$ and $\delta = \sqrt{2\nu/\omega} \approx 0.38 \mu\text{m}$, respectively arise from the diffusive parts of these equations (values are given for 2 MHz ultrasound in water at room temperature), which set the thicknesses of the thermoviscous boundary layers near rigid surfaces. The radiation force $\mathbf{F}^{\text{rad}} = \oint_R da \mathbf{n} \cdot [\langle \boldsymbol{\sigma}_2 \rangle - \rho_0 \langle \mathbf{v}_1 \mathbf{v}_1 \rangle]$ depends on the time-averaged second-order contribution $\langle \boldsymbol{\sigma}_2 \rangle$ to the stress tensor.

Including the temperature dependence of the viscosity,

$$\eta = \eta_0 + \eta_1 = \eta_0 + (\partial_p \eta)_0 p_1 + (\partial_T \eta)_0 T_1 \approx \eta_0 + (\partial_T \eta)_0 T_1, \quad (2)$$

the time average of the second-order continuity equation and Navier–Stokes equation is

$$\rho_0 \nabla \cdot \langle \mathbf{v}_2 \rangle = -\nabla \cdot \langle \rho_1 \mathbf{v}_1 \rangle, \quad (3)$$

$$\begin{aligned} -\nabla \langle p_2 \rangle + \eta_0 \nabla^2 \langle \mathbf{v}_2 \rangle + \beta \eta_0 \nabla (\nabla \cdot \langle \mathbf{v}_2 \rangle) &= -\langle \nabla \eta_1 \cdot [\nabla \mathbf{v}_1 + (\nabla \mathbf{v}_1)^T] \rangle - (\beta - 1) \langle (\nabla \cdot \mathbf{v}_1) \nabla \eta_1 \rangle \\ &\quad - \langle \eta_1 \nabla^2 \mathbf{v}_1 \rangle - \beta \langle \eta_1 \nabla (\nabla \cdot \mathbf{v}_1) \rangle + \langle \rho_1 \partial_t \mathbf{v}_1 \rangle + \rho_0 \langle (\mathbf{v}_1 \cdot \nabla) \mathbf{v}_1 \rangle, \end{aligned}$$

while the relevant second-order part $\langle \boldsymbol{\sigma}_2 \rangle$ of the stress tensor is

$$\langle \boldsymbol{\sigma}_2 \rangle = -\langle p_2 \rangle \mathbf{I} + \eta_0 \langle \nabla \mathbf{v}_2 + (\nabla \mathbf{v}_2)^T \rangle + \langle \eta_1 [\nabla \mathbf{v}_1 + (\nabla \mathbf{v}_1)^T] \rangle + (\beta - 1) \left[\eta_0 \langle \nabla \cdot \mathbf{v}_2 \rangle + \langle \eta_1 \nabla \cdot \mathbf{v}_1 \rangle \right] \mathbf{I}. \quad (4)$$

Numerical method and results

We implement and solve the above thermoacoustic equations numerically using the finite element method software COMSOL Multiphysics 4.3a in a two-step procedure. First we calculate the "incoming" standing ultrasound wave fields T_{in} , p_{in} , and \mathbf{v}_{in} , here taken to be the approximate sinusoidal planar wave along the z -direction that arises due to co-oscillating velocity boundary conditions $v_{\text{in}} = \omega l e^{-i\omega t}$ at the end-surfaces of the cylindrical domain, inset Fig. 1.

Given a numerical solution of T_{in} , p_{in} , and \mathbf{v}_{in} , we move on to step two, where the scattered fields $T_{\text{sc}} = T_1 - T_{\text{in}}$, $p_{\text{sc}} = p_1 - p_{\text{in}}$, and $\mathbf{v}_{\text{sc}} = \mathbf{v}_1 - \mathbf{v}_{\text{in}}$ are calculated after placing an elastic sphere of radius a , compressibility κ_p , and Poisson's ratio $\bar{\nu}_p$ at $(r, z) = (0, \lambda/8)$, where F^{rad} is maximum. For the particle, the standard linear elastic equations for the displacement field \mathbf{u}_p are implemented using the material parameter for polystyrene often employed in acoustophoresis experiments. The boundary conditions at the particle surface are no-slip, $\mathbf{v}_1 = -i\omega \mathbf{u}_p$, while an adiabatic condition $\mathbf{n} \cdot \nabla T_1 = 0$ is imposed on the temperature of the fluid. Thermal effects are neglected inside the particle. Finally, the fluid domain is surrounded by a concentric cylindrical shell containing a perfectly matched layer (PML) that absorbs the outgoing scattering field while leaving the incoming field untouched. At the fluid-PML interface all fields are continuous. The outer surface of the PML is a hard wall, and in our implementation, the parameters are chosen such that outgoing scattered fields are damped 40 dB on the way out through the PML, and another 40 dB on the way back through the PML after reflection at the outer surface of the PML. The cylindrical domain has height and diameter 3λ .

Examples of results from our numerical simulation of F^{rad}/V_0 [GN/m³] are shown in Fig. 1.

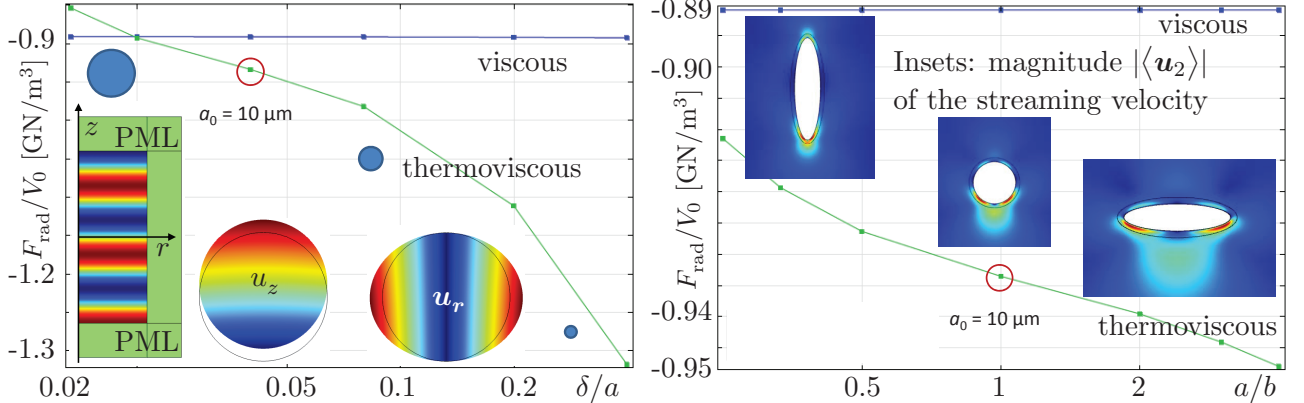


Figure 1: (Left) Numerical simulation of the radiation force per volume, F_{rad}/V_0 on a spherical particle of radius a at $(r, z) = (0, \lambda/8)$ in the thermoviscous case (green line) deviating from the analytical isothermal viscous case [3] (blue line) as a function of δ/a . Color plot insets are p_{in} in the fluid and the elastic deformation u_z and u_r of the particle. (Right) F^{rad}/V_0 vs. aspect ratio a/b for ellipsoids with same volume V_0 at $(r, z) = (0, \lambda/8)$.

Conclusion

We have derived, implemented and successfully tested a full thermoviscous simulation of the radiation force on a microparticle using parameters for typical acoustofluidic applications.

References

- [1] A. A. Doinikov, J. Acoust. Soc. Am. **101**, 722-730 (1997).
- [2] S. D. Danilov and M. A. Mironov, J. Acoust. Soc. Am. **107**, 143-153 (2000).
- [3] M. Settnes and H. Bruus, Phys Rev E **85**, 016327 1-12 (2012).
- [4] P. M. Morse and K. U. Ingard, *Theoretical Acoustics* (Princeton Univ. Press, Princeton NJ) (1986).
- [5] A. D. Pierce, *Acoustics* (Acoustical Society of America, Woodbury) (1991).
- [6] D. T. Blackstock, *Physical acoustics* (John Wiley and Sons, Hoboken NJ) (2000).



THEORETICAL AND EXPERIMENTAL EVALUATION OF THE TIME-AVERAGED VISCOUS TORQUE FOR THE ROTATION OF MICRO PARTICLES

Andreas Lamprecht, Thomas Schwarz,
Jingtao Wang, and Jurg Dual

Center of Mechanics
Swiss Federal Institute of Technology
Tannenstrasse 3, Building CLA
CH-8092 Zurich, Switzerland
Email: lamprecht@imes.mavt.ethz.ch
URL: www.zfm.mavt.ethz.ch

Introduction

Ultrasonic manipulation offers a wide range of possibilities to handle particles in a fluid. Particles can be aligned and clumps can be formed by a standing wave field. By changing the properties of the exciting standing wave, particles can be moved or rotated. There is an increase of interest in chip based microrobotics for the manipulation of micrometer sized particles with ultrasound. The acoustic rotation of particles gives a new degree of freedom to such systems.

In previous investigations with micro fluidic chambers, a fast rotation of spherical particles was observed under the excitation of two orthogonal standing waves with a phase shift. In those experiments, the acoustic viscous torque, which is generated by the near boundary streaming around the spherical particle, dominates the rotation and not the acoustic radiation torque. In theory the general physics are known, but are not understood in detail and little information was found for experimental data.

A literature review on the viscous torque has shown that so far theoretical investigations were done to calculate a torque on spheres, cylinders and circular plates [1]. A very specific analytical information of the viscous torque on a fixed sphere is given by the paper of Lee [2] based on W. Nyborg's theory [3]. However, the case that the sphere is free to move has not been presented in the literature. Furthermore, the possibility to use this acoustic viscous torque in micro manipulation devices has not been studied.

Analytical Calculations

The steady angular velocity Ω of the sphere is predicted, by using a perturbation assumption for the total fluid velocity \mathbf{u} of the form

$$\mathbf{u} = \mathbf{u}_1 + \mathbf{u}_2 + \mathbf{u}_B \quad (1)$$

where \mathbf{u} is split up in an acoustic velocity \mathbf{u}_1 , a time averaged component \mathbf{u}_2 and the background Stokes flow \mathbf{u}_B to consider the influence of the particle rotation. The property of the different time scales of \mathbf{u}_1 and \mathbf{u}_2 allows this separation. For the evaluation the sound field the first order Navier-Stokes equation is used by neglecting the terms $\rho_0 \mathbf{u}_1 \cdot \nabla \mathbf{u}_1$. The time-averaged field has to be solved by the Stokes equation to predict the time-averaged second order velocity \mathbf{u}_2 , which induces a shear stress on the sphere surface and generates the viscous torque. The influence of \mathbf{u}_B on \mathbf{u}_1 and \mathbf{u}_2 was investigated. It was shown that \mathbf{u}_B does not have any influence on \mathbf{u}_1 and \mathbf{u}_2 . The solution for the time-averaged viscous torque $\Gamma(\Omega)$ on a sphere within two orthogonal plane standing waves is

$$\Gamma(\Omega) = \frac{3}{4} \delta S_s A_x A_y (\rho_0 c_F^2)^{-1} \sin \zeta \cos kX \cos kY - 2\pi \mu_F R^3 \Omega \quad (2)$$

where δ is the Stokes-layer thickness, S_s the sphere surface area, ρ_0 the density, c_F the speed of

sound of the fluid, k the wavenumber in the fluid, μ_F the fluid dynamic viscosity and, $(A_x; A_y)$ the pressure amplitudes of the two orthogonal standing waves. The phase shift ζ and the sphere position $(X; Y)$ are responsible for the rotation direction. The result of $\Gamma(\Omega)$ can be split up into a driving torque by the acoustic excitation and a drag torque of the fluid viscosity on the moving surface. This expression for $\Gamma(\Omega)$ is analyzed in detail and the time evolution of Γ and the steady Ω are predicted.

Experimental Results

A set of experiments was designed to verify the analytical results for the viscous torque. Therefore a macroscopic manipulation device was needed which provides the necessary condition for the formation of two homogeneous orthogonal standing waves. The analytical results revealed the properties of the viscous torque which are of interest to investigate. The experimentally investigated properties of the particle rotation by viscous torque are:

- ❖ Rotation direction (Fig. 2.)
 - Location dependency (X, Y)
 - Phase dependency (ζ)
- ❖ Angular velocity Ω of the rotation
 - Influence of excitation amplitude (A_x, A_y)
 - Influence of particle size (R)
 - Influence of particle shape

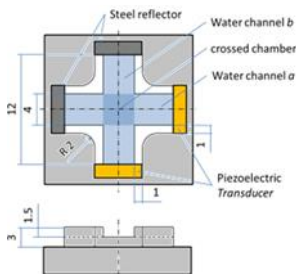


Fig. 1. Crossed fluid chamber device design for the experimental investigations on the viscous torque.

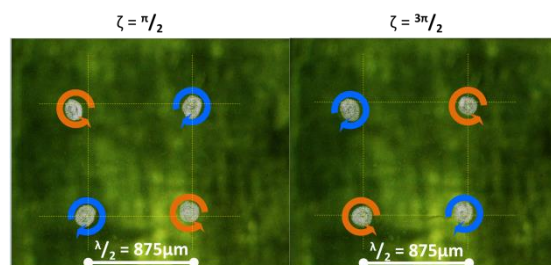


Fig. 2. Change of rotation direction at 846kHz for a jump from $\zeta = 90^\circ$ (left) to $\zeta = 270^\circ$ (right). The blue arrows are indicating a rotation in clockwise direction and the orange arrows are indicating a counter clockwise rotation.

Conclusion and Outlook

The analytical calculations have provided a deeper understanding of the viscous torque and were necessary to evaluate the experimental observations of rotating particles. It was shown that a rotating sphere has an equilibrium state between the driving viscous torque and the drag torque. The analytical results agree well with the observed particle behaviour in the experiments, where the particles rotate in the predicted direction and Ω increases quadratically with the excitation amplitudes. The phase and the radius dependency of $\Gamma(\Omega)$ were evaluated too. Measurements with a large variety of different particle sizes show the expected behaviour.

An additional parameter fitting of the unknown pressure amplitudes A_x and A_y leads to the information about the product of the two pressure amplitudes of the acoustic waves within the water chamber. Therefore this method can be used for the experimental evaluation of two orthogonal standing waves. The investigation on the measurement of the pressure amplitude of a single standing wave will be one of the challenges in the future research work.

For a single microfluidic channel it was already possible to measure the acoustic pressure amplitude by particle tracking [4]. Future work is focusing on the use of an optical trap. There it is possible to predict the force on a particle by the change of the thermal motion of the particle within the force potential of the optical trap. The optical trap also allows further experiments on the viscous torque to evaluate the influence of the phase dependency ζ and the particle position (X, Y) in more detail.

References

- [1] F. H. Busse and T. G. Wang, *Torque generated by orthogonal acoustic waves – Theory*, Acoustical Society of America, **69**, 1634-1638 (1981).
- [2] C. P. Lee and T. G. Wang, *Near boundary streaming around a small sphere due to two orthogonal standing waves*, Acoustical Society of America, **85**, 1081-1088 (1989).
- [3] Nyborg, W. L., (1958), *Acoustic Streaming near a Boundary*, Acoustical Society of America, **30**, 329-339 (1958).
- [4] R. Barnkob, P. Augustsson, T. Laurell, and H. Bruus, *Measuring the local pressure amplitude in microchannel acoustophoresis*, Lab Chip, **10**, 563-570 (2009).



Interaction force between rigid spheres in a micro channel

Shahrokh Sepehrirahnama¹, Kian-Meng Lim^{1,2} and Fook Siong Chau¹

¹Department of Mechanical Engineering
National University of Singapore
9 Engineering Dr 1
Singapore 117576
Email: shahrokh.sepehri@nus.edu.sg

²NUS (Suzhou) Research Institute
377 Lin Quan Street
Suzhou Industrial Park
Jiangsu, PRC 215123

Introduction

In microfluidic devices, the fluid carries suspended particles in the micro channels. By applying an ultrasound field, an acoustic radiation force acts on the particles in the wave direction, pushing them to the pressure node or anti-node [1, 2]. This force is called the primary radiation force [3]. It has been shown that there is a secondary radiation force which is the interaction force between particles [3]. For pulsating bubbles, it is called Bjerknes force which was reported in early 1900s [4].

Studies on the interaction of scattered waves from multiple rigid spheres and the interaction radiation force had been reported in the literature. The scattered waves from other spheres in the channel affect the distribution of the pressure and velocity field on the surface of each sphere, yielding an interaction force. In this study, the problem has been solved for two rigid spheres in a standing wave; however, the method can be generalized to any number of spheres. For two immovable rigid spheres, the interaction force is found to be attractive. For some configurations, the interaction force causes nonzero transverse force at pressure node and anti-node. Also, it affects the primary radiation force. Studying this interaction force helps to better understand the formation of particle aggregates at the pressure nodes [5, 6].

Methodology

Suppose that N rigid spheres are placed in a planar standing wave with wavenumber k . The total velocity potential is:

$$\varphi_{tot} = \varphi_{inc} + \sum_{n=1}^N \varphi_{sc}^{(n)}$$

where the velocity potential of the incident wave and the scattered wave from n^{th} sphere are φ_{inc} and $\varphi_{sc}^{(n)}$ respectively. The velocity potentials are written in a series form using multipole expansion. The $\varphi_{sc}^{(n)}$ is expanded around the center of the n^{th} sphere using the spherical harmonics Y_l^m and Hankel functions, $h_l^{(2)}$; however, φ_{inc} can be expanded around any local coordinate system.

$$\varphi_{sc}^{(n)} = \sum_{l,m} C_{lm} Y_l^m(\theta_n, \varphi_n) h_l^{(2)}(kr_n) e^{i\omega t} \quad \text{and} \quad \varphi_{inc} = \sum_{l,m} A_{lm} Y_l^m(\theta_n, \varphi_n) j_l(kr_n) e^{i\omega t}$$

where $(r_n, \theta_n, \varphi_n)$ are the spherical coordinates measured in the coordinate system attached to the n^{th} sphere, and j_l is the spherical Bessel function. The coefficients of the scattered wave C_{lm} are found by enforcing the boundary conditions on the surface of the scatterer using a weighted residual integral over the surface, with the spherical harmonics as the weights. This is considered as a numerical extension of multipole expansion.

Results

For two rigid spheres, two different configurations have been investigated. Fig. 1(a) and Fig 2(a) show the configurations. In both cases the planar standing wave is in z direction. In Fig. 1(b), the results show that the total radiation force, F_z , changes from an attractive force to a repulsive force as

the distance between two spheres reduces. The results compare well with a COMSOL finite element model for two spheres.

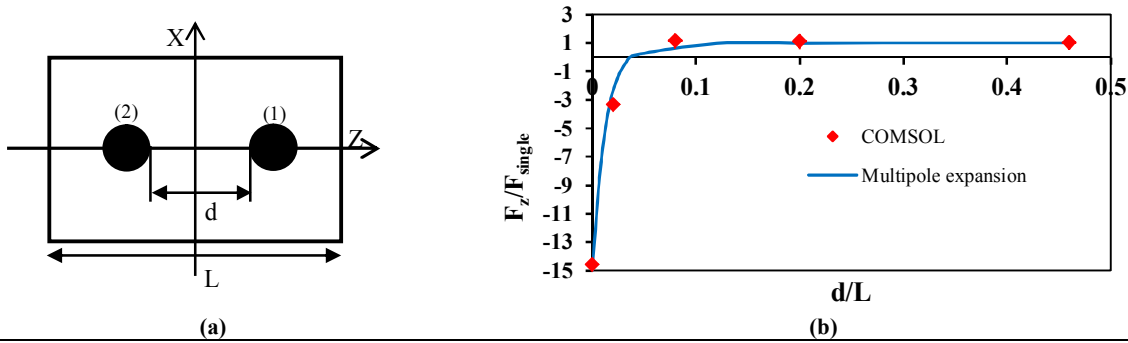


Fig. 1. (a) arrangement of two rigid spheres placed in the wave direction, z , (b) the radiation force, F_z , acting on the sphere (1) is divided by its value, F_{single} , for the case of single sphere. The length of the channel, L , is the half of wavelength, λ .

In Fig 2(a), two spheres are located at the same distance from the pressure node along the wave direction, z_c . In Fig 2(b), it is shown that by reducing the vertical distance between two spheres, d , the radiation force in the wave direction acting on the sphere (2), F_z , increases by 5% compared to the force acting on a single sphere, F_{single} . Fig. 2(c) shows that the other component of the radiation force acting on sphere (2) in the x direction, F_x , is nonzero. Again the results compare well with the COMSOL finite element model. This lateral force F_x is small for large distances but become larger than F_z when the distance, d , is close to zero. The lateral radiation force is attractive and causes cell aggregation at the pressure nodes

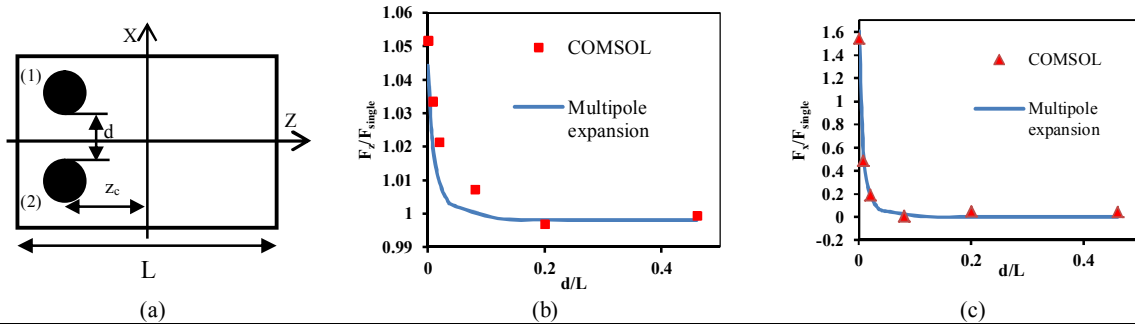


Fig. 2. (a) arrangement of two rigid spheres placed in the x direction, (b) the radiation force, F_z , acting on the sphere (2) is divided by its value, F_{single} , for the case of single sphere, (c) the radiation force, F_x , acting on the sphere (2) is divided by F_{single} in order to illustrate its comparable magnitude to F_z . The length of the channel, L , is the half of the wavelength, λ .

Conclusion

For a pair of rigid spheres in a micro channel, it is shown that the interaction between scattered waves causes interaction force. Based on the locations of the spheres in the channel, the interaction force may change different components of the radiation force acting on all the spheres. In the two configurations studied, it is observed that the interaction force is attractive, which justifies the formation of cell aggregates at the pressure nodes in micro channels. The present numerical extension of multipole expansion can be easily extended to study the case of many spheres in the channel.

References

- [1] L. V. King "On the acoustic radiation pressure on spheres" Proc. Royal Soc. of London A, (1934) Vol. 147, pp 212-240.
- [2] K. Yosioka, Y. Kawasima "Radiation pressure on spheres" Acustica (1955), Vol. 5, pp 167-173.
- [3] A. A. Doinikov "Acoustic radiation interparticle forces in a compressible fluid" J. Fluid Mech (2001), Vol. 444, pp 1-21.
- [4] V. F. K. Bjerknes "Fields of Force" (Columbia University Press, New York 1906)
- [5] M. Ohlin, A. E. Christakou, T. Frisk, B. Onfelt, M. Wiklund "Influence of acoustic streaming on ultrasonic particle manipulation in a 100-well-ring-transducer microplate" J. of Micromech. Microeng. (2012), Vol.23, No. 035008
- [6] S. Harput, B. Raiton, J. R. McLaughlan, S. D. Evans, S. Freear "The periodicity between the aggregated microbubbles by secondary radiation force" IEEE IUS (2011), art. no. 6293086, pp 1630-1633

Sorting and controlling cells and drops using surface acoustic waves

Thomas Franke

Softmatter and Biological Physics, University Augsburg

Summary:

We describe a versatile microfluidic fluorescence-activated cell sorter that uses acoustic actuation to sort cells or drops at ultra-high rates. Our acoustic sorter combines the advantages of traditional fluorescence-activated cell (FACS) and droplet sorting (FADS) and is applicable to a multitude of objects including cells, particles and drops.

The use of acoustics in microfluidics has become very popular for the past few years because it provides a versatile tool to manipulate small amounts of fluid on a chip in a highly controlled manner. Mixing, pumping, focusing and deflection has been successfully demonstrated and already included in commercial available products.

In this presentation we show sorting of biological cells and drops at high speed in microfluidic channels. We apply a surface acoustic wave (SAW) generated on a piezo-electric substrate to actuate cells and drops and direct them into one or more collect channels. The sort is triggered by the fluorescence signal of the sample objects similar to detection in a fluorescence activated cell sorter (FACS). Every single cell is interrogated in a laser spot and a decision to select is made based on its fluorescence level.

We can sort cells at rates as high as several 1000 cells/s. The sorting does not depend on cell size or another physical property such as charge, dielectric or compressibility contrast to the surrounding medium. Therefore, the sorting principle is very versatile and can be applied to large magnitude of different objects including particles and drops.

Drops have been shown to be useful in many application for example to encapsulate cells and drugs and to serve as templates for microparticle formation in drug delivery. Using our acoustic technique we are able to robustly control drop size and volume.

Ref.:

1. L. Schmid and T. Franke (front cover article), *Lab Chip*, 2013, 13 (9), 1691 – 1694 : SAW-controlled drop size for flow focusing



Surface Acoustic Waves for On-Demand Single Picoliter Droplet Production

Adrian Neild¹, David J. Collins¹,
Kristian Helmerson², and Tuncay Alan¹

¹Department of Mech. & Aero. Engineering
Monash University
Clayton, VIC 3800
Australia
Email: adrian.neild@monash.edu

²School of Physics
Monash University
Clayton, VIC 3800
Australia

Introduction

A new method is presented for the on-demand production of microfluidic water-in-oil droplets. Surface acoustic waves (SAW) are used as the actuation method required to distort a water/oil interface such that droplets are pinched off. The interdigital transducers, IDTs, used are designed to generate a high frequency focussed SAW which couples into the aqueous solution, at the interface the impedance mismatch between the oil and water results in the pressure field gradients required to generate acoustic radiation forces. These forces act to achieve the required interface distortion. Using this method, which is easily incorporated into microfluidic chips, single 12 picolitres can be produced on-demand, as such the droplets are orders of magnitude smaller than other methods using ultrasonic bulk waves [1, 2]. Additionally, pre-concentration and encapsulation of particles and cells is demonstrated, creating a platform on which a single cell can potentially be encapsulated in water-in-oil droplet: the smallest possible bioreactor [3].

Device fabrication

40 μm and 80 μm wavelength focussed IDTs were fabricated on a single-side polished 128° Y-X lithium niobate substrate. The 10 nm chrome/200 nm aluminium FIDTs were aligned on the substrate with the SAW propagation direction aligned in the X direction of the crystal orientation. A modified PDMS T-junction with height of 20 μm and orifice width of 20-30 μm , shown in Figure 1, was bonded to the lithium niobate after 1.5 minutes of oxygen plasma exposure. Using oil as the disperse phase and applying an AC signal to the FIDTs at their resonant frequency (96 MHz and 48 MHz for 40 μm and 80 μm wavelength devices) a SAW is focused at the water-oil interface which occurs at a modified T-junction between two channels containing oil and water phases. Upon actuation a water-in-oil droplet is produced.

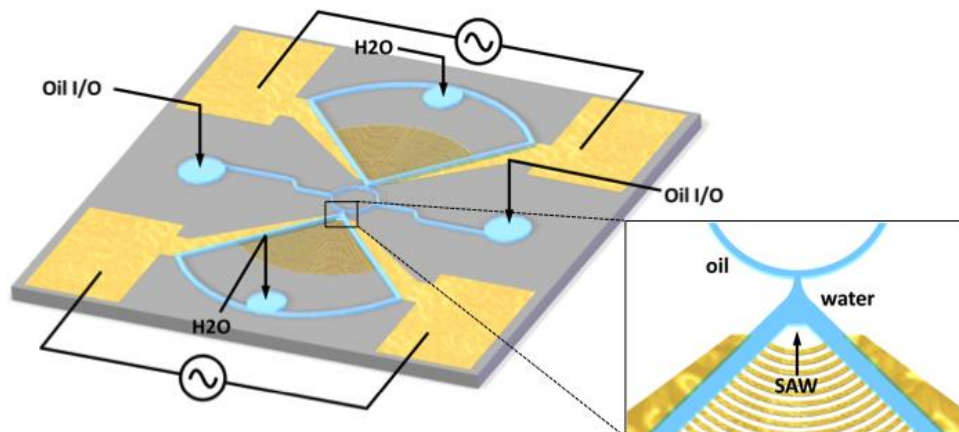


Fig. 1. Sketch of the SAW picoliter on-demand droplet generation system and close-up of the modified T-junction at which the water and oil form an interface.

Results

The application of increased applied powers (2.5 W – 5 W) and pulse durations (50 ms – 1500 ms) to the FIDTs can be used to control droplet volumes (12 pL – 50 pL) and the numbers of droplets produced (1 – 5), as shown in Figure 2. Using a 96 MHz SAW and relatively low powers (<2 W) it is possible to concentrate 10 μm polystyrene particles at the water-oil interface prior to droplet production for the purpose of particle encapsulation, as shown in Figure 3.

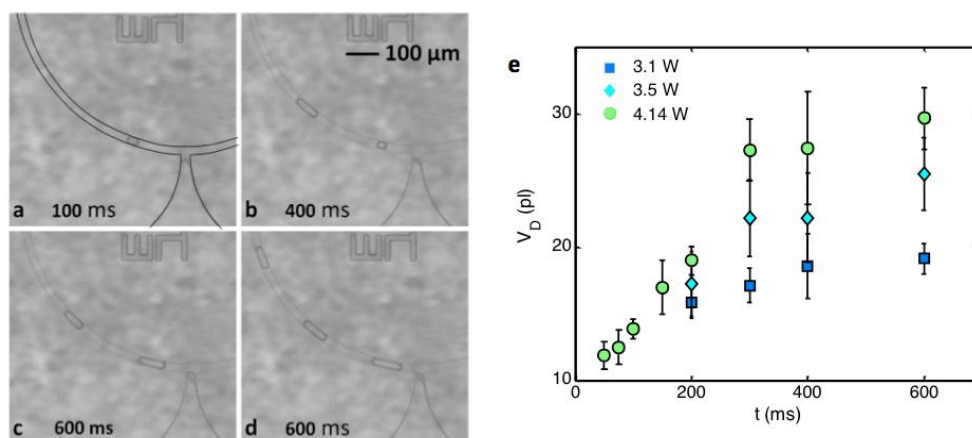


Fig. 1. (a-d) Multiple droplet can be produced using different pulse durations. Note that in (a) the outline of the channel has been drawn onto the image for clarity. Below 200 ms pulse duration single droplets are produced.

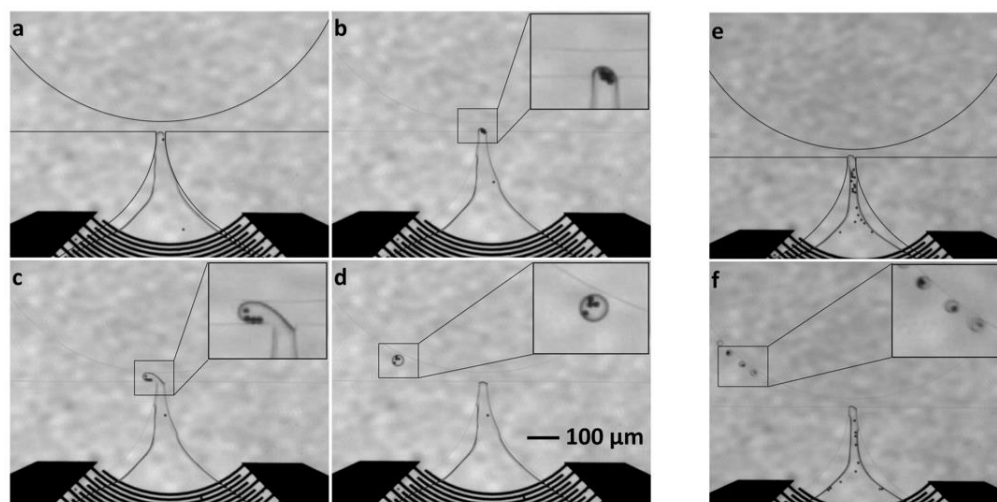


Fig. 2. Applying a low power SAW (<2 W) concentrates 10 μm particles at the oil-water interface, with a high power pulse (>2.5 W) sufficient to create a particle-encapsulating water-in-oil droplet, shown in the image sequences in (a-d) and (e, f), each spaced ~ 30 ms apart.

Conclusion

The work presented combines on-demand picolitre-scale microfluidic water-in-oil droplet generation with particle concentration and encapsulation for digital microfluidic applications. Future work will concentrate on optimizing the concept for multiple devices working in proximity and concept.

References

- [1] Bransky, Avishay, et al, *A microfluidic droplet generator based on a piezoelectric actuator*, Lab Chip, 9, 516 (2009).
- [2] A. Yusof et al., *Inkjet-like printing of single-cells*, Lab Chip, 11, 2447 (2011).
- [3] Doerr, Allison, *The smallest bioreactor*, Nature, 2, 326, (2005).



Multipole expansion method for calculation of acoustic radiation force on non-spherical objects

Kian-Meng Lim^{1,2} and Shahrokh Sepehrirahnama¹

¹Department of Mechanical Engineering
National University of Singapore
9 Engineering Dr 1
Singapore 117576
Email: limkm@nus.edu.sg

²NUS (Suzhou) Research Institute
377 Lin Quan Street
Suzhou Industrial Park
Jiangsu, PRC 215123

Introduction

The multipole expansion method using spherical harmonics is commonly used to calculate the acoustic radiation force acting on spheres. Most approximate formulae [1, 2] are based on just the monopole and dipole terms. However, the series of spherical harmonics are known to be divergent inside the Brillouin sphere [3]; hence, the use of spherical harmonics in calculations for non-spherical shapes can be erroneous. For ellipsoidal shapes, elliptical coordinates were used to obtain analytical results based on Mathieu functions, Lamé functions or electromagnetic analogy [4, 5].

In this study, we investigate the applicability of the multipole method using spherical harmonics for shapes of low eccentricity. Using spheroids as models, we examine the error incurred as a function of the aspect ratio (or eccentricity) and the number of multipoles used. The results showed that good approximate solutions of the radiation force can be obtained, especially when more multipoles are used. These calculations are useful in situations where shapes of biological cells and bubbles deviate slightly from spheres as they interact with or “get squeezed” by the surrounding.

Multipole Expansion

The scatterer is placed in a planar standing wave with wavenumber k . Both the incident φ_i and scattered φ_s waves are expanded using the spherical harmonics Y_l^m , spherical Bessel j_l and Hankel $h_l^{(1)}$ functions:

$$\varphi_i = \sum_{l,m} A_{lm} Y_l^m j_l(kr) e^{-i\omega t} \quad \text{and} \quad \varphi_s = \sum_{l,m} C_{lm} Y_l^m h_l^{(1)}(kr) e^{-i\omega t}.$$

The coefficients of the scattered wave C_{lm} are found by enforcing the boundary conditions on the surface of the scatterer using a weighted residual integral over the surface, with the spherical harmonics as the weights.

Results

Fig. 1(a) shows the normal velocities from the incident and scattering waves along the meridian of a sound-hard prolate spheroid ($b/a=1.4$), where b is the radius along the axis of rotation and a is the equatorial radius. The solid line shows the negative of the normal velocity due to the incident wave. The series of points show the normal velocity from the scattering wave when different numbers of spherical harmonics were used. As the number of terms used increases, the scattering wave data get closer to the incident wave so that the total normal velocity approaches zero (which is the boundary condition for sound-hard surface). Deviations between the (negative) incident wave and the scattered wave persist near the equator ($s=0.5$) as this region is inside the Brillouin sphere, where convergence is not achieved. The root mean square (RMS) residue of the normal velocity is calculated by sampling 30 points on the meridian, and this is plotted in Fig 1(b) against the number of terms used in the scattering wave. It can be seen that the residue decreases with the number of multipoles/spherical harmonics used, and the convergence is worse for larger eccentricity (aspect ratios deviating from 1).

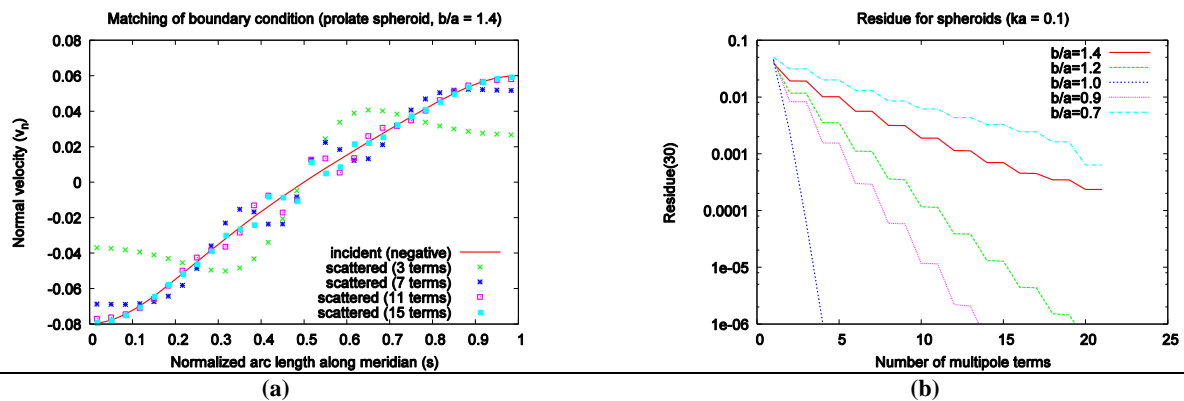


Fig. 1. (a) Matching of velocity boundary condition on sound-hard surface. The negative of the normal velocity from the incident wave should match the normal velocity from the scattered wave for the total normal velocity to be zero. The deviation is large for a small number of multipole terms used. (b) The RMS residue of the boundary condition taken from 30 sampled points is seen to decrease with the number of multipoles used in the scattered wave.

The acoustic radiation force is calculated by integrating the radiation stresses over the surface of the spheroid. The results for small spheroids ($ka=0.1$) are compared with those given by Marston [5]. Fig 2(a) shows the percentage error against the number of multipoles used. It can be seen that less than 1% error can be achieved with six multipole terms used for the cases of aspect ratio between 0.7 and 1.4. In Fig 2(b), the multipole results (using 10 multipole terms) are compared against a COMSOL finite element model for large sizes of a spheroid (up to $ka=1.3$). The non-dimensional force (Q_{st} , as defined in [5]) obtained by multipole and finite element are close to each other. Marston's results deviate for larger sizes since the formulation, which only includes the monopole and dipoles, is only valid for small spheroids.

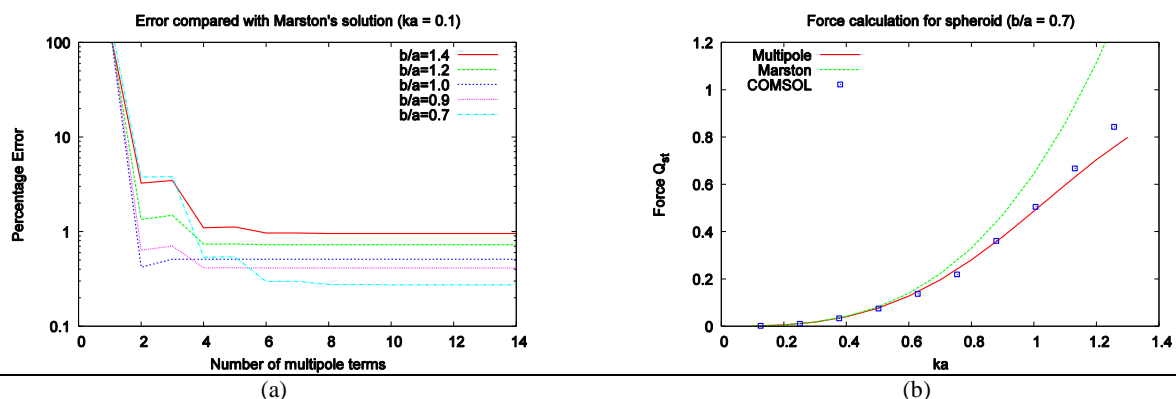


Fig. 2. (a) Comparison of the multipole results for small spheroids with Marston's results. The percentage error decreases to 1% when more than six terms are used. (b) Plot of non-dimensional radiation force Q_{st} [5] against spheroid size. Results from finite element (COMSOL) and multipole are close to each other.

Conclusion

The multipole expansion method with spherical harmonics is shown to give good approximation for acoustic radiation force on spheroids with low eccentricity. The use of more multipole terms helps to decrease the residue and error. In view of the non-convergence within the Brillouin sphere, inclusion of more singular sources (multiple multipole method, generalized multipole techniques) or a more general numerical scheme, such as the boundary element method, should be used for shapes with high eccentricity.

References

- [1] L. V. King (1934) "On the acoustic radiation pressure on spheres" Proc. Royal Soc. of London A, Vol. 147, pp 212-240.
- [2] K. Yosioka, Y. Kawasima (1955) "Radiation pressure on spheres" Acustica, Vol. 5, pp 167-173.
- [3] D. Dechambre, D.J. Scheeres (2002) "Transformation of spherical harmonic coefficients to ellipsoidal harmonic coefficients" Astronomy & Astrophysics, Vol. 387, pp. 1114-1122.
- [4] M. Hasheminejad, R. Sanaei (2007) "Acoustic radiation force and torque on a solid elliptic cylinder" J. Comp Acoustics, Vol. 15, pp. 377-399.
- [5] P. L. Marston, W. Wei, D. B. Thiessen, (2006) "Acoustic radiation force on elliptical cylinders and spheroidal objects in low frequency standing wave", AIP Conf. Proc. 838, 495.



Numerical simulation of acoustophoresis for particles of arbitrary shape, size and structure

Philipp Hahn, Thierry Baasch and Jurg Dual

Institute of Mechanical Systems
Dept. of Mechanical and Process Eng.
ETH Zurich
CH-8092 Zurich, Switzerland
hahnp@ethz.ch

Introduction

Acoustic standing wave fields can be used to move particles within acoustofluidic devices. Most of the important variables like the time-harmonic pressure field, the radiation forces on particles inside the acoustic field or the time-averaged fluid streaming cannot be observed directly. If an experimental setup is to be analysed in detail, this is a major problem because most of the important information remains hidden. Numerical tools for the calculation of the particle motion are very valuable since they provide access to all hidden variables. Furthermore, they can be validated or tuned by comparison with the particle motion which is easily observed experimentally. There are a number of solutions in the literature that simulate the particle traces under the effect of the inviscid radiation forces and the Stokes drag [1] as well as a solution that includes a viscous correction for the radiation forces and a detailed streaming model [2]. In contrast to these existing models for small, homogeneous, spherical particles, we present a numerical model for particles of arbitrary geometry and structure. It involves the calculation of the inviscid acoustic forces as well as a model for the particle dynamics inside the fluid. Though not implemented in the current work, we describe how acoustic streaming can be incorporated in the simulation setup.

Method

Figure 1 shows the structure of the presented simulation setup. Depicted in the upper two boxes are

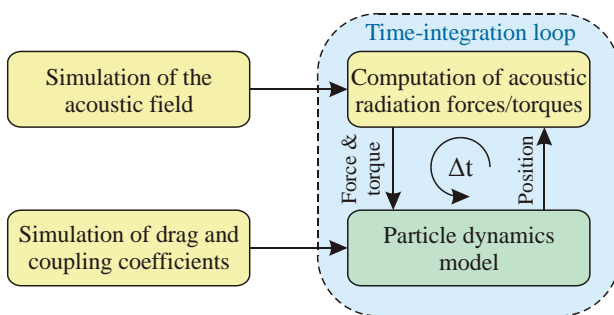


Fig. 1. Structure of the numerical setup for the simulation of acoustophoretic particle motion. In a first step, the time-harmonic acoustic field inside an acoustofluidic device is simulated or prescribed analytically. The acoustic field is used inside the time-integration loop to simulate the time-averaged acoustic forces and torques on the particle. These are necessary to determine the instantaneous particle velocity which is then used to update the particle position within the acoustic field. Prior to the simulation of the particle motion, the drag and coupling coefficients need to be determined with a fluid-dynamic simulation. The yellow boxes represent Finite Element simulation done in Comsol while the rest of the numerical calculations are done in Matlab.

the simulation steps that concern the acoustic radiation forces and torques on the arbitrarily shaped particle. Assuming a small fraction of particles inside the fluid chamber of an acoustofluidic device, the acoustic field is only affected in the vicinity of the particles due to scattering but the global field remains almost unchanged. This is why the time-harmonic field inside the acoustofluidic device has to be calculated only once without the presence of particles. This modelling step involves the piezoelectric transducer, the structural parts of the device, the acoustic field inside the fluid chamber as well as the mutual coupling between them. Subsequently, the obtained time-harmonic pressure serves as a background field in a scattering simulation to determine the inviscid radiation forces and torques on a particle. In contrast to analytical approaches, there are no restrictions on the particle shape, structure or size [3]. Particle-particle or particle-wall interaction is incorporated easily through a second particle or reflecting boundary conditions in the scattering simulation. Besides the

zero-viscosity assumption in the simulation of the radiation forces, we assume that all inertial effects can be neglected for the time-averaged fluid and particle dynamics. The conditions that have to hold are found using dimensional analysis. In the Stokes flow regime, there is a linear relation between the velocity of a particle and the drag forces and torques. This is exploited to determine resistance and coupling coefficients that are specific to each particle geometry [4]. As depicted in the lower left box of Fig. 1, they can be found with six separate simulations of the creeping flow around the particle, corresponding to the Cartesian translations and rotations. With given acoustic radiation forces and torques at the current particle location and the known drag and coupling coefficients for the specific particle geometry, the particle velocity is calculated. A simple time integration scheme allows to update the particle position and to calculate the updated acoustic forces which are used to determine the updated particle velocity and so forth. Caution must be taken to choose the time increments small enough, so that the radiation forces change only slightly over one integration step. In a typical acoustofluidic micro chamber, streaming is primarily due to the viscous boundary layer at fluid-solid interfaces such as chamber walls or particle surfaces. Strictly speaking, this means that the particles need to be incorporated in the calculation of the time-averaged fluid motion. However, in some situations, the streaming field may be regarded as independent on the particle position. In this case, the streaming field has to be computed only once and can be used throughout the particle-trace simulation as a background fluid motion. This changes the particle-fluid relative velocity which can be easily integrated in the simulation.

Example

As an illustrative example, the rotation of a fibre in a time-dependent acoustic field is simulated [5]. The radiation forces tend to align the fibre (angle β) with the lines of zero pressure in the acoustic field (angle α) (see Fig. 2). Amplitude modulation is used to rotate the line of zero pressure. The fibre follows the rotation but it lags behind due to the fluid dynamic resistance. The simulation of one fibre trajectory took 6 hours on a desktop PC. Comparison of the simulated and experimental rotation rates allows to estimate the time-harmonic pressure amplitudes to be around 1.2×10^5 Pa.

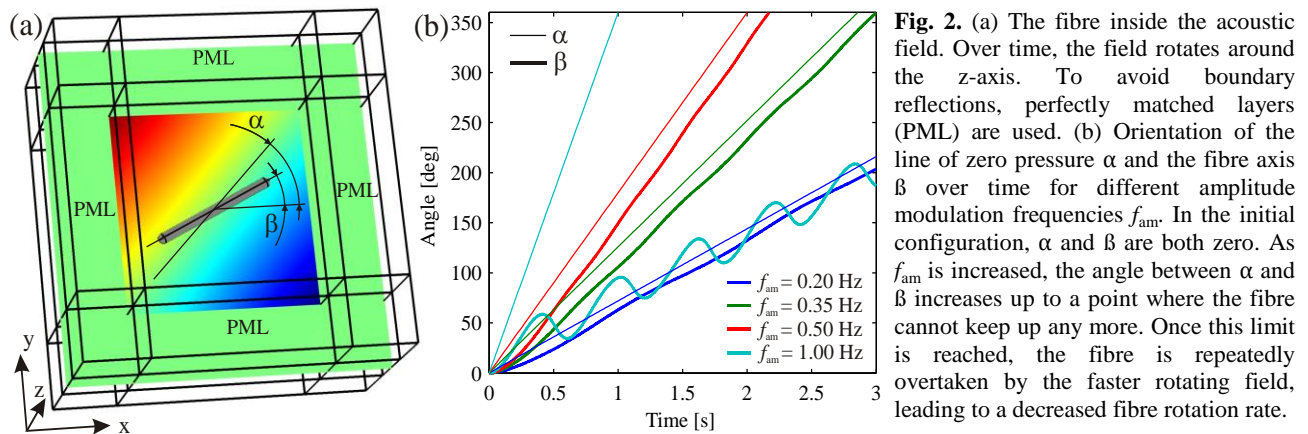


Fig. 2. (a) The fibre inside the acoustic field. Over time, the field rotates around the z-axis. To avoid boundary reflections, perfectly matched layers (PML) are used. (b) Orientation of the line of zero pressure α and the fibre axis β over time for different amplitude modulation frequencies f_{am} . In the initial configuration, α and β are both zero. As f_{am} is increased, the angle between α and β increases up to a point where the fibre cannot keep up any more. Once this limit is reached, the fibre is repeatedly overtaken by the faster rotating field, leading to a decreased fibre rotation rate.

Conclusion

We have implemented a numerical setup for the simulation of acoustophoretic particle motion. It consists of a model for the calculation of the inviscid radiation forces and a model for the particle dynamics inside a Stokes flow. In contrast to other reported solutions, our setup can handle particles of arbitrary geometry and structure in 3D, it works with arbitrary acoustic fields, it covers particle translation as well as rotation and it is numerically efficient. If a particle interacts with a wall or another particle, the fluid dynamic resistance coefficients begin to depend on the particle position. This is not reflected accurately in the current setup and represents an area of future work.

References

- [1] R.J. Townsend, M. Hill, N.R. Harris, N.M. White, *Ultrasonics* **42**, 319-324 (2004), DOI: 10.1016/j.ultras.2004.01.025.
- [2] P. Barkholt Muller, R. Barnkob, M. J. Herring Jensen, H. Bruus, *Lab Chip* **12**, 4617-4627 (2012), DOI: 10.1039/C2LC40612H.
- [3] J. Dual, P. Hahn, I. Leibacher, D. Möller, T. Schwarz, J. Wang, *Lab Chip* **12**, 4010-4021 (2012), DOI: 10.1039/C2LC40733G.
- [4] O. Gonzalez, A. Graf and J. Maddocks, *J. Fluid Mech.* **519**, 133-160 (2004), DOI: 10.1017/S002211200400128.
- [5] T. Schwarz, G. Petit-Pierre and J. Dual, *J. Acoust. Soc. Am.* **133**, 1260-1268 (2013), DOI: 10.1121/1.4776209.

Underlying physics of the emergence of negative radiation forces on spheres illuminated by zero-order Bessel beams

Mahdi Azarpeyvand

Engineering Department, University of Cambridge,
Cambridge, CB2 1PZ, UK.

Email: ma559@cam.ac.uk

Introduction

Understanding the mechanisms through which acoustic fields move objects in the direction of the wave propagation, or congregate particles at local intensity-maxima is relatively straightforward using the conventional radiation force theory. However, using a single gradientless symmetric acoustic beam to produce negative axial radiation forces on a particle placed on the beam axis is counter-intuitive and its underlying physics is not yet

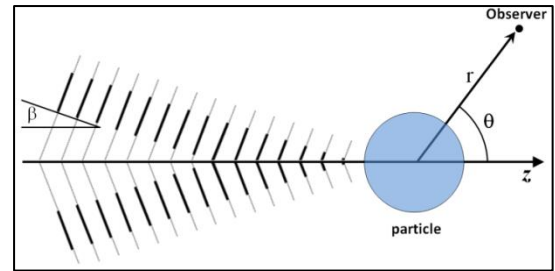


Figure 1- Interaction of a zero-order Bessel beam with a spherical particle.

fully understood, see Fig. 1. In the case of a zero-order Bessel beam (symmetric and non-diffractive), for instance, numerical studies have shown that the radiation force on rigid/soft particles is always repulsive, while that for acoustically penetrable objects may become negative under specific conditions. Unlike high-order Bessel beams, an ordinary Bessel beam does not carry an orbital momentum and has no on-axis phase singularity. Therefore, the emergence of negative radiation forces (NRF) using an ordinary Bessel beam must somehow be related to the structural dynamic of the object. The only NRF prediction tool proposed so far is that of Marston's [1], in which the emergence of NRFs have been related to the suppression of the scattering into the backward hemisphere relative to the scattering into the forward hemisphere. In this work, we shall further study the emergence of NRFs due to symmetric zero-order Bessel beams and will show that NRFs on drops and solid elastic spheres occur only at some specific Rayleigh and Whispering-Gallery modes of the object.

Mathematical modelling and results

The incident zero-order Bessel beam can be defined as [1, 2]

$$\phi^{(inc)}(R, z, \varphi) = \phi_0 J_0(\mu R) e^{i\gamma z - i\omega t},$$

where ϕ_0 is the real-valued incident field amplitude constant, $\gamma = k \cos \beta$ and $\mu = k \sin \beta$ are, respectively, the transverse and longitudinal wavenumbers of the incident field, β is the beam conical angle, $k = \omega/c_f$, and $J_0(\cdot)$ is the Bessel function of order zero. The experienced time-averaged acoustic radiation force on a sphere due to a ZOBBS can be expressed as $Y_p(ka, \beta) = -4(ka)^{-2} \sum_{v=0}^{\infty} Y_{p,v}$, where the v -th modal contribution term ($Y_{p,v}$) are given by [1, 2]

$$Y_{p,v} = (v + 1)[\alpha_v + \alpha_{v+1} + 2(\alpha_v \alpha_{v+1} + \beta_v \beta_{v+1})]P_v(\cos \beta)P_{v+1}(\cos \beta).$$

To better understand the structural behavior of the object, one also needs to find the eignefrequencies (Rayleigh, Whispering-Gallery and Franz modes), which can be readily done by calculating the backscattered form-function over two-dimensional complex plane of ka . The complex eigenfrequencies can be defined by $X_{v,l} = \alpha_{v,l} - \frac{1}{2}i\Gamma_{v,l}$, with $v = 0,1,2, \dots$ (fundamental frequencies) and $l = 1,2,3, \dots$ (overtones) and the quantity $(\Gamma_{v,l})^{-1}$ is a measure of the lifetime and the bandwidth of the resonance.

The acoustic radiation force and complex eigenfrequencies have been calculated for a wide range of liquid and solid elastic cases with different mechanical properties. The inspection of the modal radiation force contributions ($Y_{p,v}$) and the corresponding eigenfrequencies of the particle ($X_{v,l}$) has shown that the dominant NRF islands occur at the Rayleigh modes of the particle. In the case of liquid drops, it has been found that the most dominant NRFs occur at the first or second Rayleigh modes (R_{01} and R_{11}). In the case of solid elastic spheres, on the other hand, NRFs occur at the R_{21} mode (spheroidal) or higher-order Rayleigh modes of the particle; see Fig. 2. Results have also shown that the Whispering-Gallery modes can cause high-frequency NRFs. The exact location and the frequency extent of the NRF islands and the significance of each mode can also be explained using the structural properties of the particle (liquid or elastic). It is worth mentioning that the back-scattered form-function at the R_{21} frequency shows a significant dip, as per Marston [1]. The spheroidal R_{21} mode has the lowest frequency for a free elastic sphere and the formation of a strong dip in the back-scattering form-function spectrum at this frequency is a well-studied matter. However, this for higher-order modes is less obvious in the form-function spectra. Thus, using the above criterion, one can readily predict the location the NRF islands of any particle using its structural properties.

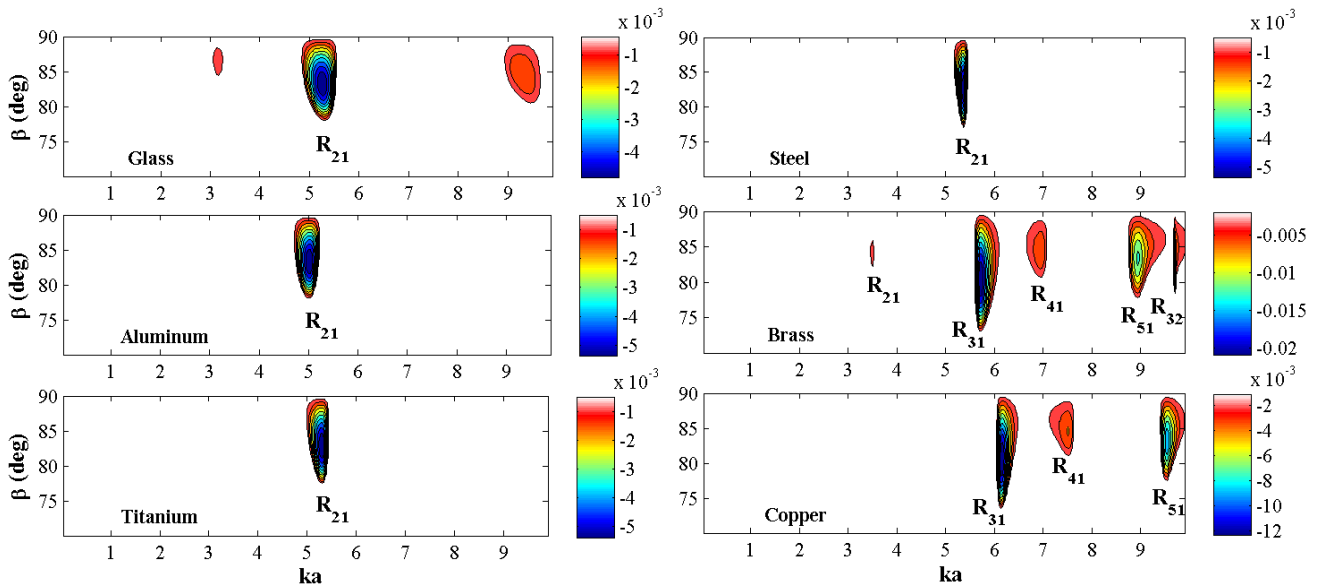


Figure 2- Negative radiation force islands for elastic spheres in water and the corresponding Rayleigh and Whispering Gallery resonance modes

Reference

- 1) P.L. Marston, "Axial radiation force of a Bessel beam on a sphere and direction reversal of the force," J. Acoust. Soc. Am. **120**, 3518–3524 (2006).
- 2) M. Azarpeyvand, "Acoustic radiation force of a Bessel beam on a porous sphere." J. Acoust. Soc. Am. **131**, 4337-4348 (2012).



Cold water cleaning using acoustofluidics

T. G. Leighton¹, P. R. Birkin², D. G. Offen²

¹ISVR, Faculty of Engineering and the Environment, University of Southampton, Highfield, Southampton SO17 1 BJ, UK

²School of Chemistry, University of Southampton, Highfield, Southampton SO17 1 BJ, UK

Traditional ultrasonic cleaning baths are limited in that they cannot clean objects that are too large to fit in the bath, and cannot be taken to objects with complex geometries in order to ‘clean in place’. Furthermore the object to be cleaned sits in a ‘soup’ of contaminated liquid, and whilst cavitation fields can be set up under test conditions, immersion of the object to be cleaned can significantly degrade the bath’s performance by disrupting the sound field. An alternative technique, which does not use ultrasound is the commercial pressure- or –power washer, where high speed jets of water and cleaning agent are pumped onto a surface. Although these can ‘clean in place’, they pump large volumes of water, and produce significant volumes of contaminated run-off and contaminated aerosol, both of which are hazards for secondary contamination of users and water supplies. The momentum of the water and pump requirements mean they are difficult to scale up. This paper presents a low volume flow technique for ultrasonic cleaning in place, benefits being that it operates with low flow rates (1-2 litres per minute), and there is no need to expend energy on heating the water.

Impedance matched channel walls in acoustofluidic systems

Ivo Leibacher¹, Sebastian Schatzer¹, and Jürg Dual¹

¹Institute of Mechanical Systems
Department of Mechanical and Process
Engineering
Swiss Federal Institute of Technology ETH Zurich
CH-8092 Zurich, Switzerland
Email: leibacher@imes.mavt.ethz.ch
URL: www.zfm.ethz.ch

Introduction

In conventional bulk acoustophoresis devices [1], cell-sized particles within a water channel are attracted to the pressure nodal lines of an ultrasonic standing wave in x -direction. Hereby the channel walls have to fulfill two tasks: First, they are the fluidic boundary. Second, they act as an acoustic reflector for the generation of the acoustic standing wave. This double assignment limits the feasible pressure fields within the acoustic domain. With novel devices as proposed in this paper, we can overcome these limitations by an additional acoustic layer.

Experiment outline

As illustrated in Fig. 1, we introduce an additional acoustic layer made of polydimethylsiloxane (PDMS) within a microfluidic channel. The characteristic acoustic impedance of PDMS is very similar to the suspending fluid. Therefore it allows to decouple the two wall tasks: the PDMS-water interface is the fluidic boundary, whereas the silicon walls remain the acoustic reflectors, as marked in Fig. 1. This allows to generate unprecedented arbitrary pressure fields within the water channel.

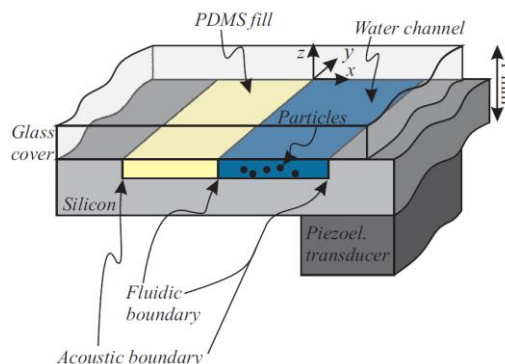


Fig. 1. Sketch of a microfluidic device. A microfluidic channel in y -direction is partially filled with water and a PDMS fill. Regarding the pressure field within the water channel, the PDMS fill gives an additional degree of freedom for acoustophoresis on the suspended particles.

Our design allows for example the movement of particles towards a wall, which is of significant biotechnological relevance for e. g. sensors or particle concentration as highlighted by Wiklund et al. [2]. This is a very delicate task as described by the latter review paper. Existing methods to attract particles on a wall (such as quarter-wavelength resonators [3]) are experimentally challenging, which has encouraged the search for more robust alternatives. Our method differs conceptually from all previous work and results in stable, strong and reproducible attraction of particles towards a channel wall.

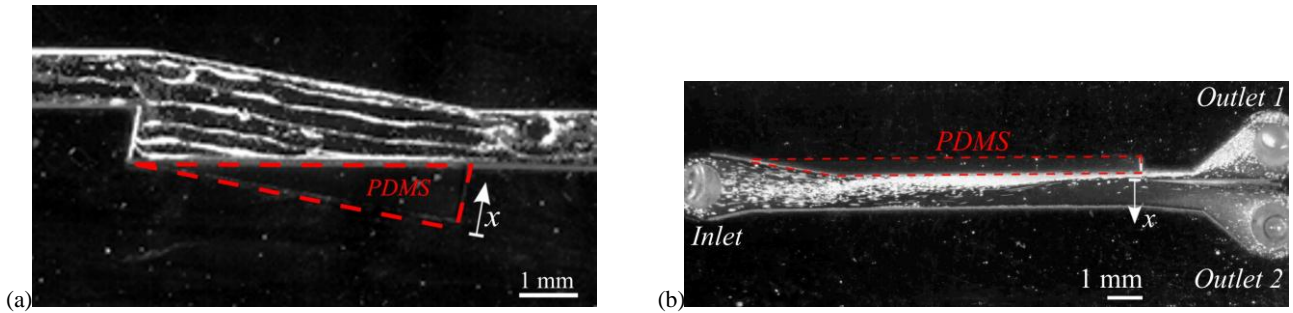


Fig. 3. (a) Proof of concept of a device with a triangular PDMS layer. 6 parallel lines show the pressure nodal lines of an ultrasonic standing wave in x -direction. (b) Application of PDMS boundaries for particle concentration in a flow-through experiment. A concentrated particle flow leaves through outlet 1.

Results

The experimental results are documented in Fig. 3. Fig. 3(a) is a proof of concept on the example of a rectangular microfluidic chamber (depth $150\ \mu\text{m}$), where a triangle on the lower right is filled with PDMS. The $17\ \mu\text{m}$ particles suspended in isopropanol aligned on 6 parallel lines at an excitation of $1.574\ \text{MHz}$, which is the same behavior as without the PDMS layer. This result shows that a suitable acoustic field could be generated even though the PDMS layer might add damping to the system. Fig. 3(b) shows an application of PDMS boundaries for particle concentration in a flow-through experiment with a $\lambda/2$ mode as plotted in Fig. 4(a). The microchannel has a total width of $1.5\ \text{mm}$ in x -direction and a depth of $150\ \mu\text{m}$. The upper $0.5\ \text{mm}$ are filled with PDMS. In the lower $1\ \text{mm}$, water flows to the right with suspended $25\ \mu\text{m}$ particles. The PDMS boundary allows to focus particles on the fluidic channel wall in a $\lambda/2$ mode at $467\ \text{kHz}$, so a concentrated particle flow leaves the device through outlet 1. Fig. 5(b) gives the calculated result for an advanced configuration with two PDMS walls, such that the particles can be focused on either the left or the right channel wall depending on the applied frequency.

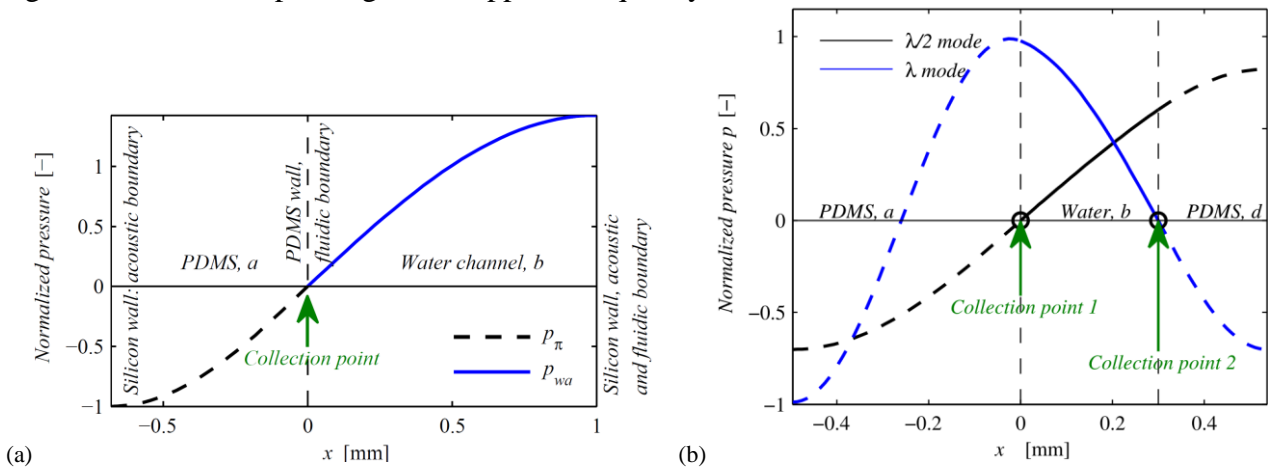


Fig. 5. (a) Pressure plot in a microfluidic PDMS/water channel with a standing wave in the $\lambda/2$ mode (first eigenmode). (b) Pressure plot of the first and second eigenmodes in a PDMS/water/PDMS channel. The collection points of the particles can be placed at the left and right channel wall.

Conclusion

The microdevices at hand demonstrate impedance matched channel walls by a layer of PDMS. Impedance matched channel walls allow to build acoustophoretic microdevices with much more freedom in the design of the particle manipulation, since the fluidic and the acoustic boundaries do not have to coincide. This approach offers potential for biotechnological applications such as particle concentration and separation as well as enhanced particle sensors.

References

- [1] A. Lenshof, M. Evander, T. Laurell, and J. Nilsson, *Acoustofluidics 5: Building microfluidic acoustic resonators*, Lab Chip, **12**, 684 (2012).
- [2] M. Wiklund, S. Radel, and J. J. Hawkes, *Acoustofluidics 21: ultrasound-enhanced immunoassays and particle sensors*, Lab Chip, **12**, 4667 (2012).
- [3] P. Glynne-Jones, R. J. Boltryk, and M. Hill, *Acoustofluidics 9: Modelling and applications of planar resonant devices for acoustic particle manipulation*, Lab Chip, **12**, 1417 (2012).



Acoustic trapping used for bead incubation in a Luminex-based multiplex biomarker assay

Maria Tenje¹, Hongyan Xia^{2,3}, Mikael Evander¹, Björn Hammarström¹, Axel Tojo¹, Sándor Belák^{2,3,4}, Thomas Laurell^{1,5} and Neil LeBlanc^{3,4}

¹Division of Nanobiotechnology
Department of Electrical Measurements
Lund University
S-221 00 Lund, Sweden
Email: Maria.Tenje@elmat.lth.se

²Department of Biomedical Sciences and
Veterinary Public Health (BVF),
Swedish University of Agricultural Sciences
S-750 07 Uppsala, Sweden

³The World Organization for Animal
Health (OIE) Collaborating Centre for
the Biotechnology-based Diagnosis of
Infectious Diseases in Veterinary
Medicine
Uppsala, Sweden

⁴Department of Virology, Immunobiology
and Parasitology
The National Veterinary Institute (SVA)
S-751 89, Uppsala, Sweden

⁵ Department of Biomedical Engineering
Dongguk University
Seoul, 100-715 Korea

Introduction

Bead-based assays are commonly used within veterinary and medical diagnostics [1, 2]. This work presents the transfer of a commercial bead-based assay onto a microfluidic platform, with several gained benefits. The Luminex assay detects antibodies to four different viruses: Infectious Bursal Disease Virus (IBDV), Infectious Bronchitis Virus (IBV), Newcastle Disease Virus (NDV) and Avian Reovirus (REO) in poultry sera. The assay uses magnetic beads internally dyed with a red/infrared mixture. An acoustic trap is used to maintain the beads stationary in a microfluidic channel during the fluid exchanges in the assay protocol. Subsequently, the bead cluster is released directly into a 96-well-plate from the microchannel for analysis in a Luminex instrument. Our results show that the bead recovery can be significantly improved in the acoustic trap format. Furthermore, the assay time can be reduced by 50% without reducing assay performance.

Experiment

A rectangular glass capillary (Vitrotubes, VitroCom) is used as the microfluidic channel in this set-up [3]. The capillary is mounted on top of a 0.8 mm wide transducer (PZ26, Meggitt A/S) actuated at 4 MHz. Figure 1 shows the set-up.

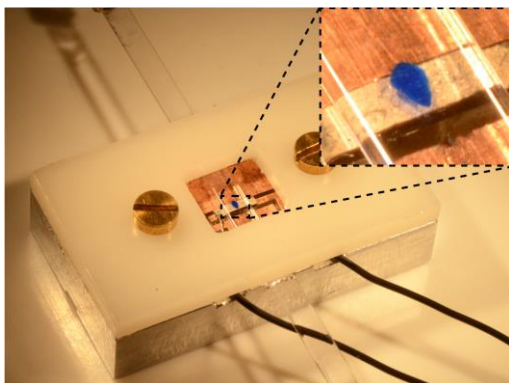


Fig. 1. The transducer is soldered onto a PCB, placed in an aluminium holder. The glass capillary is clamped onto the transducer and held stationary by a lid that is screwed onto the aluminium base. A thin layer of glycerol is placed in-between the transducer and the glass capillary for improved acoustic coupling. Tubing is connected directly onto the ends of the glass capillary.

In the figure, a cluster of blue 10-µm-beads has been trapped for visualisation, as shown in the inset.

Bead recovery is compared for three different protocols; (i) using an automatic wash station, (ii) using manual wash steps and (iii) performing the whole assay in the microfluidic format. The beads are counted with the Luminex instrument.

Seven different serum samples from vaccinated poultry are subjected to the complete assay in triplicate. The results are analysed in a Luminex 200 instrument. ELISA control assays have also been performed.

Results

The bead recovery of the acoustic trap is found to be 75%, which is significantly higher than using an automated wash station. By performing the wash steps manually, it is also possible to obtain a high bead recovery. This is however a significantly slower, labour intensive processed that is more prone to human error.

	Number of beads (n=4)	Recovery
Original solution	6,440 ± 740	
Automatic wash station	2,000 ± 260	31 %
Manual wash	5,120 ± 430	80 %
Acoustic trap	4,860 ± 1,200	75 %

The Luminex readout from the assay is given in S/P ratio, which relates the signal strength of the analyte to the signal strength of a positive control sample. The readout is taken as positive for S/P value ≥ 0.14 , 0.12, 0.20, 0.20 for IBDV, IBV, NDV, and REO respectively. Figure 2(a)–(d) shows the assay readout for all samples and all viruses. Our results show that the assay readout when performing all steps in the microfluidic format correlates well with the control ELISA assay for all samples and all viruses. When performing the assay in the conventional format we do however obtain two false-positive and one false-negative value, as marked with the red arrows in the figure below.

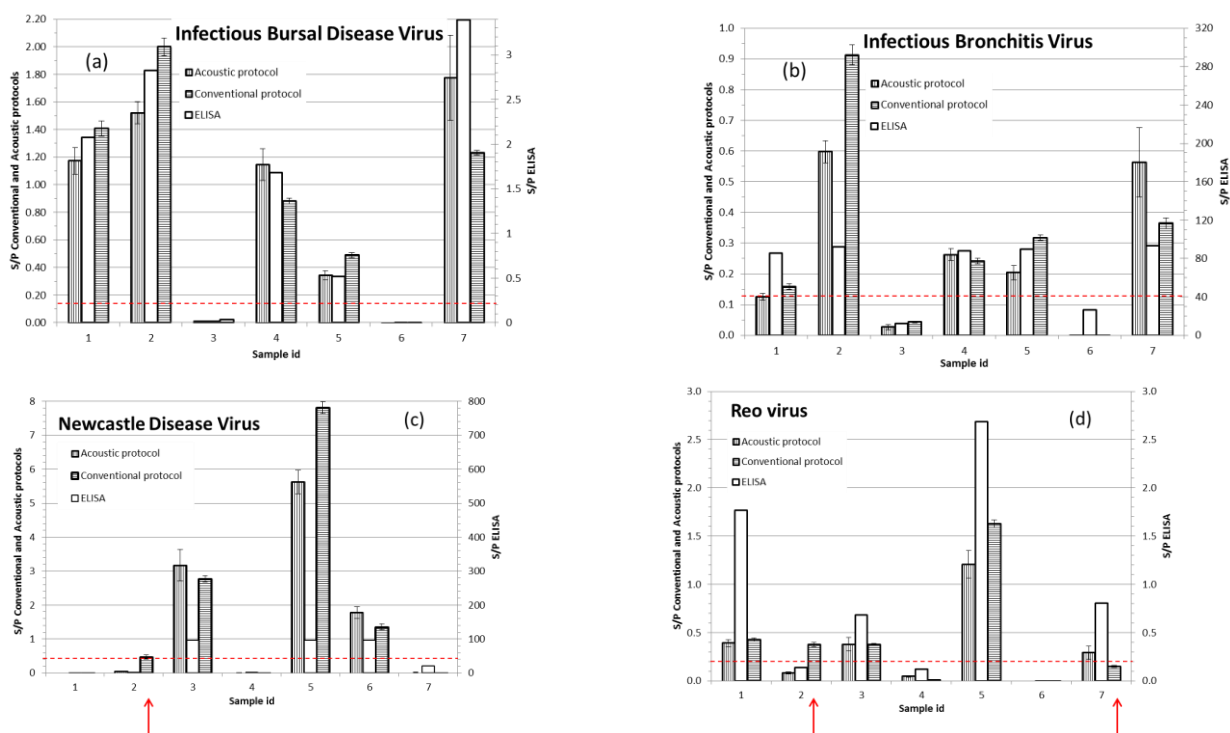


Figure 2(a)–(d) S/P readout from all three different assay methods on the seven poultry serum samples used in this study. The red dotted lines mark the cut-off S/P values. The red arrows mark the three occasions where the conventional assay reported differently than the control ELISA and the acoustic protocol.

Conclusion

We show the complete transfer of a commercial bead-based multiplex assay onto a microfluidic platform utilising acoustic trapping. In this format, we can reduce the assay time by 50% with maintained assay sensitivity. The reported bead recovery is 75%, which is a significant improvement compared with performing the assay in the conventional automated format.

References

- [1] H. Y. Xia *et al.*, *Journal of Virological Methods*, vol. 168, pp. 18–21, Sep 2010.
- [2] M. Wiklund and H. M. Hertz, *Lab Chip*, vol. 6, pp. 1279–92, Oct 2006.
- [3] B. Hammarstrom *et al.*, *Lab Chip*, vol. 10, pp. 2251–7, Sep 7 2010.



Particle attraction to membranes with evanescent standing waves

Jeremy J. Hawkes

Manchester Institute of Biotechnology (MIB)
The University of Manchester
131 Princess Street, Manchester, M1 7DN, UK
Email: J.Hawkes@Manchester.ac.uk
URL: www.uswnet.org/people.htm

Evanescent waves are an interface phenomenon where waves in a solid move into an adjacent fluid and then return to the solid but do not propagate into the fluid. This happens when the wave's velocity in the solid is lower than the velocity in the fluid[1]. In general, wave velocity in solids is higher than in liquids but some geometries (such as membranes and thin plates) reduce the wave velocity in the solid[2] and vibrations from these waves cannot propagate into the fluid. In 2002 Black and White[3] used 3 μm silicon membranes to show that particles could be trapped and manipulated in the nodes of evanescent standing waves (in the same way that particles are held and manipulated in nodes of bulk USW). Two other examples where ultrasound standing waves are used to trap particles at a liquid:solid interface are the movement of particles to a half-wave thickness solid layer (Hawkes *et al.*, Townsend *et al.*)[4, 5] and movement of particles to a thin plastic membrane Glynne Jones *et al.* [6]. In these two examples the trapping of particles at the interface has been explained as an unusual pressure release condition at the walls created in the first case because, the wall is resonating in phase with the fluid and in the second case because, the wall is thin enough not to act as a substantial reflector.

The reason for developing systems which bring particles to a surface is to increase the sensitivity of particle sensors where the sensor is located on a surface.

The experiments to be presented here also use thin membranes (25 and 50 μm polystyrene). The results support the concept of particles moved by evanescent waves. Pressure release walls and evanescent waves need not be incompatible concepts but recently evanescent waves have been a more useful concept for developing novel designs.

The experimental results

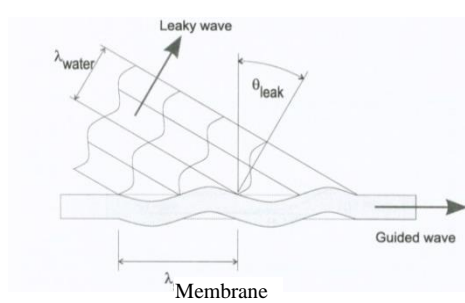
1. Particles always move to the membrane when the membrane is driven. Reliable results are not always obtained when other walls or the fluid is driven.
2. When the fluid layer is thin ($< \frac{1}{2}$ wavelength in water λ_{water}), the particles form a pattern of clumps on the membrane the distance between clumps is $< \frac{1}{2} \lambda_{\text{water}}$. Different patterns with longer clump-clump distances are produced with thicker fluid layers.
3. A membrane under tension increases the reliability of particle movement.

Description of evanescent standing waves with, an interpretation of the experimental results

- A. Surface vibrations and the energy decreases exponentially from the interface. (**1 above:** It is important to ensure that the surface is vibrating and not reliant on undefined coupling).
- B. With $< \frac{1}{2} \lambda$ fluid thickness non-evanescent modes are unlikely to form. (**2 above:** In thick fluid layers evanescent domination falls and particles are drawn to other modes).
- C. The velocity of waves in the fluid is higher than in the solid. (**2 above:** Nodes in the solid layer are closer than nodes in the bulk fluid, clumps form at the nodes of the solid).

APPENDIX Condition for creation of an evanescent standing wave

When a solid with a wave on its surface is in contact with a fluid, waves radiate out (leak) into the fluid at an angle as in fig. 1 where the crests and troughs match in the fluid and the solid waves.



$$\theta_{leak} = \sin^{-1} \left(\frac{\lambda_{fluid}}{\lambda_{solid}} \right) = \sin^{-1} \left(\frac{v_{fluid}}{v_{solid}} \right) \quad \text{Eqn 1}$$

Fig. 1 Taken from [7]. λ = wavelength and v = wave phase velocity.

When the wavelength in the fluid is greater than the solid eqn 1 implies the angle will be imaginary, or more than 90° . In this case the wave is not radiated but instead short circuited back to the solid with no energy lost. This “vanishing or evanescent” wave skims along the surface and does not radiate into the fluid bulk. When there is a standing wave in the flexing surface then the evanescent wave associated with it will also be stationary and particles will be drawn to the nodes.

Construction	Mode phase velocity	Mode shapes : Showing angle of radiation
<div style="background-color: #cccccc; padding: 5px;">Air</div> <div style="background-color: #e0e0e0; padding: 5px;">1 mm polystyrene</div> <div style="background-color: #00bfff; padding: 5px;">Water</div>		<div style="display: flex; justify-content: space-between;"> <div style="width: 45%;"> </div> <div style="width: 45%; text-align: right;"> <p>Air: Leaky wave Water: Leaky wave</p> <p>c</p> </div> </div> <div style="display: flex; justify-content: space-between; margin-top: 10px;"> <div style="width: 45%;"> </div> <div style="width: 45%; text-align: right;"> <p>Air: None Water: Evanescent wave</p> <p>d</p> </div> </div>
<div style="background-color: #cccccc; padding: 5px;">Air</div> <div style="background-color: #e0e0e0; padding: 5px;">50 μm polystyrene</div> <div style="background-color: #00bfff; padding: 5px;">Water</div>		<div style="display: flex; justify-content: space-between;"> <div style="width: 45%;"> </div> <div style="width: 45%; text-align: right;"> <p>Air: Leaky Water: Evanescent wave</p> <p>e</p> </div> </div>

Fig. 2 Modes predicted by Disperse a dispersion curve modelling program. a) and d) Show modes which could be found in 1 mm and 50 μm polystyrene membranes sandwiched between infinite air and water. b), c) and e) 3 modes at 3 MHz. 1 mm and 50 μm polystyrene layers are scaled to the same thickness in these figures. The vibration displacements are normalised and exaggerated.

On a 1 mm polystyrene layer sandwiched between air and water, only A_0 and S_0 are evanescent modes. A carefully designed support structure or the pressure release condition is needed to consistently select only these modes.

On a 50 μm polystyrene membrane sandwiched between air and water only two modes, A_0 and S_0 exist (S_0 is not plotted) both are evanescent in water.

The message here is: Thick polystyrene layers (1 mm) produce evanescent and leaky wave in water, predominantly leaky. Thin polystyrene layers (50 μm) produce only evanescent waves. (True for water but not air, therefore a drum will not work underwater because the wave will be evanescent).

References

- [1] Albrecht Haake, Adrian Neild, Gerald Radziwill, Jurg Dual, *Positioning, Displacement, and Localization of Cells Using Ultrasonic Forces*, Biotech Bioeng (2005) **92** 8-14
- [2] P. Luginbuhl, S.D. Collins, *et al.*, *Microfabricated lamb wave device based on PZTsol-gel thin film for mechanical transport of solid particles and liquids*, J. Microelectromech. Syst. (1997) **6** 337–346.
- [3] J. P. Black, R. M. White and J. W. Grate, *Microsphere capture and perfusion in microchannels using flexural plate wave structures*, Proc. IEEE Ultrason. Symp. (2002) 475–479.
- [4] J.J. Hawkes, M.J. Long, W.T. Coakley and M.B. McDonnell, *Ultrasonic deposition of cells on a surface*, Biosens. Bioelectron., (2004) **19** 1021-1028
- [5] R. J. Townsend, M. Hill, N. R. Harris and M. B. McDonnell, *Performance of a quarter-wavelength particle concentration*, Ultrasonics, (2008) **48** 515–520.
- [6] P. Glynn-Jones, R. J. Boltryk, M. Hill, N. R. Harris and P. Baclet, *Robust acoustic particle manipulation: A thin-reflector design for moving particles to a surface*, JASA Express letts, (2009) **126** EL75-EL79.
- [7] Disperse User’s Manual, version 2.0.11 2001. Brian Pavlakovic and Mike Lowe, Imperial College.



High-speed camera observation of droplet atomization and coagulation in an ultrasonic standing wave field

Marina Reißenweber, Felix Brand, and Gerhard Lindner

Institute of Sensor and Actuator Technology
Coburg University of Applied Sciences and Arts
Am Hofbräuhaus 1b
D-96450 Coburg, Germany
Email: spma1100@stud.hs-coburg.de
URL: www.isat-coburg.de

Introduction

It is well-known, that an acoustic levitator can be used to aggregate small particles slightly below the nodes of a standing pressure field in a gaseous or liquid fluid. Recently there are some efforts to use this effect e.g. for cleaning exhaust gas [1, 2]. While most of the experiments focus on the determination of particle size and shape after acoustic irradiation [3], there are only few publications which describe the coagulation of particles [4].

The observation by a high-speed camera offers the possibility to study the processes phenomenologically but resolved in space and time.

Experiment

For creating an ultrasonic standing wave field in air a sound source and a plane reflecting surface were arranged vertically facing each other in a distance of $3\frac{\lambda}{2}$ so that three pressure nodes can be used for levitation. We have used a conventional ultrasonic processor constructed for homogenizing fluids with a frequency of 24 kHz. The ultrasonic horn reaches a maximal oscillation amplitude of 12 μm , which can be regulated by the input power.

Firstly a water droplet was directly introduced into one node in order to optimize the ultrasonic standing wave field by adjusting the distance and the acoustic intensity [5]. For the experiment we deposited some amount of water on the vibrating surface of the sonotrode, where it begins to atomize as described by [6]. This and the following processes were recorded by a high-speed camera and analysed.

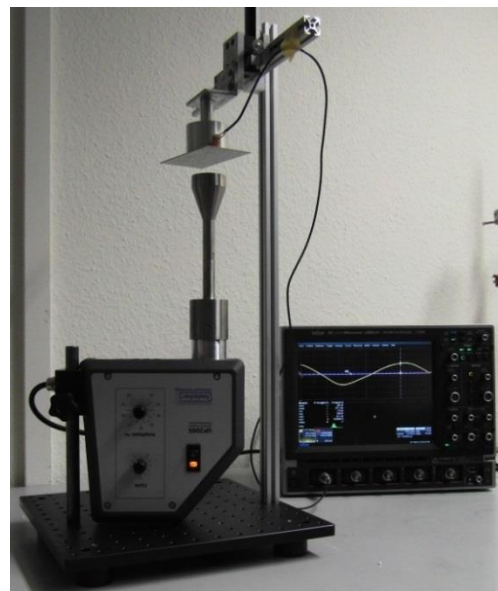


Fig. 1. The experimental set-up: ultrasonic processor with the sonotrode ($\text{Ø} = 40 \text{ mm}$), vertically displaceable plane reflector with a piezo sensor on its top and an oscilloscope for distance controlling.

Results

During the atomization the space above the sonotrode gradually fills with finest spray droplets which are accumulating at the levels of the pressure nodes and forming rotating ellipsoidal clouds there similar to observations by [7]. This happens at first only at the lowest level but in the course of the process the droplets also jump to higher levels. At those levels the droplets inevitably collide

with each other and coagulate to bigger droplets. The outer droplets were pulled to the middle slightly below the pressure node. This process continues until all nebula droplets are collected there in a single big droplet on each level.

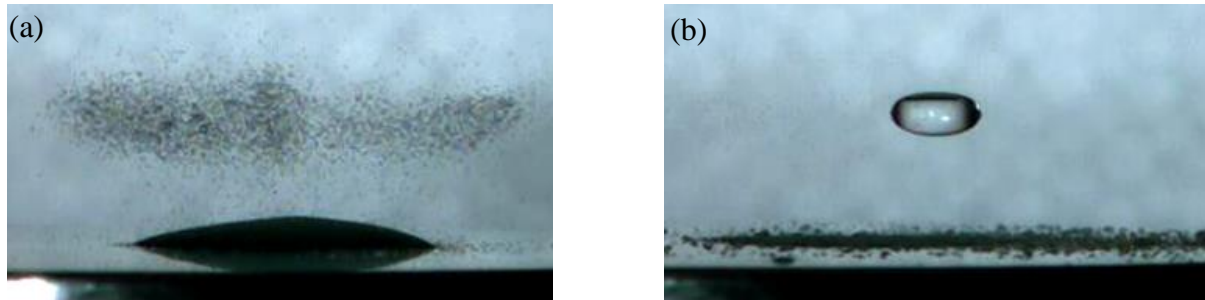


Fig. 2. (a) The water begins to atomize because of the oscillations of the vibrating surface and first spray droplets are arranged at the lowest level. (b) After coagulation processes a droplet of about 3 mm diameter is firmly levitated beneath the pressure node of the ultrasonic standing wave field while there aren't any aerosol particles left in the space above the sonotrode.

Conclusion

In our experiments we observed a complete atomization of a water volume in an ultrasonic standing wave field and a subsequent complete coagulation of all of the nebula droplets into single large levitated droplets near each pressure node. The predominant reason for the observed coagulation is the Bernoulli effect caused by differences in sound velocity. Due to an inhomogeneous but symmetrical radiation characteristic of the ultrasonic horn the axial component of the sound velocity decreases from the central levitation axis to the edge with the result that there exists an underpressure component at the side facing to higher velocities which traps the droplets in the central region of the resonator.

Acknowledgement

This work is part of the young scientist innovative project program of the Institute of Sensor and Actuator Technology and has been supported by TechnologieAllianzOberfranken (TAO). The technical support of Sandro Krempel is gratefully acknowledged.

References

- [1] M. Khair, M. Treuhaft and I. Abdul-Khalek, *Improved diesel particulate filter performance using sonic particle agglomeration*, WO/2007/101246.
- [2] M. Evander and J. Nilsson, *Acoustofluidics 20: Applications in acoustic trapping*, Lab Chip **12** (2012), 4667 – 4676.
- [3] E. Riera-Franco de Sarabia and J. Gallego-Juárez, *Ultrasonic agglomeration of micron aerosols under standing wave conditions*, Journal of Sound and Vibration **3** (1986), 413 – 427.
- [4] E.G. Lierke, *Acoustic Levitation – a comprehensive survey of principles and application*, Acustica **2** (1996), 220 – 237.
- [5] W. Shi and R. Apfel, *Deformation and position of acoustically levitated liquid drops*, J. Acoust. Soc. Am. **4** (1996), 1977-1984.
- [6] P. Deepu, S. Saptarshi, A. Abhishek and R. Kumar, *Spreading and atomization of droplets on a vibrating surface in a standing pressure field*, Applied Physics Letters **14** (2012), 143108.
- [7] R. Tuckermann, B. Neidhart, E.G. Lierke and S. Bauerecker, *Trapping of heavy gases in stationary ultrasonic fields*, Chemical Physics Letters **363** (2002), 349 – 354.



Live Cell Imaging in a Micro-Array of Acoustic Traps Facilitate Quantification of Natural Killer Cell Heterogeneity

A.E. Christakou¹, M. Ohlin¹, B. Vanherberghen¹, M.A.Khorshidi¹, N. Kadri², T. Frisk¹, M. Wiklund¹ and B. Önfelt^{1,2}

¹Department of Applied Physics
Albanova University Center
KTH - Royal Institute of Technology,
SE-10691, Stockholm, Sweden
Email: athachris@kth.se

²Department of Microbiology, Tumor and Cell Biology
Nobels Väg 16, 17177, Karolinska Institute
Stockholm, Sweden

Introduction

Our multi-well microdevice for ultrasonic manipulation of living cells in a single cell level, was first presented on USWNet 2009 and was published in *Lab On a Chip* on 2010 [1]. In this paper we present the most recent published work with experiments performed entirely on living cells. We investigate and characterize the Natural Killer Cells killing function against cancer cells. We quantify the trapping performance of the system for different cell types (adherent and non-adherent) for different actuation voltages (0 – 10 V_{pp}), in order to confirm that the acoustic forces are in the same range as natural biological forces. We have been able for the first time to quantitatively characterize the cytotoxic heterogeneity of NK cells against cancer cells.

Experiments

The microchip is square (22×22 mm²) with 10×10 centrally positioned square wells covering an area of 3.9×3.9 mm² (each well with a 300×300 μm² bottom area separated by 100 μm walls). The gasket is polydimethylsiloxane (PDMS) and is plasma-bonded to the silicon surface creating a 50 μl basin above the microwells. The silicon chip is glued into the metal holder and the wedge transducer on the chip with a thin layer of conductive adhesive gel (see fig1). Ultrasonic actuation was performed by cycling linear frequency sweeps (saw-tooth modulation) with center frequency 2.54 MHz, bandwidth 120 kHz, modulation rate 1 kHz and actuation voltage between 0 and 10 V_{pp}. In experiments not examining the voltage dependence, the actuation voltage was 10 V_{pp}.

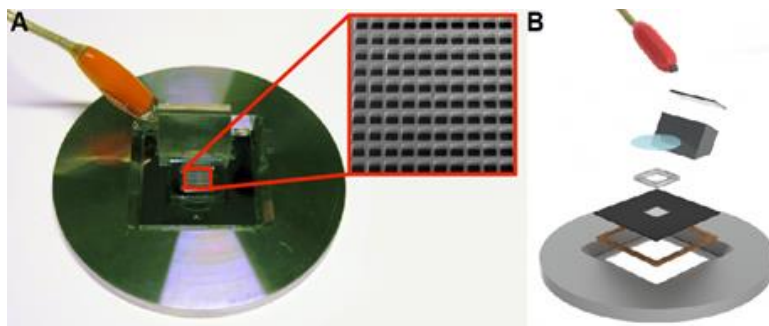


Figure 1: (A) Photo of the sono-cage platform, and a SEM picture of the array of microwells. (B) Schematic illustration of the different parts of the device (described in Ref. 1 and 2).

The cell lines used in order to investigate the trapping efficiency of our system at different actuation voltages were the 721.221 non-adherent cell line and the HEK 293T adherent cell line. 293T cells were stained and seeded in the chip together with 221 (unstained). They were allowed to settle and adhere for about one hour before imaging. For the cytotoxic experiments, as effector cells we have used primary polyclonal human NK cells that were harvested from blood of healthy donors by centrifugation and separation of peripheral blood mononuclear cells followed by negative magnetic bead sorting. NK cells were cultured for 7 days in growth medium with the IL-2 activating factor.

Results

The acquired data indicate that already at low voltage ($<2 V_{pp}$), the majority of non-adherent 221 cells aggregated to a central position, with a plateau of about 90% cells aggregated at voltages $>3 V_{pp}$. In contrast, even at higher voltages the majority of non-adherent cells were not aggregated, showing that the force of adhesion to the glass was stronger than the aggregation force delivered by the ultrasound (Figure 2)

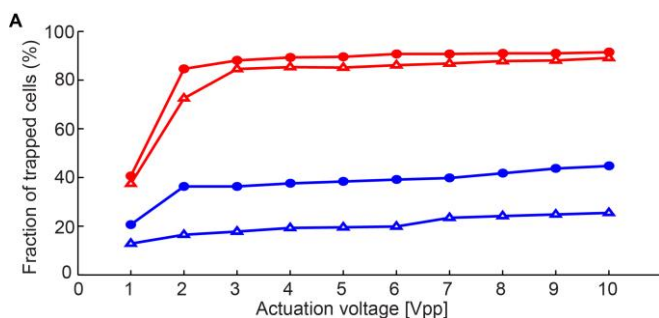


Figure 2. Adherent and non-adherent cells show different trapping efficiencies under ultrasonic actuation. (a) Percent trapped adherent (blue lines) and non-adherent (red lines) cells for different actuation voltages. Two sets of experiments were performed with a mixture of adherent 293T cells ($n=279$, triangles and 255, circles) and non-adherent 221 cells ($n=412$, triangles and 433, circles).

Furthermore, cytotoxic single-cell experiments were performed where NKs and targets were stained, seeded in the chip, and then imaged over 4 hours during continuous ultrasonic actuation. The distribution of NKs and targets is shown in Fig. 3A (pooled data from four experiments). Analysis of the data revealed a significant heterogeneity in NK killing efficiency. Surprisingly, 36% of the NK cells were completely inactive over 4 hours (Fig.3B). The remaining 64% were active (*i.e.*, killing at least one target), but few NK cells were shown to be ‘serial killers’ eliminating up to six targets [2].

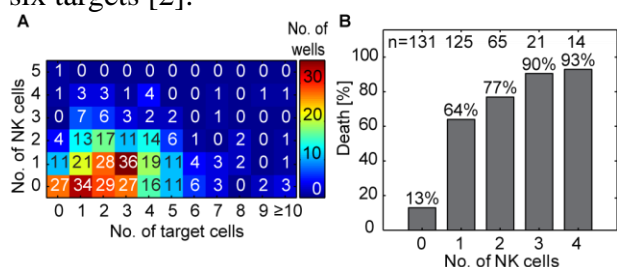


Figure 3. Target cell death increases with the number of NK cells per well. (A) Distribution of NK cells and 221 target cells in 400 wells studied (summarized data of four experiments). (B) Frequency of wells where target cell death was detected plotted versus the number of NK cells per well.

Conclusion

We have investigated our multi-well device in terms of trapping efficiency and we can conclude that the acoustic forces acting on cells are in the range of cell-cell interaction forces. Using our method we have shown that there is a significant heterogeneity among a NK cell population in terms of cytotoxicity against cancer cells. Furthermore, we observe that NK cells kill more efficiently when the target cell number increases from one to three targets (data not shown) [2].

References

- [1] Vanherberghen, B. et al. Ultrasound-controlled cell aggregation in a multi-well chip. *Lab Chip* 10, 2727-2732 (2010).
- [2] A. E. Christakou, M. Ohlin, B. Vanherberghen, M. A. Khorshidi, N. Kadri, T. Frisk, M. Wiklund, and B. Onfelt, "Live cell imaging in a micro-array of acoustic traps facilitates quantification of natural killer cell heterogeneity," *Integr Biol (Camb)*, vol. 5, pp. 712-9, Apr 2013.



Application of a novel perfusion bioreactor with integrated ultrasound standing wave trap for augmentation of cartilage tissue engineering

S Li¹, P Glynne-Jones²,
M Hill², R O C Oreffo¹, and R S Tare¹

¹Bone and Joint Research Group
Faculty of Medicine
University of Southampton
Institute of Development Sciences Building
Southampton General Hospital
Tremona Road, Southampton, SO16 6YD, U.K.
Email: Siwei.Li@soton.ac.uk

²Engineering Sciences Unit
Faculty of Engineering & the Environment
University of Southampton
Highfield, Southampton, SO17 1BJ, U.K.
Email: P.Glynne-Jones@soton.ac.uk

Introduction

In the absence of effective pharmacological agents and limited success of surgical interventions to treat cartilage defects, application of tissue engineered cartilage grafts is a promising approach to address the problem of cartilage regeneration. However, cartilage grafts generated using conventional tissue engineering strategies are typically characterised by suboptimal cell viability, cartilage formation and mechanical competency, limiting their application in cartilage repair. Ultrasound standing wave trap (USWT), a relatively less exploited non-destructive cell manipulation technique, is capable of spatially organising cells into levitating 3-D agglomerates. Moreover, stimulation by ultrasound of bovine chondrocytes in 2-D and 3-D cultures in bioreactors is shown to enhance cell proliferation, viability and expression of chondrogenic genes [1,2]. This presents an exciting opportunity to extend the application of ultrasound to augment conventional cartilage bioengineering strategies.

Aim

By utilising a unique multidisciplinary approach, the study aims to bioengineer 3-D scaffold-free neocartilage grafts of human articular chondrocytes (HACs) in custom-built perfusion bioreactors with integrated ultrasound standing wave trap (USWT) to create a dynamic environment conducive for optimal cartilage formation.

Experiment

The custom-built USWT bioreactor employed a piezoelectric transducer that was fitted on an etched glass capillary (Figure 1).

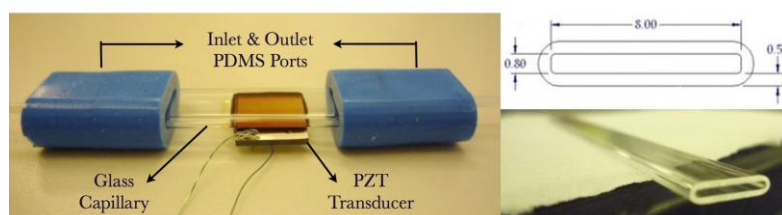


Figure 1. Design of perfusion bioreactor with integrated USWT.

HACs (1×10^6 cells) were introduced into the bioreactors to promote rapid formation of levitating 3-D agglomerates by ultrasonic force fields. The bioreactors were maintained at 37°C in humidified atmosphere and the agglomerates were cultured in chondroinductive media perfused continuously for 21 days. Day 21 explants [~ 2 mm (diameter) \times ~ 0.15 mm (thickness)] were analysed for cell viability, cartilage formation, expression of cartilage-specific proteins and biomechanical properties.

Results

The structure of the explants was reminiscent of native articular cartilage and composed of chondrocytes expressing SOX-9 located in lacunae embedded within dense extracellular matrix constituted by proteoglycans and collagen Type II (Figure 2a-c). CellTrackerTM Green/Ethidium homodimer-1 labelling demonstrated negligible cell death in the explants, indicating no adverse effects from prolonged ultrasonic exposure (Figure 2d). The elastic modulus of the explants determined by indentation-type atomic force microscopy was comparable to native human articular cartilage.

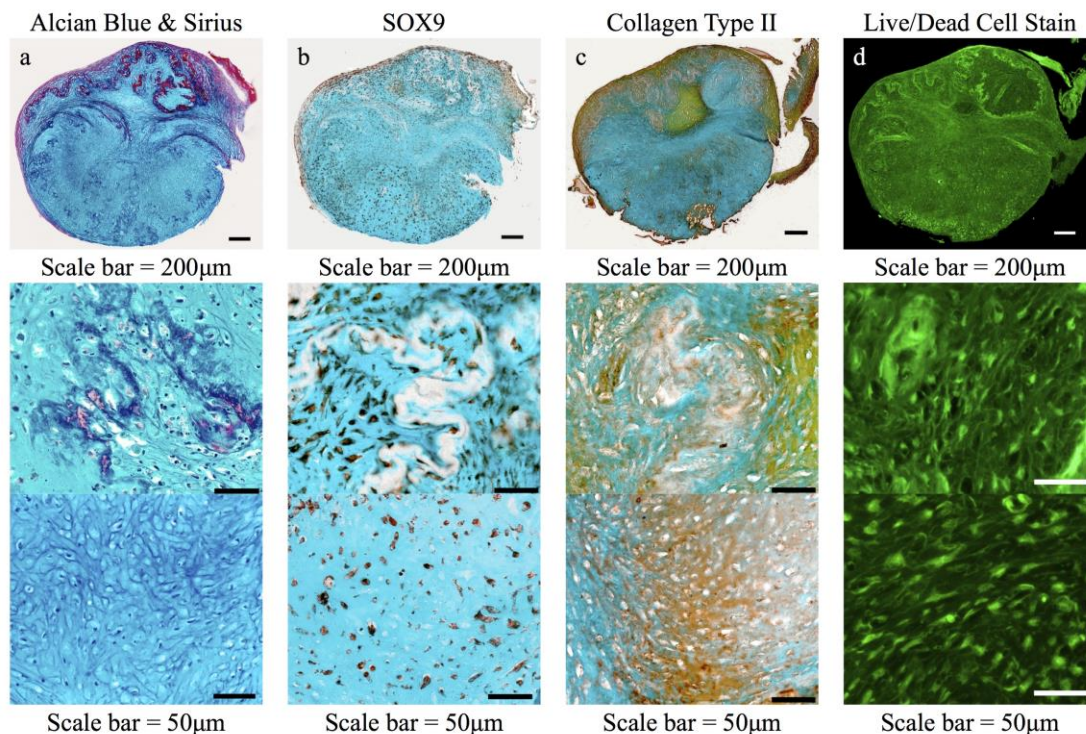


Figure 2. Histological analysis of chondrogenic differentiation in day-21 neocartilage explant (a-c) and fluorescence microscopy image of day-21 neocartilage explant stained with CellTrackerTM Green and Ethidium homodimer-1 (d).

Conclusion

We have demonstrated the first successful application of USWT in combination with perfusion bioreactor technology for bioengineering robust 3-D neocartilage grafts that are analogous to native articular cartilage.

References

- [1] Hasanova G., et al. *J Tissue Eng Regen Med* 2011; 5(10): 815-822.
- [2] Subramanian A., et al. *Tissue Eng* 2013; 19(3): 244-255.



Sonoporation in the absence of contrast agent: a “gentle” way to deliver therapeutic agents

Dyan Ankrett, Dario Carugo, Peter Glynn-Jones and Martyn Hill

Electromechanical Engineering, Engineering and the Environment, University of Southampton, Southampton SO17 1BJ, United Kingdom

Introduction

Sonoporation, the use of ultrasound to create transient pores in biological cell membranes, is traditionally undertaken in presence of contrast-agent microbubbles (CA). Although CAs drastically enhance the formation of membrane pores [1], their cavitation activities and their propensity to initiate high velocity streaming local to cells are known to compromise cell viability [2]. Moreover, CAs add complexity the elucidation of mechanisms involved in membrane poration since it is difficult to delineate CA effects from ultrasound “alone” effects on cell membranes.

In our pervious study [3] we demonstrated sonoporation in the absence of CA using a cardiac myoblasts cell line (H9c2). We showed the facilitated uptake of therapeutic agents, achieved by generating an ultrasonic standing wave (USW) within a glass capillary micro-device. Notably, this “gentle” CA-free system proved to be highly biocompatible, maintaining high cell viability.

Here we use a similar capillary micro-device, employ frequency sweeping, and expose H9c2 cells to “gentle-to-aggressive” CA-free ultrasonic conditions, allowing the identification of conditions that create only transient cell stress and conditions that significantly reduces cell viability. Our findings may facilitate the understanding of mechanisms governing transient membrane stress associated with sonoporation and enable improvements in the use of ultrasound for the delivery of therapeutic agents.

Experimental

The micro-device (Fig. 1) comprised of a squared cross-section borosilicate glass micro-capillary, acoustically coupled to a piezoelectric transducer. A frequency sweep was employed (2.13-2.40 MHz) and the sweep duration varied (0.02-0.50 sec). H9c2 cardiac myoblasts were grown in Dulbecco’s Modified Eagle Medium (DMEM) culture medium supplemented with 10% (v/v) foetal calf serum and 1% (v/v) penicillin-streptomycin and were maintained at 37 °C, 5% CO₂ in air with 95% humidity. Harvested cells were suspended at a density of 2 x10⁶ cells/mL in serum free DMEM and infused into the device using a syringe pump and subjected to varied ultrasound-alone conditions.

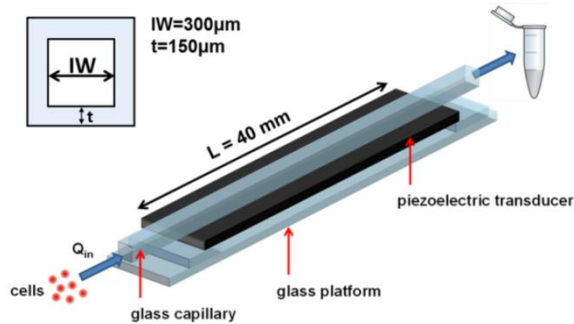


Fig. 1. Micro-device comprising of a squared cross-section glass capillary (length: 50 mm, internal width: 300 μm and wall thickness: 150 μm), coupled to a PZT transducer (length: 40 mm, width: 0.9 mm and thickness: 1 mm) and mounted on a glass platform.

Results

Cells were subjected to a variety of gentle-to-aggressive, CA-free ultrasonic conditions in order to assess the effect of ultrasound-alone on cell viability. In particular we focused on the effect of frequency sweep duration (Fig. 2) at a fixed sweep range (2.13-2.40 MHz) and at 29 Vpp. At the longer frequency sweep durations ($t_{\text{sw}} \geq 0.08$ sec) cell viability was virtually unaffected. However, at the shorter sweep duration ($t_{\text{sw}} < 0.08$ sec) cell viability decreased, with a minimum viability ($\sim 40\%$) detected at $t_{\text{sw}} = 0.05$ sec.

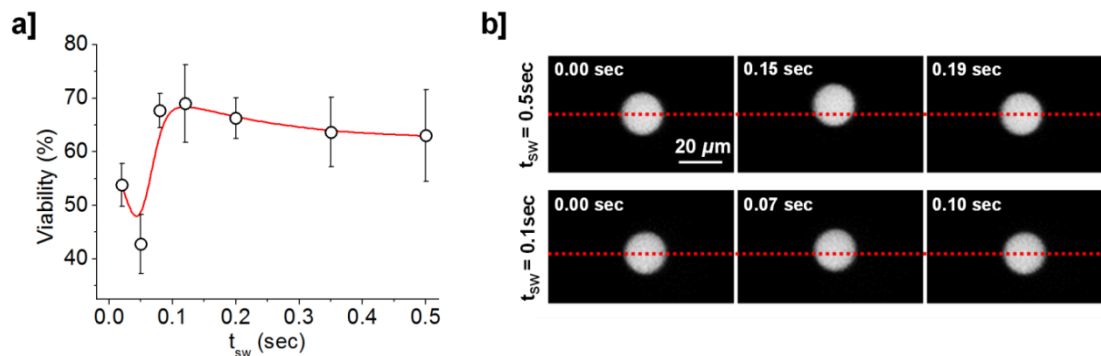


Fig. 5. a) Effect of frequency sweep duration (t_{sw} : 0.02-0.50 sec, frequency range: 2.13-2.40 MHz) on cell viability at a fixed 29 Vpp. b) Oscillatory dynamics of 20 μm diameter fluorescent beads at a sweep rates of 0.5 and 0.1 sec

Conclusions

Longer duration frequency sweeps were identified to have little or no effect on cell viability, whereas short sweeps resulted in reduced cell viability. This effect may be attributed to mechanical stress generated by rapid oscillatory movements of the cell within the fluidic domain. In support of this, imaging of fluorescent tracer beads showed that beads oscillate more rapidly during short sweep durations compared with longer sweep durations. Our findings may be of potential interest to researchers in the field of ultrasonically induced drug delivery and ultrasonic manipulation of biological cells.

Acknowledgements

We are very grateful to Agilent Technologies, Santa Clara, CA, USA for funding this research

References

- [1] C. D. Ohl, M. Arora, R. Ikin, N. De Jong, M. Versluis, M. Delius and D. Lohse, *Biophysical journal* **91** (11), 4285-4295 (2006)
- [2] A. A. Brayman, M. Azadniv, C. Cox and M. W. Miller, *Ultrasound in medicine & biology* **22** (7), 927-938 (1996)
- [3] D. Carugo, D.N. Ankrett, P. Glynn-Jones, L. Capretto, R.J. Boltryk, X. Zhang, P.A. Townsend, M. Hill, Contrast agent-free sonoporation: The use of an ultrasonic standing wave microfluidic system for the delivery of pharmaceutical agents. *Biomicrofluidics* 5(4) (2011) 044108.



Integrated acoustic micro particle manipulation and imaging system

A.L. Bernassau, M. Al-Rawhani and D.R.S. Cumming

University of Glasgow
School of Engineering
G12 8LT, Glasgow
Email: Anne.Bernassau@glasgow.ac.uk

Introduction

There has been an increasing interest in the use of manipulation and recognition of cells and particles in bio-analytical and diagnostic biosensors applications [1, 2]. For example, quantitative immuno-fluorescent detection is an important area of research, as it provides an intracellular indicator of the metabolism and physiology of the cells. Furthermore, compact and easy to use set-ups are attractive for the end-users e.g. life scientist and clinicians.

In this paper, we propose the use of single-photon avalanche diode (SPAD) matrix integrated in acoustic particle manipulator for precise patterning, positioning and imaging of particles without the need of a microscope setup.

Experiment

Particle patterning and manipulation was achieved by an octagonal array of acoustic transducers surrounding a fluid filled chamber. The acoustic octagonal device allows various patterns to be formed from the interference of travelling waves including lines, squares or more complex shapes by exciting two, four, six or eight transducers [3]. The detection and recognition of fluorescent particles is achieved by counting the photons hitting each single SPAD of the matrix. Thanks to the high sensitivity of SPADs in the wavelength of emission, it is possible to perform quick and accurate analysis.

In order to generate the desired patterns, a device consisting of eight transducers, with lateral dimensions substantially greater than the wavelength of the generated waves, was fabricated. Eight 5 mm x 5 mm plates of NCE51 Noliac ceramic lead zirconate titanate (PZT) had alumina loaded epoxy matching layer applied. The thickness of the matching layer was optimised using one dimensional transmission line model to minimise the reflection of the incident waves. The matched plates were bonded to a flexible kapton ribbon that was then folded into an octagon. Synchronisation between channels was achieved using two linked arbitrary waveform generators providing four output channels each (TGA12104, Aim and Thurlby Thandar Instruments, UK) allowing independent control of the amplitude, phase and frequency of each channel. The signals from the waveform generators were amplified and electronically matched by high speed buffers (BUF634T, Texas Instruments, USA).

The detection was achieved by a 32 x 32 SPAD array imager chip which was fabricated using austriamicrosystem 350 nm CMOS technology. The pixel size resolution is 75 μm and the total active area of the array is 2.4mm x 2.4 mm [4]. The SPAD array is biased using an integrated charge pump. When fully operational, the chip consumes 1.7 mA at 3V power supply. The excitation and detection wavelength of the imager was comprised between 430-490 nm and 510-550 nm, respectively. The high sensitivity of the SPAD imager allows the system to run effectively at a very low excitation source using a narrow viewing angle LED which is biased at 2.5 V and draws less than 4 mA. Fig. 1 shows the integrated system which consists of the SPAD array imager chip, an infinity corrected objective lens, a fluorescence interference filter, a narrow viewing angle LED, a secondary convex lens and the acoustic octagonal device. The excitation light coming from the LED is reflected off a beam splitter situated in the interference cube which then passed through

the objective lens to the glass surface of acoustic device. The generated fluorescence signal is then magnified by the objective lens and passed through a green band pass filter (510-550 nm) into the secondary lens to be detected finally by the SPAD array.

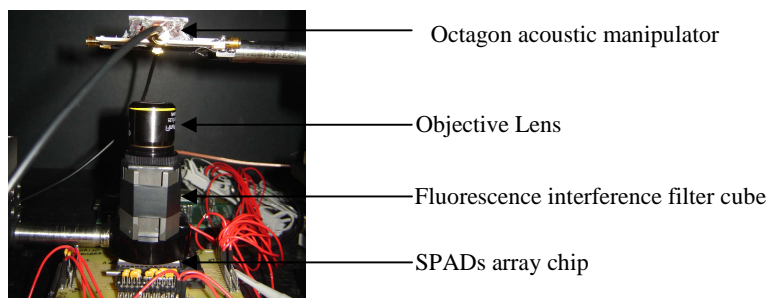


Fig. 1. Photograph of the setup. The octagon acoustic manipulator sets above the detector system which mainly consists of the SPAD array chip, fluorescence filter cube and an objective lens.

Results

Patterning and displacement experiments were performed using 10 μm diameter fluorescent polystyrene microparticles (Polysciences Europe, Germany). The transducers were excited at a frequency of 4.00 MHz with amplitude 8 V_{pp} . At this frequency, the wavelength of the sound waves in water was $\lambda = 375 \mu\text{m}$. Fig. 2 (a) shows the computer simulation results of the acoustic landscape obtained with two transducers, (b) microscope micrograph and (c) SPAD imager detection of the fluorescent particles. The micro-particles are trapped at the minima of the potential acoustic energy density¹⁵. For two active transducers, a linear pattern of nodes and antinodes is formed (Fig. 2). The distance d between the nodes is $d = 188 \mu\text{m}$, as expected. From Fig. 2, it can be seen that the patterning of the trapped particles experimentally follows this behaviour.



Fig. 2. (a) Simulation of the acoustic landscape when 2 transducers are excited simultaneously, (b) microscopic photograph of the aligned fluorescent particles, (c) image acquired with SPAD imager detector of the fluorescent particles.

Conclusion

We have presented an integrated system allowing precise and versatile manipulation microscope-less detection and permits a compact and easy-to use set-up. The SPAD imager has the advantages to have very low power consumption and very high detection capability. The set up allow changing the magnification lens.

References

- [1] P. Wang, G. Xu, L. Qin, Y. Xu, Y. Li, and R. Li, "Cell-based biosensors and its application in biomedicine," *Sensors and Actuators B: Chemical*, vol. 108, pp. 576-584, 2005.
- [2] L. Su, W. Jia, C. Hou, and Y. Lei, "Microbial biosensors: A review," *Biosensors and Bioelectronics*, vol. 26, pp. 1788-1799, 2011.
- [3] A. L. Bernassau, C. R. P. Courtney, J. Beeley, B. W. Drinkwater, and D. R. S. Cumming, "Interactive manipulation of microparticles in an octagonal sonotweezer," *Applied Physics Letters*, vol. 102, p. 164101, 2013.
- [4] Al-Rawhani, M.A.; Chitnis, D.; Beeley, J.; Collins, S.; Cumming, D. R S, "Design and Implementation of a Wireless Capsule Suitable for Autofluorescence Intensity Detection in Biological Tissues," *Biomedical Engineering, IEEE Transactions on*, vol.60, no.1, pp.55, 62, Jan.2013



Online Frequency Tracking in Acoustic Trapping

Björn Hammarstöm¹, Mikael Evander¹, Jacob Walström, Thomas Laurell¹, and Johan Nilsson¹

¹Division of Nanobiotechnology
Department of Measurement Technology and
Industrial Electrical Engineering
Lund University
S-221 00 Lund, Sweden
Email: Björn.Hammarstrom@elmat.lth.se

Acoustic trapping devices designed as high Q value resonators can provide improved performance by allowing higher acoustic intensities without a corresponding increase in temperature. However, in such devices it is critical to maintain an optimal operation frequency over time as performance will be greatly influenced by any drift in frequency, caused by e.g. temperature variations. This creates a trade-off between performance and stability for all resonator-based devices. Here, we present a new transducer fabrication method utilizing a 4 MHz PZT-transducer with kerfs to create strongly resonating acoustic trapping devices as well as a method for continuously tracking the optimal frequency over time.

The device used for acoustic trapping is shown in figure 1, and uses the cross-sectional resonance in a $2 \times 0.2 \text{ mm}^2$ glass capillary to facilitate acoustic trapping [1]. The device is used in aspirate/dispense-mode to draw beads and sample to and from the trapping site. To remove spurious resonance modes and allow for frequency tracking, a $3.2 \times 0.9 \text{ mm}^2$ transducer was diced using a silicon dicing saw to form $150 \text{ }\mu\text{m}$ ridges with $100 \text{ }\mu\text{m}$ kerfs. In the mounted device (with capillary in place) only a single thickness resonance was present in a 1 MHz wide band, as shown by the impedance characteristics in figure 2. The impedance spectrum was obtained using a HP 4194A Impedance/Gain-Phase Analyzer (Hewlett-Packard Company, CA, US).

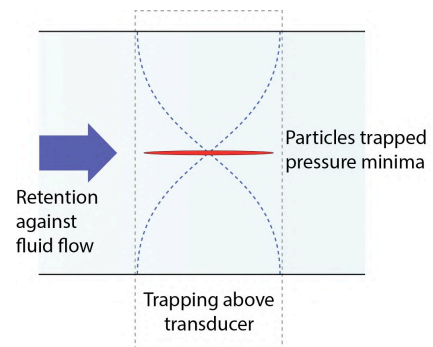
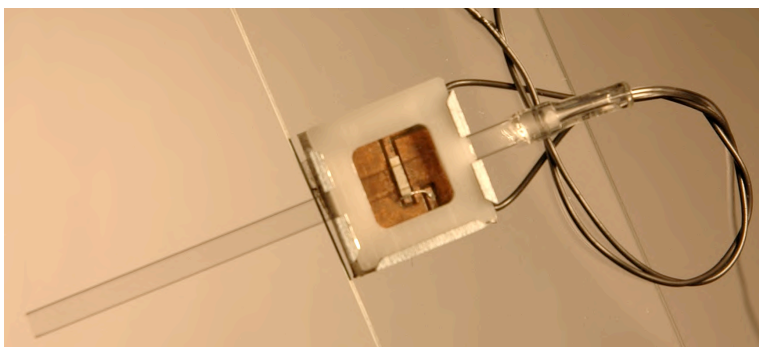


Fig. 1. Acoustic trapping device utilizing a miniaturized transducer and a $2 \times 0.2 \text{ mm}^2$ cross-section glass capillary to realize non-contact acoustic trapping in aspirate/dispense mode.

To benchmark the trapping performance, a cluster of $3 \text{ }\mu\text{m}$ beads were trapped and the maximum retention flow rate was evaluated by gradually increasing the flow rate in the channel until the cluster was lost. The highest flow where the beads could be retained (at 10 V amplitude) was recorded for each frequency, and was taken as a metric of the trapping performance.

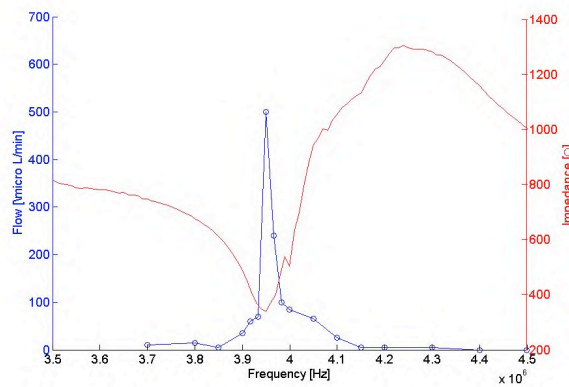


Fig. 2. The blue trace shows the trapping performance as a function of frequency and the red trace shows the impedance of the mounted device utilizing a kerfed transducer. As seen here, the trapping performance is highly frequency dependent and the impedance minima and the optimal trapping frequency coincides, forming the basis for the frequency tracking method.

Figure 2 shows that the results from the performance study optimal frequency based on flow rate coincides with the minimum impedance frequency. By utilizing the coincidence of the electrical resonance and the acoustic resonance in this system, the optimal trapping frequency could be selected by monitoring the amplitude over the piezo at fixed actuation amplitude. Impedance spectra were continuously acquired using a peak-detector circuit coupled to a data acquisition device. Data sampling was synchronized to a waveform generator, performing 10 ms scans with 2 s intervals. The optimal trapping frequency was found by selecting the frequency with the lowest amplitude for each frequency sweep. Through continuous frequency tracking, the optimal frequency could be continuously updated. To demonstrate the online frequency tracking method, the system was subjected to changes in the ambient temperature ranging from 15 to 45 °C while continuously tracking the frequency. As shown in figure 3 the frequency tracking system is able to adjust the frequency according to the temperature changes and therefore maintain an efficient trapping frequency regardless of changes in the ambient temperature.

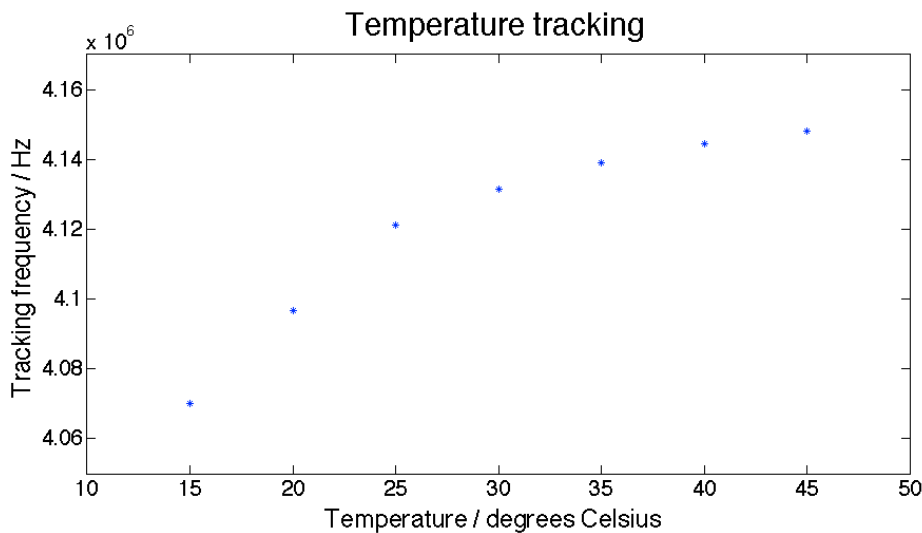


Fig. 3. The graph shows selected frequency as a function of changes in the ambient temperature, demonstrating the online frequency tracking in the system.

Not only does automatic frequency tracking accommodate for high Q factor devices it is also highly useful as it accommodates for variations in individual capillary dimensions, and temperature changes over time.

References

- [1] Hammarstrom, B., et al., *Non-contact acoustic cell trapping in disposable glass capillaries*. Lab on a Chip, 2010. **10**(17): p. 2251-2257



Electronic Controlled Piezoelectric Array for Ultrasonic Particle Manipulation in an Acoustic Resonator

Han Wang¹, Yongqiang Qiu¹, Peter Glynne-Jones², Martyn
Christine Demore¹, Sandy Hill²
Cochran¹

¹Institute for Medical Science and Technology,
University of Dundee, Dundee, United Kingdom
Wilson House, 1 Wurzburg Loan, Dundee Medipark,
Dundee, DD2 1FD
Email: hywang@dundee.ac.uk
URL: <http://www.imsat.org/MU.htm>

²Faculty of Engineering and the Environment, University
of Southampton, Southampton, United Kingdom
Highfield, Southampton, SO17 1BJ

Introduction

Electronic Sonotweezers are a topic of significant emerging interest because of their potential for manipulation in solid state systems with larger working volumes than other systems. One example is found in devices combining ultrasonic standing waves and microfluidics for particle concentration [1]. Devices incorporating single element transducers have been widely studied for cell manipulation [2]. One dimensional piezoelectric arrays for particle manipulations have also been investigated [3]. Here we report on a fine-pitch multi-element piezoelectric array to achieve precise lateral control and manipulation with bespoke electronics.

Materials and Methods

The device comprises a 30-element, 1D piezoelectric transducer array with 200- μ m element pitch coupled to a glass capillary. The ultrasonic transducer array was fabricated from PMN-PT single crystal and made into a 1-3 piezocomposite to enhance the behaviour of the active materials. The control electronics consist of an FPGA board (Spartan 3a development board, Xilinx Inc., San Jose, CA, USA) with a multichannel analogue signal switching array for transducer excitation and multiplexing [4]. The electronics are designed and constructed in a reconfigurable, concise and robust form to make it easy for researchers to control the microparticles by ultrasonic manipulation.

Results and Conclusion

The functioning of the device with control electronics was verified in various experiments and compared with theoretical results drawn from analytic solutions relating to ultrasonic radiation forces and microfluidics. We tested the device efficiency with polystyrene beads and with cells. Results are demonstrated in Fig. 1. The results show that we can position a single particle agglomerate arbitrarily and precisely in the lateral direction under straightforward electronic control.

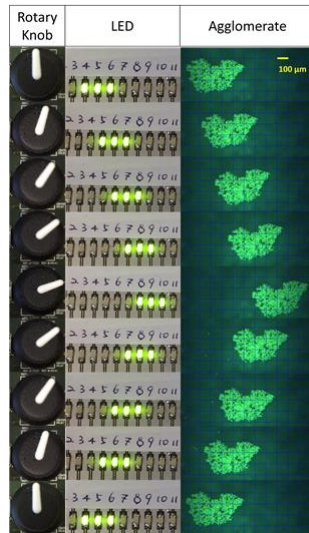


Fig. 1. An agglomerate of 10 μm polystyrene beads 500 μm in length manipulated laterally in steps corresponding to the spacing of the elements in the ultrasound array by operation of a rotary knob to control custom circuitry

References

- [1] M. Hill, "The selection of layer thicknesses to control acoustic radiation force profiles in layered resonators," *The Journal of the Acoustical Society of America*, vol. 114, no. 5, p. 2654, 2003.
- [2] P. Glynn-Jones, R. J. Boltryk, N. R. Harris, A. W. J. Cranny, and M. Hill, "Mode-switching: a new technique for electronically varying the agglomeration position in an acoustic particle manipulator.," *Ultrasonics*, vol. 50, no. 1, pp. 68–75, Jan. 2010.
- [3] P. Glynn-Jones, C. E. M. Démore, C. Ye, Y. Qiu, S. Cochran, and M. Hill, "Array-controlled ultrasonic manipulation of particles in planar acoustic resonator.," *IEEE transactions on ultrasonics, ferroelectrics, and frequency control*, vol. 59, no. 6, pp. 1258–66, Jun. 2012.
- [4] H. Wang, Y. Qiu, C. Demore, S. Cochran, P. Glynn-jones, and M. Hill, "Particle Manipulation in a Microfluidic Channel with an Electronically Controlled Linear Piezoelectric Array," *Proc. 2012 IEEE International Ultrasonics Symposium* pp. 1998–2001, 2012.



Multi-frequency characterisation of a chip for microbubble trapping

Chris Fury^{1,2}, Pierre N. G elat^{1,3},
Philip H. Jones², Gianluca Memoli¹

¹ Department of Acoustics
National Physical Laboratory
Teddington, United Kingdom
Email: gianluca.memoli@npl.co.uk
URL: <http://www.npl.co.uk/pop>

² Department of Physics and Astronomy
University College London
London, United Kingdom
Email: chris.fury@npl.co.uk
URL: <http://www.ucl.ac.uk/~ucapphj/>

³ Department of Mechanical
Engineering
University College London
London, United Kingdom
Email: pierre.gelat@npl.co.uk

Introduction

The characterisation of a resonant acoustofluidic chip is the first step towards its use for particle trapping (i.e. when aggregation at nodes/antinodes occurs). As device complexity increases, however, it becomes more and more difficult to match experimental findings with predictive theory, especially in terms of determining the optimal trapping frequencies and the acoustic pressures acting during manipulation. In this work, the authors characterise an acoustically actuated microchannel over a relatively large range of frequencies using simultaneously (1) microscope observation, (2) laser vibrometry, (3) finite-elements (FEM) modelling. Comparison with analytical theories (i.e. Lamb, Rayleigh and Love-Kirchhoff dispersion curves [1]) led to a non-invasive method of monitoring the pressure distribution inside the microchannel.

Experimental set-up

Two glass structures were used for this study. The first, consisting of a simple 3-mm thick square piece of glass, was used to calibrate the method: a PZT transducer mounted at one of the corners was used in thickness mode to generate surface oscillations whose wavelength, once measured by a Polytec laser vibrometer scanning the surface, showed the typical dispersion curve of an anti-symmetric Lamb wave. The second glass structure – Fig. 1a – had a similar thickness (2.4 mm), but contained a K-shaped manifold of microchannels, filled with water-diluted Expancel microbubbles. Acoustic manipulation was observed in this second structure by classical microscopy all through the experimental range of frequencies (70–230 kHz), but trapping only occurred at ~104 kHz and ~163 kHz, Fig. 1b. Again, the Polytec laser vibrometer was used to measure the vertical velocity on the top surface, 0.17 mm above the channel – Fig. 2a – and these data were compared with classical propagation theories and with a dedicated FEM model of the system, Fig. 2b.

Results and discussion

The wavelength measured along the direction of the longest microchannel (dotted blue line in Fig 2a) was used to calculate propagation speed, showing a resonant behaviour on top of the expected asymmetric Lamb dispersion curve. Since resonances corresponded to the observed trapping frequencies (Fig. 3a), the laser vibrometer could then be used to highlight candidate trapping frequencies from outside: a method potentially applicable to an unknown structure.

In order to get the pressure distribution inside the manifold, it was necessary to match the two experimentally observed peaks with the 9 resonances appearing in the FEM calculated spectrum (range: 130-180 kHz). Precise measurements of glass properties, use of non-dimensional plots – like the one in Fig. 3a – and analysis of the spatial cross-correlation (between vibrometer-measured and FEM-calculated velocities on the top surface) allowed matching experiments (at 163 kHz) with theory. As a further proof of the correct match, the calculated pressure distribution was found to be consistent with the one observed by microscope (i.e. at least in terms of node/antinode position under trapping conditions), thus closing the characterisation loop.

As a final step, pressures in the FEM model were linearly scaled using the displacements observed on the top surface, thus giving an indirect measurement of the unperturbed pressure in the channel.

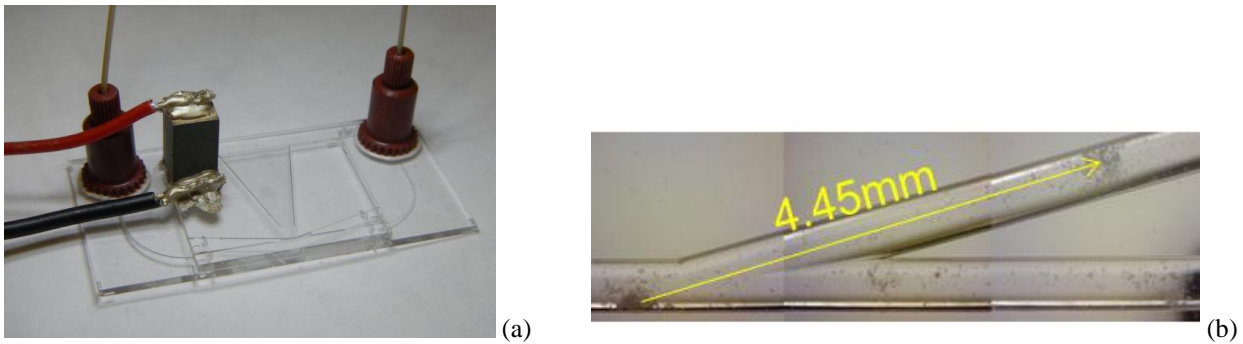


Fig. 1. (a) The microchip used for manipulating microspheres in this study (b) Composite microscope image showing aggregation of Expancel microspheres at 163.4 kHz in the right half of the K-structured manifold.

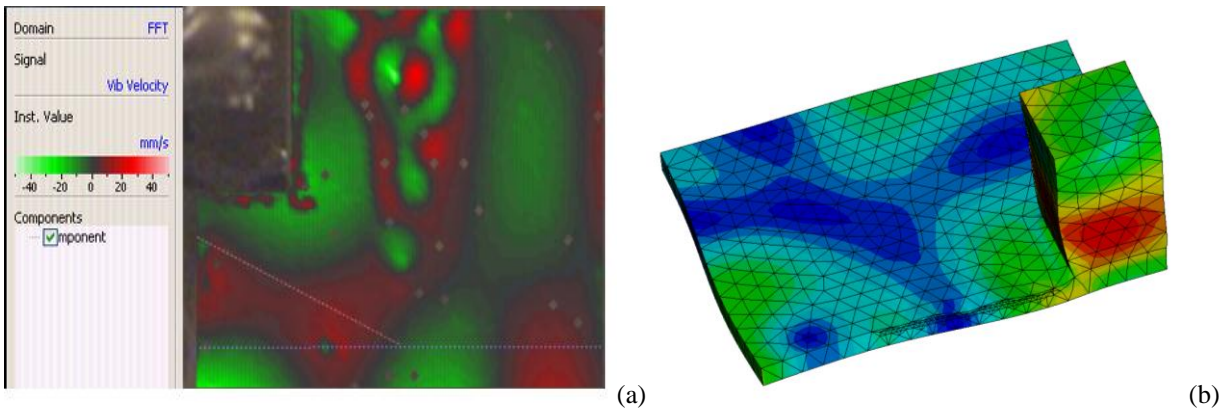


Fig. 2. (a) A typical scan using the laser vibrometer (162 kHz), with the microchannel structure highlighted by dotted lines (b) Deformation of the structure, according to the FEM model, at 164 kHz.

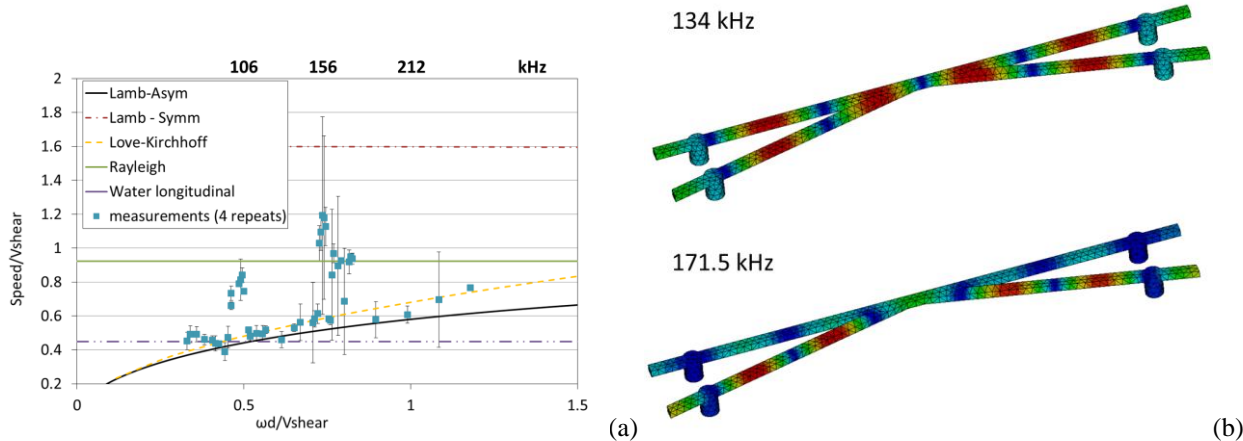


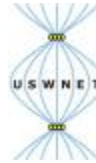
Fig. 3. (a) Laser vibrometer results in non-dimensional form, compared with different classical theories of wave propagation in solids. (b) Pressure distribution inside the channel at 134 kHz and 171.5 kHz, according to the FEM model: the position of nodes/antinodes is similar to the one observed experimentally in Fig. 1b.

Conclusions

Comparing theoretical and experimental results over a large range of frequencies allowed a non-invasive determination of the trapping frequencies and of the unperturbed pressure distribution inside an acoustically activated microchannel manifold. This is a potentially better method than using a perturbing hydrophone [2]: future studies will investigate uncertainties and compare these estimated values of pressure with the forces calculated tracking microbubble motion.

References

- [1] J. Dual, T. Schwarz, *Acoustofluidics 3: Continuum mechanics for ultrasonic particle manipulation*, Lab chip **12**, 244 (2012).
- [2] D. Rabaud, P. Thibault, JP. Raven, O. Hugon, E. Lacot, P. Marmottant, *Manipulation of confined bubbles in a thin microchannel: Drag and acoustic Bjerknes forces*, Physics of Fluids **23** (2011).



Numerical simulation of 3D acoustophoretic motion of microparticles in an acoustofluidic device

Junjun Lei, Peter Glynne-Jones and Martyn Hill

Faculty of Engineering and the Environment
University of Southampton
University Road, Southampton, SO17 1BJ, UK
Email: j.lei@soton.ac.uk

Introduction

Acoustic streaming is typically found in addition to acoustic radiation forces in acoustofluidic devices. Simulation of acoustic streaming is a crucial step for the understanding of its origins, which can provide efficient guidance on creating designs to limit or control this phenomenon. However, most existing methods can only simulate the streaming field in a local area, typically a cross-section of fluid channel. In this work, the three-dimensional (3D) Rayleigh streaming pattern in an acoustofluidic device is simulated and its effects on the movement of microparticles with various sizes are demonstrated. The viability of the simulation of 3D Rayleigh streaming presented here not only can provide better understanding and more comprehensive prediction of experiments in full acoustofluidic devices, but also can offer instructions on the simulation of unusual acoustic streaming patterns, e.g. transducer-plane streaming.¹

Model and method

Fig. 1(a) shows the full model used to simulate the 3D acoustophoretic motion of microparticles, which is the one presented in². A schematic of different layers and the dimensions of the device are shown in Fig. 1(b). The fluid channel has a dimension of 1 mm x 0.377 mm x 0.157 mm ($x \times y \times z$). The acoustic streaming field was simulated from the *limiting velocity method*, which only predicts the streaming field outside the viscous boundary layer and does not calculate the streaming velocities inside the viscous boundary layer. This is generally useful in real acoustofluidic devices working at MHz region where the thickness of viscous boundary layer is typically several orders smaller than the dimensions of the fluid chamber such that only the streaming field outside the viscous boundary layer is of interest.

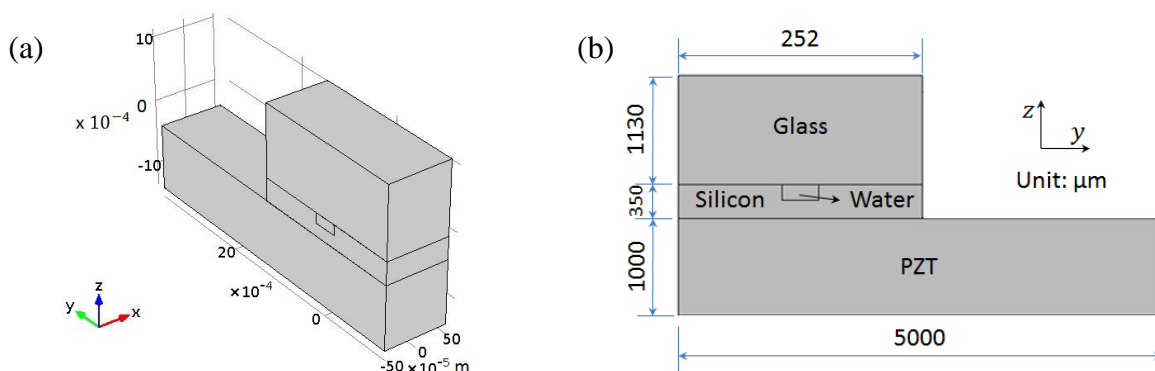


Fig. 1. (a) The 3D full model considered; (b) yz cross-section of (a)

The model was implemented in the finite element package COMSOL³. Three steps were used to simulate the acoustic streaming field and present the effects of acoustic streaming on the movements of particles. Firstly, a ‘Pressure Acoustic’ model was used to obtain the first-order acoustic pressure and velocity field, from which the limiting velocities can be derived. Then, a ‘creeping flow’ model was used to simulate the acoustic streaming field with the limiting velocities derived from the first model working as limiting velocity boundary conditions. Finally, a ‘particle trajectory for fluid flow’ model was used to simulate the particle trajectories under the combination of acoustic radiation forces (ARF) and acoustic streaming induced drag forces (ASF).

Results

The device was excited with a frequency of 1.936MHz. A lateral (y-axis) half-wavelength resonance was simulated (not shown) and a classical Rayleigh streaming pattern was obtained in the lateral direction (not shown). Based on the two models solved above, particle trajectories can be simulated with both ARF and ASF acting on the particles (polystyrene beads of diameter 0.5 μm and 5 μm), resulting in the motion shown in Fig. 3. It can be seen clearly that the movements of 0.5 μm particles are dominated by the ASF as the pattern the particle trajectories form is closely related to the acoustic streaming field. However, 5 μm particles are firstly driven to the pressure nodal plane by ARF and then slowly dragged to the up and bottom boundaries by ASF. Both of the trajectories of 5 μm and 0.5 μm are compared well with the experimental measurements from Muller et al.²

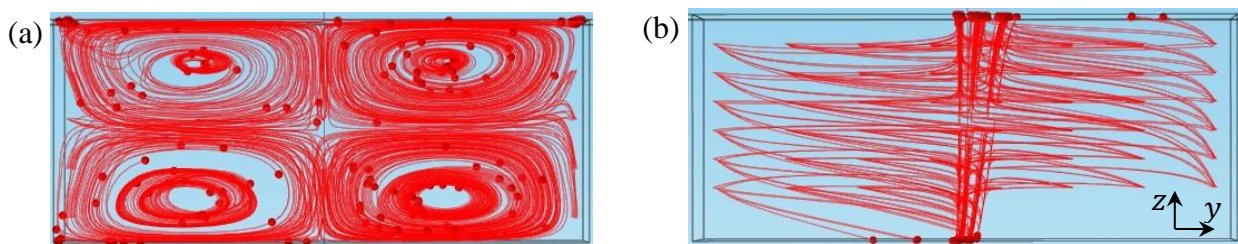


Fig. 3 Overall views along the channel axis (x-direction) of modelled trajectories of 0.5 μm particles (a) and 5 μm particles (b), where the particles are initially arranged in a 7 \times 8 \times 5 array

Conclusion

We have simulated the 3D Rayleigh streaming pattern in an acoustofluidic device using the limiting velocity method and demonstrated respectively the ARF-dominated and ASF-dominated particle motions. The results obtained from this model show much more explicitly the acoustic streaming field in full acoustofluidic devices compared to that obtained from simplified two-dimensional (2D) models and compare well with 3D measurements.

References

1. J. Lei, P. Glynne-Jones and M. Hill, *Lab Chip*, 2013, **13**, 2133-2143.
2. P. B. Muller, M. Rossi, A. G. Marín, R. Barnkob, P. Augustsson, T. Laurall, C. J. Kähler, M. J. H. Jensen and H. Bruus, *arXiv:1303.0201 [physics.flu-dyn]*, 2013.
3. Comsol Multiphysics 4.3, <http://www.comsol.com/>.



Acoustic trapping of Rayleigh-size particles using complex Gaussian-shape beams

Mahdi Azarpeyvand

Engineering Department, University of Cambridge,
Cambridge, CB2 1PZ, UK.

Email: ma559@cam.ac.uk

Introduction

Acoustic manipulation of Rayleigh-size tubular particles using 2D Gaussian-shape beams has been considered in this paper. For a particle, with density and speed of sound of ρ_l and c_l , submerged in an infinite and lossless liquid medium with density and speed of sound of ρ_0 and c_0 , the acoustic radiation force, $\mathbf{F} = F_x \mathbf{i} + F_y \mathbf{j}$, due a 2D complex beam can be calculated using the following integral over the surface of the particle [1]

$$\mathbf{F} = - \oint_A \left\{ \rho_0 \langle \mathbf{v}\mathbf{v} \rangle \cdot d\mathbf{A} - \frac{\rho_0}{2} \langle |\mathbf{v}|^2 \rangle \cdot d\mathbf{A} + \frac{1}{2\rho_0 c_0^2} \langle p^2 \rangle \cdot d\mathbf{A} \right\},$$

where $p = \rho_0 d\phi/dt$ and $\mathbf{v} = -\nabla\phi$ are respectively the acoustic pressure and particle velocity in the surrounding fluid, in which ϕ is the real part of the total potential field around the object. The radiation force can then be mathematically derived using the angular spectrum of plane wave components for the incident beam and partial-wave decomposition of the total field, as explained in Ref. [1]. In order to study the effects of the beam's lateral distribution on the performance of a single-beam acoustic manipulation device, we have considered the following Gaussian-type lateral (Y) distributions in the waist plane ($X = 0$):

$f_G(Y) = \phi_0 e^{-(\beta Y)^2}$	<i>Fundamental Gaussian</i>
$f_{HG_n}(Y) = \phi_0 H_n(\sqrt{2}\beta Y) e^{-(\beta Y)^2}$	<i>Hermite-Gaussian</i>
$f_{LG_n}(Y) = \phi_0 L_n(2(\beta Y)^2) e^{-(\beta Y)^2}$	<i>Laguerre-Gaussian</i>
$f_{PG_n}(Y) = \phi_0 (\beta Y)^{2n} e^{-(\beta Y)^2}$	<i>Dark-hollow Gaussian beam</i>

where H_n and L_n are the Hermite and Laguerre polynomial functions, $\beta^2 = 0.5 k_0 / (R + jq)$, $R = 0.5 k_0 W_0^2$ is the Rayleigh range of the beam, W_0 is the waist radius and q is a constant. The schematic of the problem is shown in Figure 1. Unlike the fundamental Gaussian beam, Hermite-, Laguerre-, and dark-hollow Gaussian beams may have several on-axis and off-axis minima and maxima, leading to strong lateral gradients and also zero-intensity (hollow) region. The emergence of such regions can be of significant importance for manipulation purposes, as already shown for optical particle handling applications.

Numerical results and discussions

Results are presented for a wide range of particle sizes, mechanical properties, and beam shapes. The numerical evaluation of the radiation force due a fundamental-Gaussian beam on different liquid particles has shown that $c_l/c_0 \approx 1$ is the critical

speed of sound ratio, above which axial/lateral manipulation is possible, such as Glycerol ($c_l = 1904 \text{ m/s}$, $\rho_l = 1260 \text{ kg/m}^3$), and below which both the lateral and axial forces are generally repulsive. It has also been shown that attractive axial/lateral forces can be achieved if the beam is operating at low frequencies, *i.e.* small (Rayleigh) particles, with large waist radius, or at very high-frequency beam ($\lambda/a < 3$) with small waist radius $W_0 < a$.

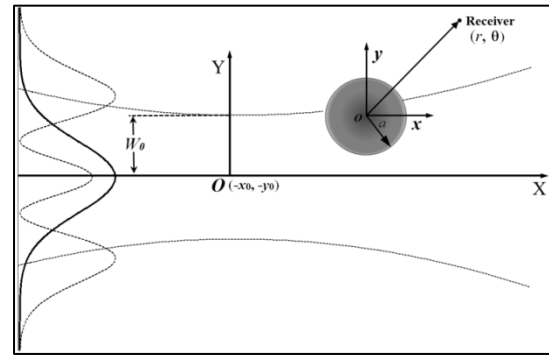


Figure 1- A circular cylinder illuminated by an off-axis Gaussian beam (solid line) or a Gaussian-type beam (dashed line).

The use of high-order Gaussian beam and dark-hollow beams (with a zero-intensity region around the propagation axis) for acoustic handling purposes is examined in Fig. 2. Results are presented for a glycerol cylinder of radii $a = \lambda$ and $a = 0.05\lambda$ (Rayleigh-size) illuminated by Hermite-Gaussian beam of $n = 1$ and a dark-hollow-Gaussian beam of $n = 2$. The beam waist is taken $W_0 = 4a$ and $q = 0.5$. Results for large particles ($a = \lambda$) show that the axial force is generally repulsive, but the lateral force can become attractive. These attractive lateral forces lead to various on-axis (*e.g.* fundamental Gaussian beam) and off-axis (*e.g.* Hermite-, dark-hollow-Gaussian beams) lateral trap positions. In the case of the dark-hollow-Gaussian beam, particles can be channeled into both on-axis and off-axis trap lines. For very small particles (Rayleigh-size), both the axial and lateral forces become attractive, pulling the particles laterally towards a trap line, and then towards the beam center. These results show that Gaussian-type beams can be used both as (a) tractor beams (for Rayleigh particle) to trap particles axially and laterally, and (b) pressor beams (large particles) to channel particles and transport them in the direction of the beam. The application of Gaussian and Gaussian-type beams for manipulation of rigid/soft and elastic particles will also be studied.

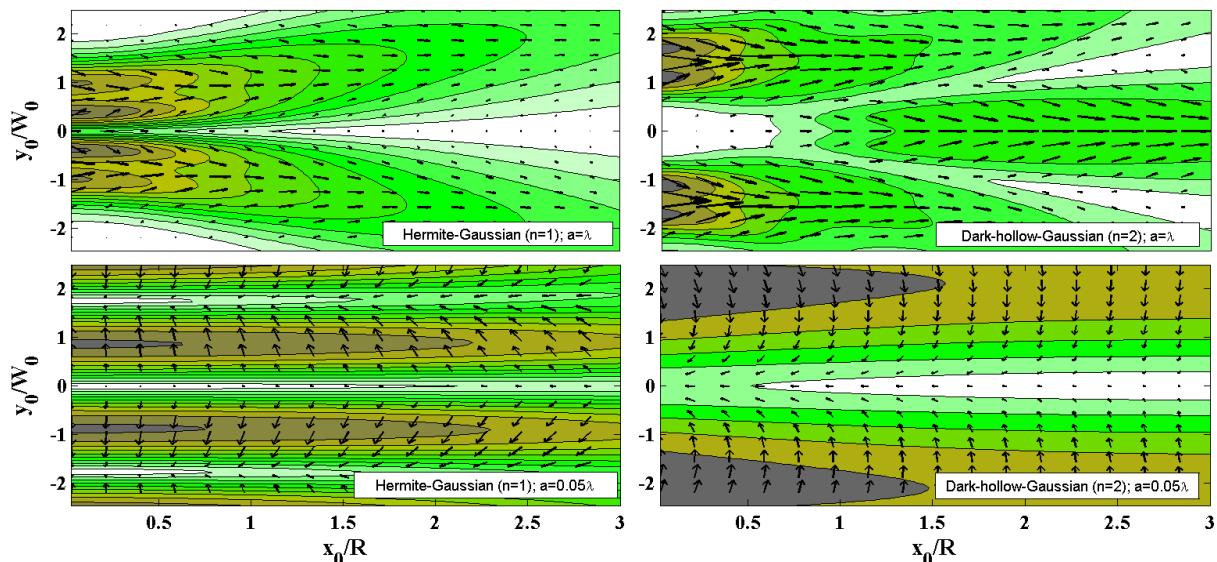


Figure 2- Acoustic radiation force and force vectors on a glycerol cylinder at different axial and lateral locations within a Gaussian-type beam.

Reference

1) M. Azarpeyvand and M. Azarpeyvand, Acoustic radiation force on a rigid cylinder in a focused Gaussian beam, *Journal of Sound and Vibration* **332**, 2338-2349 (2013).



Temperature dependence of acoustic streaming inside droplets induced by Lamb waves

Wei Liang, and
Gerhard Lindner

Institute of Sensor and Actuator Technology
Coburg University of Applied Sciences and Arts
Am Hofbräuhaus 1b
D-96450 Coburg, Germany
Email: Wei.Liang@hs-coburg.de
URL: www.isat-coburg.de

Introduction

Acoustic streaming inside droplets on LiNbO_3 substrates was intensively investigated for lab-on-a-chip applications in the last few years [1, 2]. However, piezoelectric lab-on-a-chip devices suffer from fabrication problems, costs, maintenance and cleaning. These are the reasons why current research is focused on exciting surface acoustic waves on non-piezoelectric substrates by transferring the acoustic wave from a piezoelectric substrate via a liquid coupling layer to a glass plate [3, 4]. Recently, we succeeded to induce acoustic streaming inside water droplets by Lamb waves on a glass plate by attached piezoelectric single phase transducers. In this contribution we report on the temperature dependence of acoustic streaming inside droplets on a glass plate as investigated by numerical simulations and observations with a high speed camera. demonstrated the temperature dependence of acoustic streaming inside water droplets by Lamb waves on a glass plate, which influence the acoustic streaming velocity inside the droplet.

Numerical simulations and experimental observations

In the numerical simulations antisymmetrical zero order Lamb waves with a frequency of 1 MHz and amplitude of 5.66 nm are produced on a 1 mm thick glass plate, on which a 30 μl water droplet was deposited. The streaming velocities inside the droplet were calculated for different temperatures (0°C, 10°C and 20°C). The streaming inside the droplet will be observed via the movement of tracer particles recorded with a Keyence VW9000 high speed camera.

Results

According to the simulation results, the highest streaming velocities at temperatures 0°C, 10°C and 20°C in the droplet are 0.0148 m/s, 0.0174 m/s and 0.0194m/s, respectively. A recirculation of the streaming is obtained in all cases and the center of the recirculation is moving forward with increasing the temperature. The position of the maximum of the velocity field at the surface of the droplet is also moving forward direction, which means the droplet at temperature of 20°C will have the best propulsion performance in comparison with the other temperatures (Fig.1).

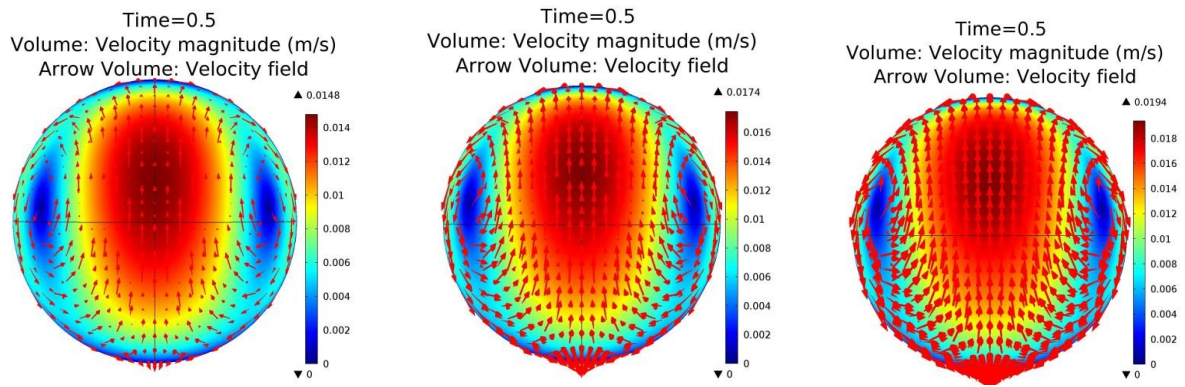


Fig.1. Comparison of simulation results on droplet acoustic streaming at different temperatures (top view on droplet). (a) Temperature 0 °C, viscosity of water 1.79×10^{-3} N s/m², (b) temperature 10 °C, viscosity of water 1.3×10^{-3} N s/m², (c) temperature 20 °C, viscosity of water 1.002×10^{-3} N s/m². The recirculation center (blue) is moving more forward by increasing the temperature and the acoustic streaming velocity is increasing. Lamb waves are propagating from down to up in the figure.

Conclusion

The viscosity of droplet, which depends on the temperature, has an important influence on the acoustic streaming of micro liter droplets on non-piezoelectric substrates. With a detailed investigation of the relevant parameters, the streaming effect can be optimized. This knowledge is relevant for technical application of acoustic streaming with respect to droplet stirring and propulsion at different temperature conditions.

Acknowledgement

This work has been supported by the special innovation program ‘Aufbruch Bayern’ of the state government of Bavaria.

References

- [1] J. R. Friend and L. Y. Yeo, *Microscale acoustofluidics: Microfluidics driven via acoustics and ultrasonics*. Reviews of Modern Physics, 83(2011).
- [2] A. Wixforth, *Acoustically driven planar microfluidics*, Superlattice and Microstructures, 33(2003).
- [3] R.P. Hodgson, M. Tan, L. Yeo, and J. Friend, *Transmitting high power rf acoustic radiation via fluid couplants into superstrates for microfluidics*, Applied Phics Letters, 94(2009).
- [4] T. Sugita and J. Kondoh, *Novel Digital Microfluidic System Using a Surface Acoustic Wave Device*, Proc. IEEE Sensors, (2010).



Temperature Controlled Multi-Well Chip Device Using a PID Regulated Liquid Heat Exchanger

Mathias Ohlin, Martin Wiklund

Department of Applied Physics
Royal Institute of Technology
KTH - Albanova
SE-10691 Stockholm, Sweden
Email: mathias.ohlin@biox.kth.se
URL: www.biox.kth.se

In this paper we propose a solution on how to control and regulate the temperature inside the multi-well chip. We have previously described the multi-well chip and its applications [1, 2] and how the acoustic manipulation performance is affected by temperature [3]. However, we have not previously been able to regulate the temperature actively. With the proposed solution the temperature will be regulated using a liquid heat exchanger implementing a PID regulator enabling selectable temperatures of the device not dependent on the acoustic energy density stored in the fluid in the multi-well chip.

With the ability to regulate the temperature inside the multi-well chip it is possible to study the effects of high energy ultrasonic actuation on cells without the risk of thermal induced damage. Furthermore, studies of the effect of acoustic streaming at low temperatures are also possible using the temperature controlled multi-well chip device.

A schematic drawing of the device is shown in figure 1. Temperature regulated liquid is flown through the device between the piezoelectric crystal and the matching layer. The PID regulated heat exchanger regulates the temperature using a thermoelectric element via feedback from a thermistor placed on the matching layer directly beneath the multi-well chip, see (9) figure 1.

The device has been fabricated (see figure 2) and is currently tested for the first time. We will report on its temperate regulation capacity at different acoustic energy densities and on the dependence of acoustic streaming on the temperature.

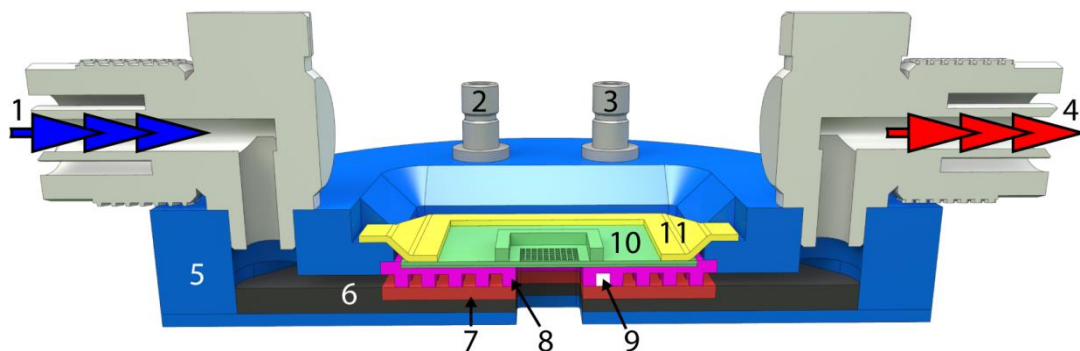


Fig. 1. Schematic drawing of a cross section made in the center of the device. (1) Inlet of liquid from heat exchanger. (2) Connection to PT1000 thermistor. (3) Connection to piezoelectric crystal. (4) Outlet of liquid to heat exchanger. (5) Plastic housing (blue). (6) Aluminum bottom bracket (black). (7) Piezoelectric crystal (red). (8) Aluminum matching layer (magenta). (9) PT1000 thermistor (white). (10) Multi-well chip (green). (11) Clamp (yellow).



Fig. 2. Picture of the complete system: the multi-well chip device (front) together with the PID regulated liquid heat exchanger (back).

References

- [1] B. Vanherberghen, O. Manneberg, A. Christakou, T. Frisk, M. Ohlin, H. M. Hertz, B. Onfelt, and M. Wiklund, "Ultrasound-controlled cell aggregation in a multi-well chip," *Lab on a Chip*, vol. 10, pp. 2727-2732, 2010.
- [2] A. E. Christakou, M. Ohlin, B. Vanherberghen, M. A. Khorshidi, N. Kadri, T. Frisk, M. Wiklund, and B. Onfelt, "Live cell imaging in a micro-array of acoustic traps facilitates quantification of natural killer cell heterogeneity," *Integr Biol (Camb)*, vol. 5, pp. 712-9, Apr 2013.
- [3] M. Ohlin, A. E. Christakou, T. Frisk, B. Onfelt, and M. Wiklund, "Influence of acoustic streaming on ultrasonic particle manipulation in a 100-well ring-transducer microplate," *Journal of Micromechanics and Microengineering*, vol. 23, Mar 2013.



Deformation and vibration of confined liquid droplets on a aluminum substrate excited by piezoelectric transducers

Matthias Streller, and
Gerhard Lindner

Institute of Sensor and Actuator Technology
Coburg University of Applied Sciences and Arts
Am Hofbräuhaus 1b
D-96450 Coburg, Germany
Email: matthias.streller@hs-coburg.de
URL: www.isat-coburg.de

Introduction

At the moment, several activities in creating tactile output devices, especially for mobile phones or tablet computers, are observable. We already described the formation of a static liquid mound at a confined water droplet on top of a single-phase-transducer [1]. Using this effect caused by acoustic radiation pressure, we are going to develop an acoustic approach to tactile displays. The local non-static deformation of liquid surfaces due to radiation pressure was used e.g. for the measurement of surface tension [2] or for acoustic ink printing [3]. Using a high-speed set-up, we investigate dynamic processes induced by acoustic radiation pressure leading to a stable deformation of liquid surfaces.

Experiment

The experimental set-up for creating a stable deformation is presented in figure 1. A PZT thickness shear vibrator is attached to a 0.35 mm thick aluminum plate. On its opposite side, a plastic housing confines the droplet within a square (5x7 mm) preventing the liquid from moving and leaving a free upper surface. The transducer is operated at approx. 400 kHz powered by an amplifier circuit. The droplet consists of 100 μ L of tap water and the measurements were performed at room temperature (20 °C). A high-speed camera system VW9000 from Keyence is used to investigate the deformation at frame rates up to 4000 frames/sec or faster.

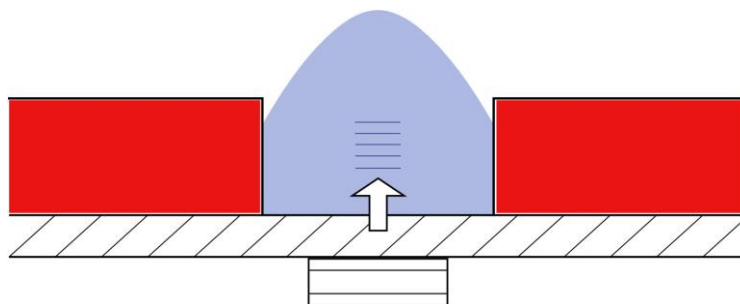


Fig. 1. Schematic set-up of the test sample being used for producing the effect of acoustic liquid deformation. Piezoelectric transducer below the aluminium substrate, confinement (red) on top.

Results

Using the set-up described before, a stable deformation with height of 1.5 mm can be achieved as shown in figure 2. Even at frame rates of 2000 frames/sec no movement of the mound was observable anymore.

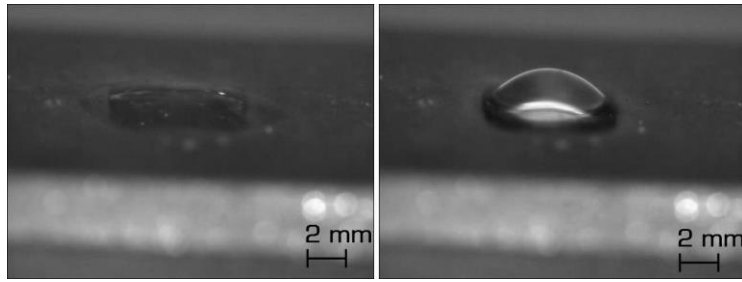


Fig. 2. Surface of the confined droplet observed with high-speed camera: without acoustic excitation (left) and after switching on the acoustic excitation (right).

Two different processes leading to this deformation have been observed: one process is a sudden switching into a stable deformation, the second process is a chaotic vibration, which changes into a periodic vibration in the course of time. Figure 3 shows the overall brightness detected by the camera sensor which represents surface vibrations. Since the video is taken at a flat angle, changes in brightness can be attributed to different sizes of liquid mounds which reflect the light back to the camera. At least three phases of vibration are observable. In the beginning the liquid is in a chaotic vibrational state with high amplitudes up to 3 mm, changing to a periodic oscillation which is damped out in the third face. The behaviour of a droplet under forced vibrations was already described for the chaotic phase using a Duffing oscillator [4, 5]. The frequency of the periodic vibration was determined to be 19.95 Hz (fig. 4).

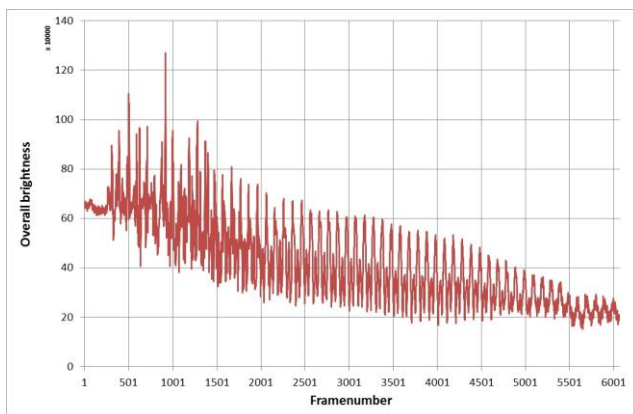


Fig. 3. Overall brightness detected by the high-speed camera as function of time.

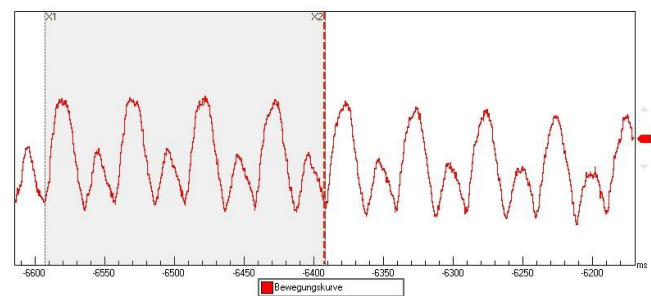


Fig. 4. Determination of the periodic vibration frequency measured over four periods.

Conclusion

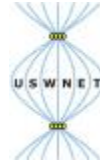
We managed to create stable liquid mounds from confined water droplets with height of 1.5 mm using acoustic radiation pressure. Two different processes were observed leading to this result: a) a switching process and b) a vibrational process. In the second case a vibrational period was measured, which may be related to the surface tension of the droplets [2].

Acknowledgement

This work is part of the ADOLIS project supported by the Bavarian Ministry of Science, Research and the Arts.

References

- [1] S. K. M. Schmitt, G. Lindner, B. Först, and F. Kaiser and S. Fromm, *Scaling up Microfluidic Acoustic Streaming Effects to Macrofluidic Applications*, 12th International Conference on New Actuators Bremen (2010), pp. 786–789.
- [2] C. Cinbis, N. N. Mansour, and B. T. Khuri-Yakub, *Effect of surface tension on the acoustic radiation pressure-induced motion of the water–air interface*, *J. Acoust. Soc. Am* (1993), vol. **94**, p. 2365.
- [3] B. Hadimioglu, S. Elrod, D. L. Steinmetz, M. Lim, and J. C. Zesch, *Acoustic Ink Printing*, Ultrasonics Symposium (1992).
- [4] K. Miyamoto, S. Nagatomo, Y. Matsui, and S. Shiokawa, *Nonlinear Vibration of Liquid Droplet by Surface Acoustic Wave Excitation*, *Jpn. J. Appl. Phys* (2002), vol. **41**, pp. 3465–3468.
- [5] S. Yamakita, Y. Matsui, and S. Shiokawa, *New Method for Measurement of Contact Angle (Droplet Free Vibration Frequency Method)*, *Jpn. J. Appl. Phys* (1999), vol. **38**, pp. 3127–3130.



Creating sheets of bronchial epithelial cells within Sonotweezers

Angela Tait¹, Peter Glynne-Jones²,
Dyan Ankrett², Martyn Hill², and Donna Davies¹

¹Brooke Laboratories, Clinical and Experimental Sciences, University of Southampton Faculty of Medicine, University Hospital Southampton, Tremona Road, Southampton, SO16 6YD,

² Engineering Science, Faculty of Engineering and the Environment University of Southampton, Highfield, Southampton SO17 1BJ

Introduction

Cell culture models are important in understanding the fundamentals of diseases as well as normal cellular physiology. We aim to create a multi-layered cell culture model to investigate the interactions of the different cells in the airways for a better insight into asthma.

We are focused on bronchial epithelium and its interaction with underlying mesenchymal cells e.g. fibroblasts. The communication between these different cell types is important for regulation of tissue homeostasis and can become dysregulated in disease. We aim to create sheets of bronchial epithelial cells within the Sonotweezers device that can be laid on top of fibroblasts, essentially making a cell 'sandwich' or allow the two cell types to arrange themselves within the device. Cohesive sheets are important when studying epithelial cells as they form cell-cell junctions that are vital for their barrier function. Previous studies have shown that levitating sheets of PZ-PHV-7 prostate epithelial cells for 1 hour (Bazou et al., 2006) allows formation of their adherens junctions. To our knowledge bronchial epithelial cell sheets have not been levitated over a short or prolonged time period.

Epithelial cells rely on integrins binding to ECM to allow polarization of the cells. Levitating over a prolonged time period the cells may release their own ECM allowing them to polarise, or the binding of cell-cell junctions may allow this to occur.

Experiment

CMRA orange stained 16HBE (Human bronchial epithelial cell line) cells were levitated for 5 days within the Sonotweezers device using a sweeping frequency to ensure that the cells remain levitated. At the end of the experiment the cells were released from the device and immunofluorescently stained for the presence of junctional proteins ZO-1 and E-cadherin, as well as their nuclei.

Results

When introduced into the Sonotweezers device, the cells were immediately levitated and aggregated at the nodal plane. Over the 1st 24 hours the cells formed a monolayer (figure 1). This multicellular structure could be maintained over 5 days within the Sonotweezers device with no apparent loss of viability.

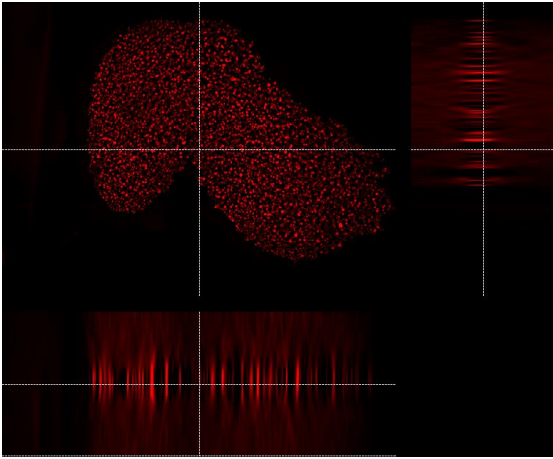


Figure 1

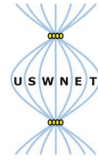
Monolayer of CMRA orange stained bronchial epithelial cells after 24 hours of levitation

Conclusion

Bronchial epithelial cells can be levitated for extended periods. Further experiments are required to optimize cell numbers and conditions for maintenance of a single cell sheet that has formed adhesive contacts similar to the epithelial barrier in vivo.

References

BAZOU, D., DAVIES, G., JIANG, W. G. & COAKLEY, T. 2006. Rapid molecular and morphological responses of prostate cell lines to cell-cell contact. *Cell Commun Adhes*, 13, 279-94.



Acoustic streaming: a general analytical solution to the driven parallel-plate system

Jonas T. Karlsen, Mikkel W.H. Ley, Peter B. Muller, and Henrik Bruus

Department of Physics
Technical University of Denmark
DTU Physics, building 309
DK-2800 Kongens Lyngby, Denmark

URL: www.staff.dtu.dk/bruus/researchgroup

Introduction

Since the seminal work by Lord Rayleigh [1], acoustic streaming has been the subject of several analytical studies most notably by Westervelt [2], Nyborg [3], Hamilton [4], and Rednikov and Sadhal [5], as well as numerical modeling in microfluidics by e.g. Muller *et al.* [6]. Most of these analytical studies (including related ones on thermoacoustic engines) are limited to the system of parallel plates separated by a height h . Moreover, the solution by Rayleigh is valid only in the regime $\delta \ll h \ll \lambda$, where δ is the thickness of the viscous boundary layer and λ is the wavelength. Hamilton lifted the requirement that $\delta \ll h$ and provided a rigorous solution including thermal effects, however still with the constraint $\delta \ll \lambda$ remaining [4].

In the literature, including the above references, the constraint $\delta \ll \lambda$ is used to neglect pressure gradients perpendicular to the wall, i.e., the first-order pressure is generally assumed to vary only parallel to the channel wall. This assumption often leads to first-order solutions that fulfill the boundary conditions to order $O(k\delta)$, where $k = 2\pi/\lambda$ is the wavenumber, but that have discontinuities of the same order at the transition from the boundary layer to the bulk [7]. For many practical applications this error is insignificant, but from a theoretical point of view a discontinuous solution is not satisfactory.

In this work we lift the requirement that $\delta \ll \lambda$ (or $k\delta \ll 1$) using an approach different from boundary layer theory. We present continuous analytical solutions of the first-order fields for the driven parallel-plate system that yields predictions in agreement with numerical simulations.

Theory

We consider a cavity bounded by acoustically hard walls and filled with a compressible fluid of density ρ , kinematic viscosity ν , and speed of sound c_0 . The Navier–Stokes equation, the continuity equation, and the thermodynamic equation of state for the pressure p and the velocity \mathbf{v} are solved analytically using perturbation theory to second order.

In the usual first-order equations,

$$\partial_t p_1 = -\rho_0 c_0^2 \nabla \cdot \mathbf{v}_1, \quad \partial_t \mathbf{v}_1 = -\frac{1}{\rho_0} \nabla p_1 + \nu \nabla^2 \mathbf{v}_1 + \beta \nu \nabla (\nabla \cdot \mathbf{v}_1), \quad (1)$$

we make a Helmholtz decomposition of the velocity field \mathbf{v}_1 into a longitudinal part \mathbf{v}_l and a solenoid part \mathbf{v}_s ,

$$\mathbf{v}_1 = \mathbf{v}_l + \mathbf{v}_s, \quad \text{with } \nabla \times \mathbf{v}_l = \mathbf{0} \quad \text{and} \quad \nabla \cdot \mathbf{v}_s = 0. \quad (2)$$

For fields with the harmonic time dependence $e^{-i\omega t}$ we thus arrive at

$$\nabla^2 p_1 = -\frac{\omega^2}{c_0^2} (1 + i\Gamma)^2 p_1, \quad \mathbf{v}_l = \frac{-i}{\rho_0 \omega} (1 - i\Gamma)^2 \nabla p_1, \quad \mathbf{v}_s = \frac{i}{2} \delta^2 \nabla^2 \mathbf{v}_s, \quad (3)$$

where $\delta = \sqrt{2\nu/\omega}$ and $\Gamma = (1 + \beta) \frac{\nu\omega}{2c_0^2}$ is the viscous length and damping factor, respectively.

Results

For a parallel-plate system of plate distance h , we impose no-slip boundary conditions on the horizontal plates in the xy -plane and drive the system with an oscillating boundary condition on the longitudinal velocity, $\mathbf{v}_l = v_{bc} e^{-i\omega t} \mathbf{e}_y$, on the vertical open boundaries. Without going into details, this configuration allows for analytical solution by separation of variables, $p_1(y, z) = p_a \sin(k_y y) \cos(k_z z)$, where the complex-valued wavenumbers are related by $k_y^2 = (i - 1)(k_z/\delta) \tan(k_z h/2) / \tanh[(1 - i)h/(2\delta)]$. The resonance frequency ω_{res} is found by tuning ω until maximum acoustic energy is obtained in the cavity for the given value of v_{bc} . An example of resulting first-order fields at resonance is shown in Fig. 1.

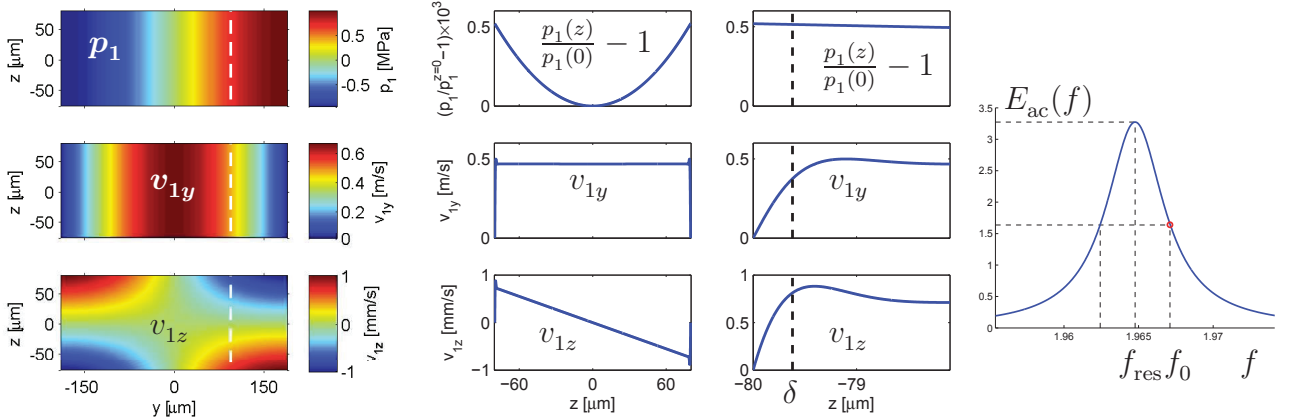


Figure 1: Analytical results for p_1 , v_{1y} and v_{1z} in a parallel-plate system of height $h = 0.16$ mm and width $w = 0.38$ mm as in Ref. [6] driven at the fundamental half-wave resonance. First column: color plots. Second column: line plots along the white dashed lines. Third column: zoom-in near the boundary layer of width $\delta = 0.38$ μm . Fourth column: The energy density E_{ac} [$\mu\text{J}/\text{m}$] versus driving frequency f [MHz] near the resonance f_{res} , which is seen to be shifted downwards from the simple resonance condition $f_0 = c_0/(2w)$.

Our analytical results can be used to calculate a wide range of properties related to acoustofluidics in the parallel-plate system, among them streaming velocity fields. Here, besides the fields shown in the figure, we mention three specific results. First, we note that our results are in full agreement with the direct numerical simulations by Muller *et al.* [6]. Second, we can predict the Q-factor of the resonance to be $Q = h/\delta = 420$ agreeing with the simulation value of 418 and experimental results of around 500. Third, we predict the resonance frequency to be $f_{res} = (1 - \frac{\delta}{2h}) \frac{c_0}{2w}$.

Conclusion

We have derived continuous analytical expressions for the first-order acoustofluidic fields without any restrictions on the length scales δ , h , and λ . These expressions allow us to predict a wide range of properties related to acoustofluidics in the parallel-plate system, among them streaming velocity fields.

References

- [1] Lord Rayleigh. *Philos. Trans. Series I* **175**, 1- 21 (1884).
- [2] P. J. Westervelt. *J. Acoust. Soc. Am.* **25**, 60-67 (1953).
- [3] W. L. M. Nyborg. *Physical Acoustics*. Academic, ed. W. P. Mason, Vol. 2B, pp. 290-295 (1965).
- [4] M. F. Hamilton, Y. A. Ilinskii, and E. A. Zabolotskaya. *J. Acoust. Soc. Am.* **113**, 153-160 (2003), *ibid* **114**, 3092-3101 (2003).
- [5] A. Y. Rednikov and S. S. Sadhal. *J. Fluid Mech.* **667**, 426-462 (2011).
- [6] P. B. Muller, R. Barnkob, M. J. H. Jensen, and H. Bruus. *Lab Chip* **12**, 4617-4627 (2012).
- [7] L. D. Landau and E. M. Lifshitz. *Fluid Mechanics*. Butterworth Heinemann, 2nd ed., (2011).



Ultrasonic Needle Device for Cell Membrane Disruption and Local Mixing in a Microfluidic Chip

Ida Iranmanesh¹, Harisha Ramachandraiah², Mathias Ohlin¹, Aman Russom², Martin Wiklund¹

1) Department of Applied Physics
Royal Institute of Technology
KTH - Albanova
SE-10691 Stockholm, Sweden
Email: isir@biox.kth.se
URL: www.biox.kth.se

2) Department of Biotechnology
Royal Institute of Technology
Science for Life Laboratory
SE-17121 Solna, Sweden
Email: harisha.r@scilifelab.se
URL: <http://www.scilifelab.se/>

Introduction

Sonication is a commonly used method for cell lysis and cell membrane disruption. Previous studies have shown that it is possible to lyse the cells in microfluidic systems using chemical, electrical or pulsed-wave ultrasound methods [1, 2]. In this paper we present a simple ultrasonic needle device that produces localized acoustic streaming. It is shown that due to the shear stresses induced by the streaming, the membrane of the cells are disrupted. In addition, this device has shown a great capacity to be used for localized acoustic mixing.

Experimental arrangement

The device is based on an acupuncture needle with the tip size of approximately 80 μm glued to a PZT element, see Fig. 1. It is attached to a three dimensional (x, y, z) translation stage with micrometer precision for controlling the position of the needle. A glass-silicon-glass microfluidic chip was used for the cell experiments.

MCF-7 cells (breast cancer cell line) stained with nuclear Hoechst 33342 that bounds to dsDNA and emits blue fluorescence. These cells were injected to a microfluidic chip. The chip has an elliptical element in the middle with an outlet hole above its center. After cell injection, the needle was submerged into the chip through the outlet hole. The device was operated at 30 V_{pp} and 100 kHz. Due to the fast needle vibrations in the cell suspension, acoustic streaming was created inside the chip.

Results

Fig. 2 shows the cell sample before (a) and after (b) ultrasonic exposure. Initially, the cell membrane is clearly visible before the ultrasonic actuation (Fig. 2a). However, after 5 min of needle vibration, the membranes of the cells are disrupted and a lot of cell debris is released into the fluid medium.

Conclusion

We have demonstrated the proof of concept of a new ultrasound-based method for cell disruption. The method utilizes a vibrating needle at 100 kHz that produces localized acoustic streaming, which in turn causes cell membrane disruption. The method is currently quantified in detail.

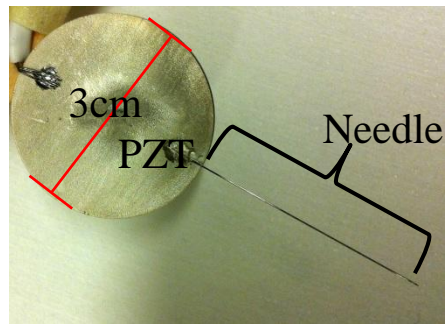


Fig. 1. The device consists of an acupuncture needle with the tip diameter of approximately $80\ \mu\text{m}$ attached to a PZT element.

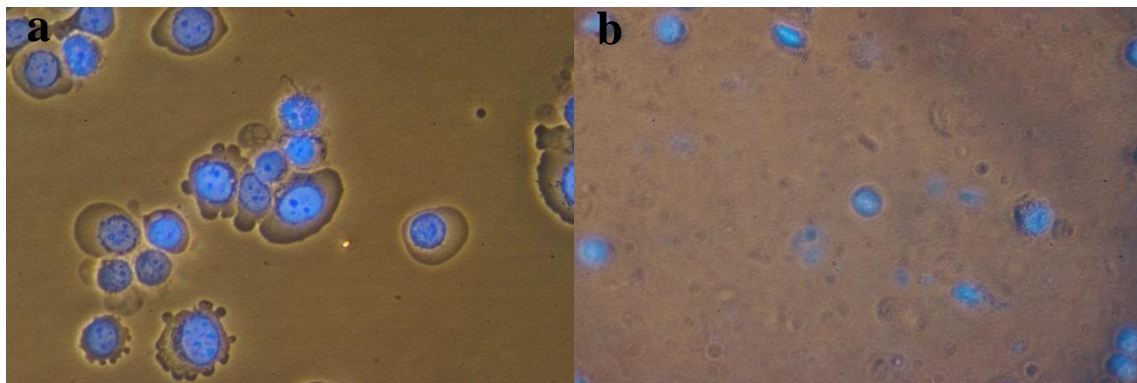


Fig. 2. (a): Before the treatment, the cell membrane can be seen clearly. (b): After five min treatment with the needle device, all the cells lose their membrane and a lot of cell debris can be observed in the cell medium inside the chip.

References

- [1] T. Tandiono, D. Siak-Wei Ow, L. Driessen, C. Sze-Hui Chin, E. Klaseboer, A. Boon-Hwa. Choo, S. Ohl, and C. Ohl, "Sonolysis of *Escherichia coli* and *Pichia pastoris* in microfluidics," *Lab on a Chip*, vol. 12, pp. 780-6, 2012.
- [2] H. R. Guzman, D. X. Nguyen, S. Khan and M. R. Prausnitz, "Ultrasound-mediated disruption of cell membranes. II. Heterogeneous effects on cells," *Journal of Acoustical Society of America*, vol. 110, pp. 597-606, July 2001.

Accelerated Cell Sorting Using In-Line Sample Pre-Enrichment

Brian Warner,* Liping Yu,* Joe Trotter,* Maria C. Jaimes,* Marko Blom,† Wilfred Buesink,† Andreas Lenshof,‡ and Thomas Laurell‡

*BD Biosciences, USA; †Micronit Microfluidics, The Netherlands; ‡Lund University, Sweden

Sample pre-enrichment is a common process strategy in cell sorting applications which is used to reduce the complexity of the sample and reduce overall sorting time. However, it can still be a time-consuming procedure and may compromise biological function.¹ Here we demonstrate an in-line sample pre-enrichment modular tool on a modified BD Influx™ cell sorter combining magnetic cell separation and acoustic cell concentration technologies² to pre-process the sample immediately before injection into the flow cell (Figure 1). This new pre-enrichment process can speed sorts 3–4 times overall and specifically eliminates the time that cells sit after pre-enrichment which greatly reduces cell-cell aggregation and subsequent additional losses due to coincidence and doublets.

Treg cells were directly sorted from a PBMC sample and from the same sample which had been pre-enriched for CD4 T lymphocytes using the BD IMag™ CD4 T Lymphocyte Enrichment Kit using the in-line process. Without pre-enrichment, the rate at which the sorted cells were collected was observed to be 244 cells/sec (total over-threshold event rate of 4,000 events/sec) while with pre-enrichment the sort rate was increased to 940 cells/sec (total over-threshold event rate of 10,000 events/sec). This higher rate allowed 1.2×10^6 Treg cells to be sorted in about 24 minutes or about 3.5 times faster than the un-enriched sort procedure. Waste fluid from the acoustic concentrator was subsequently analyzed and found to contain about 7% of the total cells coming from the magnet. Typical cell loss during the concentration step varies depending on sample concentration and flow rate through the concentrator and ranges typically from 1%–10%.

The magnetic depletion step removes sample components prone to aggregation, such as monocytes, and improves the spatial distribution of cells immediately prior to sorting. Aggregate removal was measured using the BD Influx™ Sort Analysis Tool software application which displays the position of all cells in the sample stream, calculates the proximity of the nearest neighbors, and additionally expresses a measure of dispersion as the Entrainment Factor ($EF = \text{observed frequency} / \text{expected frequency}$). When $EF = 1$, the sample distribution can be described by normal Poisson distribution, >1 indicates aggregation and <1 indicates ordering. We have observed repeatedly that the pre-enrichment process reduces EF to <1 , and we are able to measure small increases in both electronic detection and sort efficiency of 1%–5%. When $EF \gg 1$, loss of processed events occurs due to more frequent electronic aborts and reduced sort efficiencies on the processed events due to coincidence within drop packets.

We have demonstrated that the in-line enrichment modular tool on the BD Influx™ cell sorter not only cuts down the time to sort large samples, but also increases detection and sorting efficiency. The mitigating effects on cell-to-cell aggregation are transitory—a pre-enriched sample that is left to sit for some period of time (1–2 hr) begins to degrade and aggregation recurs. This suggests that time to sort after pre-enrichment is of great importance which provides a compelling argument for the advantages of the in-line procedure.

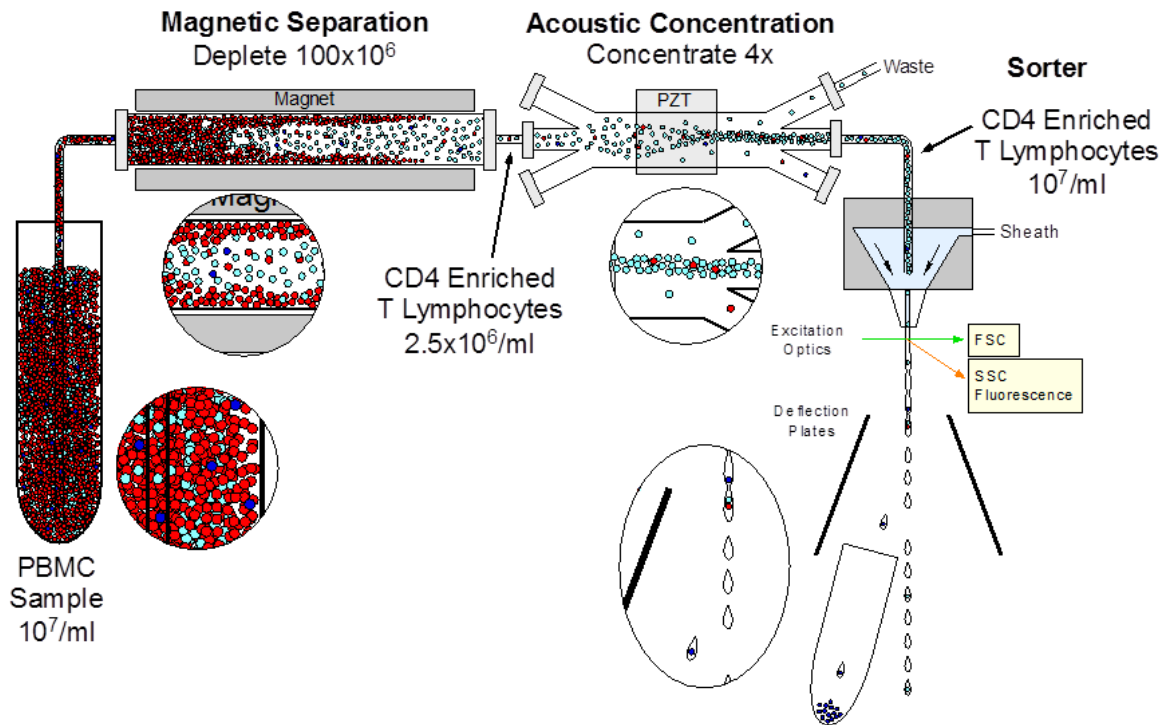


Figure 1 Sample Pre-Enrichment System

The systems, reagents, and methods presented here are for research use only and not for use in diagnostic or therapeutic procedures.

References

1. Optimizing Sorting Experiments. <http://facs.scripps.edu/SortLink/sortprep.html>. Downloaded November 26, 2012.
2. Nordin M, Laurell T. Two-hundredfold volume concentration of dilute cell and particle suspensions using chip integrated multistage acoustophoresis. *Lab Chip*. 2012;12;4610-4616.

Orientation of Erythrocytes for Flow Cytometry

Ola Jakobsson, Carl Grenvall, Thomas Laurell

Division of Nanobiotechnology, Department of Electrical Measurements, Lund University, Sweden
ola.jakobsson@elmat.lth.se

Background

Unlike most cell types, erythrocytes exhibit a bi-concave, disc-like shape. When performing flow cytometry analysis, light scattering from such cells is dependent on both their position and orientation and may cause artifacts or inconsistency in the collected signal if not accounted for [1]. While co-axial flow focusing typically is used for positioning, it does not normally control the orientation of non-spherical particles.

To compensate for this, smarter gating algorithms[2], or sphericalization[3] have been employed. To enable studies of cells in their native state it may be preferred to actually control the orientation of cells and utilize imaging cytometry.

Techniques that exist for controlling the orientation of asymmetric cells in continuous flow include the use of magnetic and electric forces[4], asymmetric nozzle geometries[5], inertial focusing[6] or fabrication of obstructions within the fluidic channels [7].

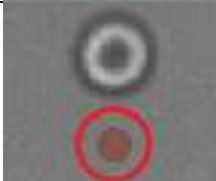
We herein report an easy to use, easy to fabricate and adjustable method for both alignment and orientation of non-spherical cell types, e.g. erythrocytes, in a continuous flow stream. By actuating a microfluidic structure with ultrasound at its resonance frequency, an acoustic radiation force will both align[8] and orient particles.

Methods

A piezoceramic transducer was glued to the bottom of a square borosilicate glass capillary (400µm ID, 800µm OD). Diluted whole blood (~1000-10000x) was injected into the capillary at different flow rates and was actuated with ultrasound at 1,88MHz or 1,89MHz at 5Vpp. Cell images were taken in a 40x microscope.

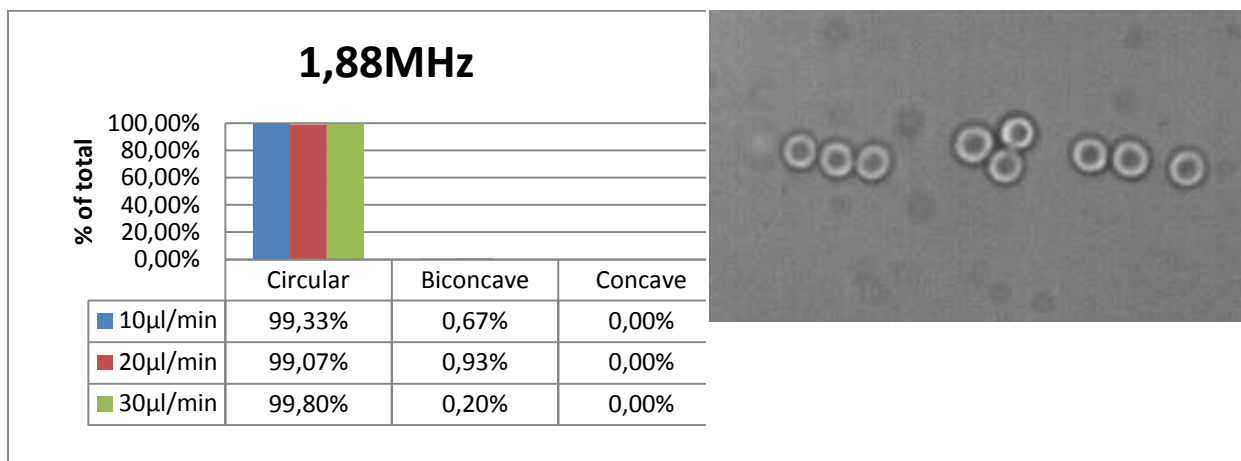
Red blood cells were manually classified into three categories depending on the observed shape. Approximately 500 cells were classified for each experiment

<i>Observed shape</i>	<i>Interpreted as orientation</i>	<i>Observation example</i>
Concave	Flat side ~90° to camera	

Biconcave	Flat side $\sim 1^\circ < 89^\circ$ to the camera	
Circular	Flat side perpendicular to camera	

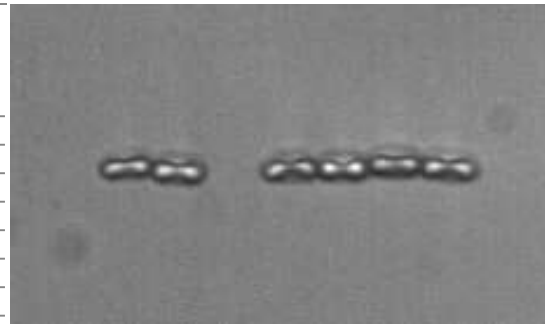
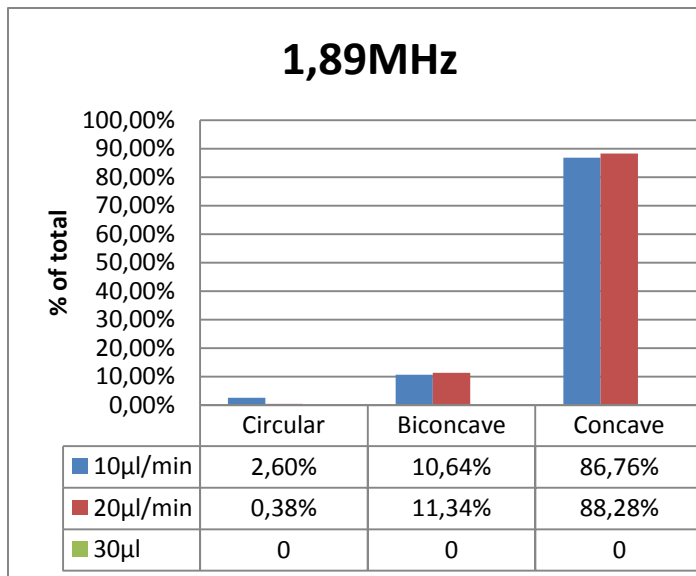
Results

As the ultrasound is turned on, two resonance modes could be observed in the capillary, one in the horizontal and one in vertical direction. Although both resonance modes were observed to exist simultaneously in the capillary, forcing particles into the cross-sectional center, one resonance mode was observed to dominate over the other. By adjusting the actuation frequency, the dominating resonance would change, thus causing the RBCs to flip horizontally 90° , presenting their smallest axis to the acoustic radiation force.



Orientation efficiency based on manual classification of observed shapes.

View from the microscope



Orientation efficiency based on manual classification of observed shapes.

View from the microscope

Conclusion

We have showed that erythrocytes can be accurately oriented in a continuous flow microchannel by means of acoustic radiation force, enabling imaging cytometry morphology analysis. The cell orientation was controlled from horizontal to vertical with respect to the optical axis by adjusting the actuation frequency.

References

1. Shapiro, H.M., Practical flow cytometry, Third edition
2. Kim, Y., et al. J. of Biomedical Optics, 2012. **17**(4).
3. Kim, Y.R. and L. Ornstein, Cytometry, 1983. **3**(6): p. 419-427.
4. Suda, T. and S. Ueno, J. of Appl. Physics, 1999. **85**(8): p. 5711-5713.
5. Dean, P.N. et al. Biophysical Journal, 1978. **23**(1): p. 7-13.
6. Hur, S.C., et al. Applied Physics Letters, 2011. **99**(4).
7. Bow, H., et al. Lab on a Chip, 2011. **11**(6): p. 1065-1073.
8. Augustsson, P., et al. Lab on a Chip, 2009. **9**(6): p. 810-818.

Finite element modeling of cell deformation by acoustic radiation forces

Puja Mishra, Peter Glynne-Jones and Martyn Hill

Engineering and the Environment
University of Southampton
Highfield
Southampton
SO17 1BJ

Introduction

The mechanical properties of cells can be used to identify cancer cells or parasitic infections such as malaria, and the compliance of individual cells has previously been measured experimentally using optical tweezers [1]. Here we demonstrate an efficient finite element method to predict the shape deformation of an osmotically expanded red blood cell (RBC) in water in an ultrasonic standing wave field. The system investigates the shape change due to presence of a relatively strong acoustic field gradient reaching force equilibrium with the elasticity of a levitated blood cell. The acoustic deformation can potentially be applied to many (e.g. thousands) of cells simultaneously, leading to higher throughput diagnostic devices.

Method

The Radiation stress tensor at a boundary due to non-linear second order effects can be approximated in the non-viscous regime as [2]

$$\Pi = \frac{1}{2\rho c^2} \langle p_1^2 \rangle - \frac{\rho}{2} \langle v_1^2 \rangle + \rho \langle u(n.u) \rangle$$

where p_1 and v_1 are the first order acoustic pressure and velocity respectively. The total radiation stress across the boundary is the difference of the radiation stress on the inner and outer surfaces of the boundary. Neglecting components parallel to the boundary, this can be written as, $\Delta p = \Pi_i - \Pi_o$, where Π_i and Π_o are the pressures due to acoustic radiation force inside and outside respectively. The resulting pressure is balanced by the elastic properties of the particle to create an equilibrium shape [1].

The model is implemented in COMSOL similar to our previous approach [3]. The approach consists of two physics models. A pressure acoustics model is used to estimate the stress acting on the cell boundary and a shell physics model predicts the deformation due to the resolution of that stress. A volume dependent internal pressure is implemented to ensure that particle volume is constrained to be constant.

Results

At first the stiffness model was verified by applying a similar stress profile to that seen by Guck [1] and the deformation of the blood cell was predicted and compared. Then the pressure acoustics was added to estimate the load on the boundary of the particle in presence of an acoustic field. Previously this had been studied on a water droplet levitated on air. In the case of the water droplet deformation due to the acoustic pressure was counterbalanced by the surface tension and an equilibrium shape was achieved. The finite element model was verified by comparing its

predictions with known results for droplet deformation [2]. The stress profile was subsequently applied to an osmotically expanded red blood cell. A linear acoustic step predicted the acoustic environment of the cell. This was combined iteratively with a non-linear thin shell representation of the cell membrane to find the resulting deformation. The properties were taken from Guck [1]. The following figure 1(a) shows the modelled scattered pressure field from a red blood cell in water at an incident pressure amplitude of 438 kPa and a frequency of 7.9 MHz. It can be observed that by applying the applied total stress there is an inward force on the pole causing compression whereas there is an outward force which leads to stretching at the equator. The final results have been compared to experimental results reported earlier [4].

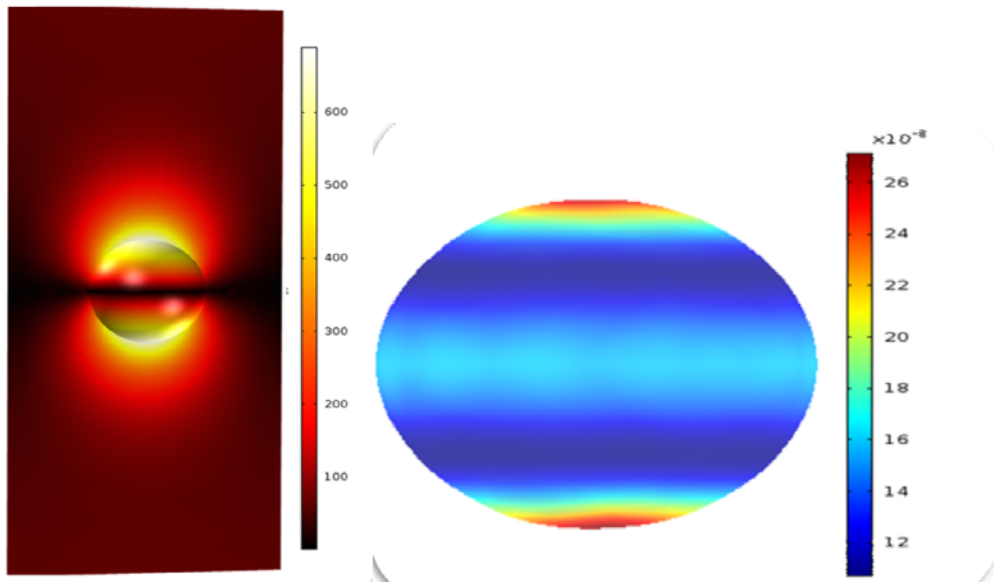


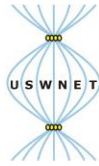
Fig. 2. (a) Scattered pressure amplitude from a red blood cell in water at incident pressure amplitude of 438 kPa. (b) Modelled cell deformation at acoustic pressure amplitude of (438 kPa): $2.5\mu\text{m}$ compression at pole and $1.5\mu\text{m}$ stretching at equator.

Conclusion

Ultrasonic standing wave fields have been shown capable of inducing deformations in red blood cells that are comparable to those demonstrated by optical methods. The deformation predicted by FE simulation has been compared with experimental results. This work has the potential to be applied to examination of the dynamics of cell deformation, and to creating new device geometries to realise the potential of deforming many cells simultaneously for high throughput diagnostics.

References

- [1] J. Guck, R. Ananthkrishnan, H. Mahmood, T.J. Moon, C.C. Cunningham, J. Kas, The optical stretcher: A novel laser tool to micromanipulate cells, *Biophysical Journal*, 81 (2001) 767-784.
- [2] P.L. Marston, Shape oscillation and static deformation of drops and bubbles driven by modulated radiation stresses---Theory, *The Journal of the Acoustical Society of America*, 67 (1980) 15-26.
- [3] P. Glynne-Jones, P.P. Mishra, R.J. Boltryk, M. Hill, Efficient finite element modeling of radiation forces on elastic particles of arbitrary size and geometry, *The Journal of the Acoustical Society of America*, 133 (2013) 1885-1893.
- [4] P. Mishra, M. Hill, P. Glynne-Jones, Acoustic deformation of cells (Abstract only), *The Journal of the Acoustical Society of America*, 133 (2013) 3278.



Acoustofluidics
2013

Ultrasonic Large-Scale Separation – Review and Application in Milk Fat Skimming

Linda Johansson^{1,2}, Thomas Leong^{1,2}, Pablo Juliano², Raymond Mawson², Sally McArthur¹,
Richard Manasseh^{*1}

¹Faculty of Engineering and Industrial Sciences, Swinburne University of Technology

²CSIRO Animal, Food and Health Sciences

ljohansson@swin.edu.au

Keywords: Ultrasonic separation, milk fat separation, standing waves, direct radiation force, large-scale systems

The last decade of acoustic manipulation research has been dominated by micro-fluidic and other small-scale systems, with focus on microfluidic applications and the exploration of fundamental acoustic manipulation principles. Our recent review of ultrasonic particle separation indicate that there are growing activity and large future potential for large-scale ultrasound separation systems.¹ Applications of interest include a broad range of chemical engineering applications such as waste water clarification, minerals separation, oil-water emulsion splitting, food and beverage manufacture, blood preparation and cell-perfusion. The technology is expected to offer a complement to conventional particle separation techniques such as centrifugation, membrane separation and floatation.

The question of how to classify this technology into large-scale and small-scale systems is not generally agreed upon. In keeping a general focus of reviewing both small and large-scale systems we suggest a few principle design classifications that the most influential systems can be categorised into, see Figure 1. This allows us to make general observations regarding limitations in process parameters and possibilities regarding what type of applications for acoustic large-scale systems to address. For instance it signifies the role of particle coalescence and aggregation for these systems. Secondly, we list throughput values for a number of systems that were selected based on performance parameters such as sample type, efficiency of separation and sample concentration. Hence, state-of-the-art systems and throughput values were identified. One conclusion is that the batch-type systems are quite competitive at this stage for large scale applications.

One promising large-scale application is the separation of milk fat globules (MFGs) from whole milk, commonly performed on an industrial scale using centrifuges. Early work by Miles et al.² using dilute milk showed that banding of the milk fat globules at the pressure antinodes occurred when the ultrasound was switched on, followed by an observed faster rising rate of the fat globules when the ultrasound was switched off. More recent trials performed by Juliano et al. in a small tube³ and a larger cubic reaction vessel⁴ showed that such a process was viable with batch scale up. In this work supported by Australian Research Council, Gardiner Foundation, CSIRO and Swinburne University, we will show some of our recent work separating MFGs from raw whole milk using ultrasound.

The benefits for this technology are likely to be application specific; ideally providing the desired values for a set of parameters regarding throughput, type of sample, separation yield, with the added benefit of gentle separation and robust operation. Key hurdles such as high throughput, concentration effects, temperature control and sample variation and sample interaction effects remain to pose challenges for the realisation of large-scale systems. In this work, we provide a framework to aid future studies of large-scale applications and provided a discussion of important aspects.

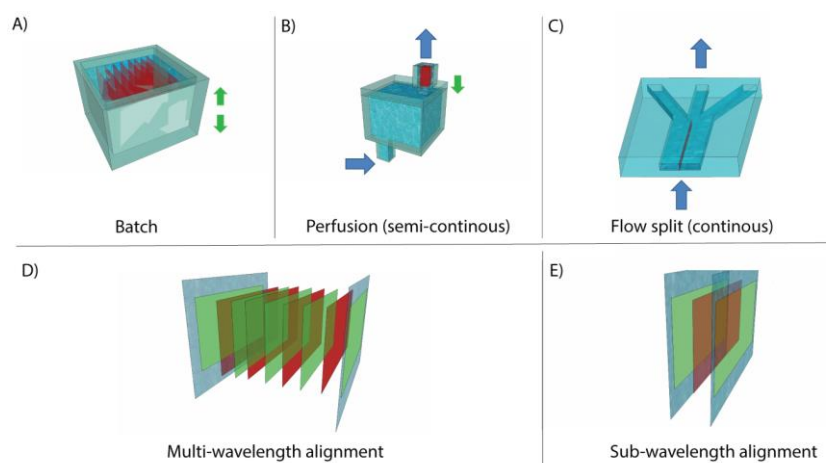


Figure 1. Classification of different acoustic particle separation systems in terms of flow arrangements (A-C) and number of particle banding planes (D, E). Alignment planes for positive acoustic contrast factor particles (red plane) and negative acoustic contrast particles (green plane) between the cavity walls (blue). In A) the alignment is combined with buoyancy or sedimentation motion (green arrow) to generate separation of the particles and the fluid. In B) the acoustic zone is used as a filter that traps particles in the perfusion flow, followed by particle aggregation and aggregate sedimentation (green arrow) back into the larger cavity.

1. Leong, T. S. H.; Johansson, L.; Juliano, P.; Mawson, R.; McArthur, S.; Manasseh, R. *submitted*.
2. Miles, C. A.; Morley, M. J.; Hudson, W. R.; Mackey, B. M. *Journal of Applied Microbiology* **1995**, *78*, 47-54.
3. Juliano, P.; Kutter, A.; Cheng, L. J.; Swiergon, P.; Mawson, R.; Augustin, M. A. *Ultrason Sonochem* **2011**, *18*, 963-973.
4. Juliano, P.; Temmel, S.; Rout, M.; Swiergon, P.; Mawson, R.; Knoerzer, K. *Ultrason Sonochem* **2013**, *20*, 52-62.



Elastomeric Negative Acoustic Contrast Microparticles for Flow Cytometry Assays

Kevin W. Cushing,^{1,4} Menake E. Piyasena,¹ Nick J. Carroll,¹ Gian C. Maestas,¹ Beth Ann Lopez,¹ Bruce S. Edwards,³ Thomas Laurell,⁴ Steven W. Graves,¹ and Gabriel P. Lopez,^{1,2}

¹ Department of Chemical and Nuclear Engineering, Center for Biomedical Engineering, The University of New Mexico, Albuquerque, New Mexico 87131, United States

² Departments of Biomedical Engineering and Mechanical Engineering & Materials Science, NSF Research Triangle Materials Research Science and Engineering Center, Duke University, Durham, North Carolina 27708, United States

³ Department of Pathology, School of Medicine, The University of New Mexico, Albuquerque, New Mexico 87131, United States

⁴ Department of Measurement Technology and Industrial Electrical Engineering, Lund University, Lund, Sweden

This report describes the development of elastomeric capture microparticles (*ECμPs*) and their use with acoustophoresis to perform flow cytometry assays (See Fig.1). We have developed simple methods to form *ECμPs* by cross-linking droplets of common commercially available silicone precursors in suspension followed by surface functionalization with biomolecular recognition reagents.^{1,2} The *ECμPs* are compressible microparticles that exhibit negative acoustic contrast in ultrasound when suspended in aqueous media, blood serum, or diluted blood.¹ In this study, these microparticles have been functionalized with antibodies to bind immunoglobulin (IgG). Specific separation of the *ECμPs* from blood cells is achieved by flowing them through an acoustofluidic chip that uses an ultrasonic standing wave to align the blood cells, which exhibit positive acoustic contrast, at the standing wave pressure node while aligning the negative acoustic contrast *ECμPs* at the antinodes. Laminar flow of the separated microparticles to downstream collection ports allows for collection of the negative acoustic contrast (*ECμPs*) and positive acoustic contrast blood cells at different outlets (Fig. 1a). Separated *ECμPs* were analyzed via flow cytometry (Fig. 1b) and demonstrated picomolar detection (*Limit of detection* = 65 pM) for IgG in diluted blood samples (Fig. 1c). The removal of high quantities of blood cells using acoustophoresis becomes crucial for accurate flow cytometry analysis of ligand-bound capture microparticles; as large quantities of blood cells can overwhelm the electronic systems of most flow cytometers. The ability to perform the biospecific capturing of a biomarker-analyte in a whole blood sample without dilution (or with minimal dilution) has potential to enhance detection and quantification of biomarkers (e.g., PSA) that are present at low concentration levels.

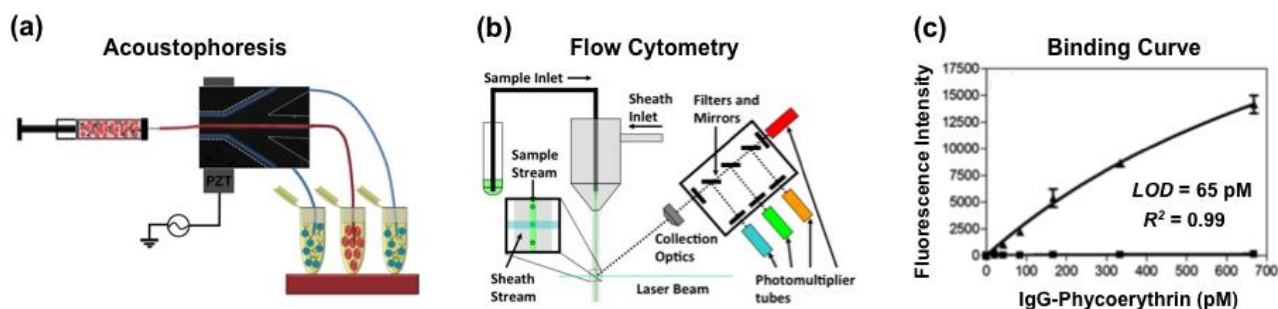


Figure 1: (a) Acoustophoresis of *ECμPs* using an acoustofluidic chip. *ECμPs* are collected from the side outlet channels and blood cells through the center. (b) Flow cytometry assay performed on collected *ECμPs*. (c) IgG-PE binding assay in 0.1 % porcine blood from *ECμPs* separated and collected using the acoustofluidic chip prior to flow cytometry analysis. (▲) denotes *ECμPs* with capture antibody and (■) denotes *ECμPs* without capture antibody.

References

1. Cushing KW, Piyasena ME, Carroll NJ, Maestas GC, López BA, Edwards BS, Graves SW, López GP: Elastomeric negative acoustic contrast particles for affinity capture assays. *Anal Chem* 2013, 85:2208–2215.
2. Johnson LM, Gao Lu, Shields IV W, Smith M, Efimenko K, Cushing KW, Genzer J, López GP: Elastomeric microparticles for acoustic mediated bioseparations. *Journal of Nanobiotechnology* 2013, 11 (1), 22.



Modeling of the formation of bands on a multiband resonator – Comparison of two approaches: diffusion equation and two phase model

Francisco Javier Trujillo,

School of Chemical Engineering
 University of New South Wales
 Kensington, NSW, 2052,
 Email: Francisco.Trujillo@unsw.edu.au
 URL:
<http://info.ceic.unsw.edu.au/about/staff/cvpage2.asp?sid=378>

Abstract

In the last decade there have been significant advances on developing mathematical models to describe the movement of suspended particles via acoustic forces on microchip configurations. Townsend et al. [1] solved the Helmholtz wave equation for the pressure amplitude of the wave, to then model the movement of single particles after calculating the acoustic force by solving Gor’kov’s equation. The path of single particle was modelled by balancing the forces acting on a particle; namely, acoustic force, drag and buoyancy, while coupling it with the fluid velocity profile predicted by computational fluid dynamics (CFD).

While this modelling approach may be sufficient for designing and modelling microchannels, it is not suitable for larger scale systems where more pronounced gradients on the acoustic field and particle concentration are present. Recently, Trujillo et al. [2] proposed to model the change of concentration of particles by solving the mass transport equation, which was modified to account for the effect of the acoustic field. This approach allowed modelling the changes of concentration of particles to form bands instead of tracking the movement of single particles. The proposed equation of the mass balance of particles is:

$$\frac{\partial}{\partial t}(x_p \rho_T) + \nabla \cdot \left(-D \nabla (x_p \rho_T) + \frac{\nabla U_{rad}}{C_D} (x_p \rho_T) \right) = 0 \tag{1}$$



Accumulation *Diffusion* *Convection*

The terms of the equation can be compared with a general transport equation by identifying the accumulation, diffusion and convective terms. The diffusivity (or diffusion coefficient) for low concentrations of particles can be calculated according to the Einstein-Stokes equation. However, this equation only accounts for the diffusion of spherical particles at low concentrations. Because the acoustic force rapidly focuses particles at the nodes (or antinodes), neglecting the effect of the concentration on diffusivity can lead to unrealistically high concentrations during modelling. To correct this, the effect of concentration on diffusivity was incorporated following the equation proposed by Garg and Ruthven [3]:

$$D = \frac{D_o}{\left(1 - \frac{c_p}{c_{sat}}\right)^2} \quad (2)$$

Where c_{sat} is the concentration at saturation and D_o is the limiting diffusivity as the concentration of particles $c_p \rightarrow 0$. According to this equation, the diffusivity will reach infinity at the saturation point which is the maximum concentration of the particles tightly packed. The equation was developed to account for the concentration dependence of diffusivity on zeolitic sorption curves. It reflects the fact that the rate of absorption and desorption depends on the availability of free spaces on the zeolite. It seems valid to use the pore diffusion approach when considering the band of particles as a porous media, where the amount of particles entering and leaving the band depends on the already occupied space within the band. If the band is saturated with particles tightly packed the diffusion term in equation (1) will balance the convective term. In other words, the concentration of particles on the band cannot be higher than the saturation concentration regardless of the extent of the acoustic force, which is a sound representation of the formation of bands.

Trujillo's model was used to predict the formation and movement of bands under a frequency ramping sawtooth pattern. The model works well at low voltages and low initial concentration of particles, because higher voltages and higher concentrations cause high acoustic forces that leads to numerical instabilities. This is because the acoustic forces rapidly localize particles at the nodes while the calculated diffusivity approaches infinity as the concentration of particles approaches saturation. In this paper an Eulerian-Eulerian two-phase model is compared with the diffusion model proposed by Trujillo et al [2]. The Eulerian-Eulerian approach models the momentum transfer equation of two phases (liquid and particles) while ensuring consistency of the volume fraction of each phase. Hence, this approach solves the problem of unrealistic concentration of particles on the bands but it highly increases the complexity of the model.

References

- [1] R.J. Townsend, et al., Modelling of particle paths passing through an ultrasonic standing wave, *Ultrasonics*, 42 (2004) 319-324.
- [2] Trujillo, F. J., S. Eberhardt, et al. (2013). "Multiphysics modelling of the separation of suspended particles via frequency ramping of ultrasonic standing waves." *Ultrasonics Sonochemistry* 20(2): 655-666.
- [3] D.R. Garg and D.M. Ruthven, The effect of the concentration dependence of diffusivity on zeolitic sorption curves, *Chemical Engineering Science*, 27 (1972) 417-423.